This is to certify that the

dissertation entitled

Life History Implications of Ribosomal RNA Gene Copy Number in Escherichia coli

presented by

Bradley Scott Stevenson

has been accepted towards fulfillment
of the requirements for

Ph.D. degree in **Microbiology**

Major professor

Date **4/19/2000**

LIFE HISTORY IMPLICATIONS OF RIBOSOMAL RNA GENE COPY NUMBER IN *ESCHERICHIA COLI*

By

Bradley Scott Stevenson

A DISSERTATION

Submitted to
Michigan State University
in partial fulfillment of the requirements
for the degree of

DOCTOR OF PHILOSOPHY

Department of Microbiology and Center for Microbial Ecology

2000

ABSTRACT

LIFE HISTORY IMPLICATIONS OF RIBOSOMAL RNA GENE COPY NUMBER IN *ESCHERICHIA COLI*

By

Bradley Scott Stevenson

Unlike the majority of prokaryotic genes, the ribosomal RNA (rRNA) genes can be found in multiple copies on the chromosome. The number of rRNA gene copies varies widely between different prokaryotic species, but among isolates of the same species the number of rRNA gene copies appears to be conserved. The research in this dissertation investigates the potential selective forces behind the occurrence of multiple rRNA gene copies in prokaryotes, and the proposed link between rRNA gene copy number and the life history of a species. The hypotheses tested state that multiple rRNA operons are an advantage in environments characterized by fluctuations in nutrient availability, and that fewer rRNA operons are an advantage under stable conditions where growth is limited by nutrient availability. The relationship between rRNA gene copy number and life history was investigated in strains of *Escherichia coli* in which additional rRNA genes were added on plasmids or deleted from the chromosome. Additional plasmid-borne rRNA gene copies caused decreased growth rates and higher concentrations of RNA in slow growing batch cultures, suggesting multiple rRNA gene copies are a metabolic expense at slower growth rates. The competitive

ability of each rRNA gene deletion strain (Δ*rrnA*, Δ*rrnB*, and Δ*rrnAB*) was measured relative to a wild type control strain in batch and chemostat competition experiments representing fluctuating and stable environments, respectively. Individual growth parameters (maximal growth rate, lag time, K_S, death rate, and yield) for each strain were measured and used in a dynamic computer model programmed to simulate the competition experiments. The model represented the dynamics of two populations competing for the same limiting nutrient, and accurately predicted the outcome of competition experiments under batch or chemostat culture conditions. As predicted by the model, the control strain was shown to have a higher competitive ability in batch culture competition experiments with the rRNA gene deletion strains, due to slightly faster growth rates and shorter lag times. These results support the hypothesis that multiple rRNA operons are an advantage when nutrient availability fluctuates. The chemostat competition experiments however, did not support the hypothesis that fewer rRNA genes are an advantage in stable, limiting nutrient conditions, because the rRNA deletion strains had lower competitive ability than the control strain. Interestingly, the decrease in relative fitness measured in chemostats depended upon which rRNA operon was deleted from the chromosome (either *rrnA* or *rrnB*), suggesting that the seven rRNA operons in *E. coli* may have differential properties that are poorly understood. Further research to confirm this observation and study the mechanism for differentiation between the *rrnA* and *rrnB* operons is currently underway.

DEDICATION

To my parents Will and Sue, and my wife Katie, for your endless love, guidance, and support.

ACKNOWLEDGMENTS

I am thankful for the support of my parents, Will and Sue, my wife, Katie, and all of my family, throughout my life. The guidance of my mentor, Thomas Schmidt, was essential to my development as a scientist and is a resource that will continue to shape my career. I thank the rest of my graduate committee, Helmut Bertrand, John Breznak, Richard Lenski, and Michael Thomashow, for their guidance and insight. Thanks to all of the past and present members of the Schmidt lab; Bonnie Bratina, Dan Buckley, Les Dethlefsen, Joel Hashimoto, Joel Klappenbach, and Paul Lepp, as well as my fellow graduate students, Keri Byzek, Joe Graber, Deb Hogan, and Mark Johnson, for their assistance, suggestions, lively discussion, and humor. Thanks to Kate Delaney and Rachael Collet for their logistical support of various experiments.

TABLE OF CONTENTS

LIST OF TABLES VIII
LIST OF FIGURES X
CHAPTER 1 1
1.1 Central observations 1
1.2 The rRNA genes 4
1.3 Non-adaptive explanations for multiple rRNA operons and their conservation 6
1.4 Multiple rRNA operons as an adaptation 8
1.5 Role of rRNA operon copy number as a life history trait 9
CHAPTER 2 12
2.1 Introduction 12
2.2 Materials and Methods 13
2.3 Results 16
2.4 Conclusions 22
CHAPTER 3 23
3.1 Introduction 23
3.2 Materials and Methods 27
Bacterial strains, plasmids, and phage 27
Bacterial growth conditions, media 30
General cloning procedures 30
PCR and XL PCR amplification 31
Visualization of rRNA operons using southern hybridization 32
Deletion of the *rrnB* operon 33
Deletion of the *rrnA* operon 38
3.3 Results 41
3.4 Discussion 47
Deletion of rRNA operons 47
Conclusion 50
3.5 Lessons learned during construction of rRNA deletion strains 50
Generalized transduction between strains of *E. coli* 50
Gene conversion 51
Marker gene orientation 54
Temperature sensitive plasmid 54
CHAPTER 4 55
4.1 Introduction 55
4.2 Materials and Methods 58
Bacterial strains 58
Media and culture conditions 58
Measurement of specific growth parameters 62
Measurement of other physiological traits 65
Batch culture competition experiments 66
Chemostat culture competition experiments 67
Calculation of chemostat-specific growth parameters 69
4.3 Results 69

Specific growth parameters 69
Measured physiological traits 73
Batch culture competition experiments 75
Chemostat competition experiments 77
Calculated chemostat-specific growth parameters 81
4.4 Discussion 81
Effect of rRNA copy number on relative fitness in fluctuating nutrient conditions 83
Effect of rRNA operon copy number on relative fitness in stable nutrient conditions 86
Possible impact of tRNA imbalance 89
Proposed explanation of cumulative results 90
Potential limitations of comparing rRNA deletion strains to control strains .. 92
Conclusion 93
CHAPTER 5 95
5.1 Introduction 95
5.2 Methods 97
Identification of variables 97
Parameterization 100
Modeling method 100
Sensitivity analyses 101
Verification of model performance 102
Validation of model performance 103
5.3 Results 103
Sensitivity analyses 103
Model Verification 108
Model Validation 116
5.4 Discussion 121
CHAPTER 6 127
APPENDIX A 136
APPENDIX B 138
APPENDIX C 140
REFERENCES 141

LIST OF TABLES

Table 2.1 Specific growth rates (μ) of the host strain and transformants carrying pEZ200 or pEZ211, grown in different media

Table 2.2 Concentration of RNA (fg/fl) of the host strain and transformants carrying pEZ200 or pEZ211, grown in different media

Table 2.3 Specific growth rate (μ) for pEZ211ΔSal transformants in different media

Table 3.1 Bacterial strains

Table 3.2 Plasmids and Phage

Table 4.1 Growth parameters measured for each strain[a]

Table 4.2 Chemostat-specific growth parameters

Table 5.1 Parameter values and results for a simulation of previously published batch culture competition experiments (76)

Table 5.2 Parameter values for simulations of previously published chemostat culture competition experiments (37)

Table 5.3 Comparison of reported and calculated *J* parameters for chemostat model verification

Table 5.4 Calculated *J* parameters for chemostat model validation at different dilution rates (*D*)

LIST OF FIGURES

Figure 1.1 Phylogenetic relationship and rRNA operon copy number of environmental isolates and representative prokaryotic species. Major phylogenetic groupings are indicated on the right. Figure taken from (46).

Figure 1.2 Typical organization of prokaryotic rRNA operon.

Figure 2.1 (A) Map of pEZ211 showing the 7.0 kb *rrn*B operon of *E. coli* cloned into pBR322 between the *Bam*HI and *Sgr*AI restriction sites. (B) Linearized representation of *rrnB* insert in pEZ211, removal of *rrn* promoters P1 and P2 in pEZ200, and internal deletion in pEZ211ΔSal.

Figure 2.2 Cellular RNA content (fg/cell) as a function of growth rate, μ (h^{-1}) for the evolved host strain (▲), and transformants with pEZ200 (●) or pEZ211 (O) compared with previously published values for *E. coli* B (Δ; (11)). Error bars represent sample standard deviations.

Figure 3.1 Location (in min) of the seven rRNA operons (*rrn*) and the origin of replication (*oriC*) on the *E. coli* K-12 chromosome (22). Arrows indicate direction of rRNA operon transcription.

Figure 3.2 The (A) general organization (19), and (B) tRNA genes of the seven *E. coli* rRNA operons (61, 62).

Figure 3.3 Steps used to delete the *rrnB* operon from the REL 4548 and BS 4548 genome, creating the BS 200 and BS 201 (Δ*rrnB*) strains.

Figure 3.4 Regions of the *E. coli* chromosome containing the *rrnA* and *rrnB* operons, showing the amplified flanking sequences (UpA, DnA, UpB, and DnB; white boxes), structural rRNA genes (16S, 23S, and 5S; dark grey boxes), tRNA genes ($tRNA^{Ile}$, $tRNA^{Ala}_{1B}$, and $tRNA^{Glu}_{2}$; dark grey boxes), and adjacent genes (*trkH, hemG, mobB, murI, murB*; light grey boxes).

Figure 3.5 Oligonucleotide primers used throughout rRNA operon deletion procedure. The non-target specific tails at 5' end of each primer are shown in boxes, the recognition sequences of restriction endonuclease are labeled and shown in shaded area of box, and the arrows indicate the restriction sites.

Figure 3.6 Southern hybridization of genomic DNA of each strain digested with *Pvu*II and hybridized with a 16S DIG-labelled probe. Hybridized bands corresponding to each of the seven rRNA operons in the control strain are labeled on the left. Sizes (kb) of each band of the λ *Hin*dIII DNA marker are labeled on the right.

Figure 3.7 XL PCR amplification of the wild type *rrnB* operon (lane 5, 6.1 kb), *rrnB*-specific marker allele (lane 6, 5.4 kb), plasmid-borne UpB:DnB deletion fragment (lane 7, 1.8 kb), and chromosomal *rrnB* deletions (lanes 9-16, 1.8 kb). Fragments sizes of a 1 kb DNA ladder in lanes 1 and 19 are marked to the left of lane 1.

Figure 3.8 XL PCR amplification of wild type *rrnA* (lane 2) and *rrnB* (lane 11) operons, intermediate *rrnA*-specific marker allele (lane 3), *rrnA* deletion in BS 101 (lane 4), *rrnB* deletion in BS 201 (lane 12), and both *rrnA* and *rrnB* deletions from BS 301 strain isolates (lanes 5-9 and 13-17 respectively). Fragment sizes of a 1 kb DNA ladder (lanes 1, 10, and 18) are marked to the left of lane 1.

Figure 3.9 Southern hybridization of a repaired chromosomal *rrnB* operon. Hybridized DNA fragments that correspond with the wild type *rrnB* operon (1), the marker *rrnB* allele (2), and the hybrid *rrnB* operon (3) are labeled with arrows.

Figure 4.1 (A) Diagram of chemostat culture system. (B) Sideview of individual chemostat culture vessel.

Figure 4.2 The death rate is shown as the change in population density (CFU/ml) of each strain in batch monocultures from 12 to 24 hours.

Figure 4.3 (A) Cell yield (10^6 cells/μg glucose), and (B) cell volume (fl) for the control (black), Δ*rrnB* (dark grey), Δ*rrnA* (light grey), and Δ*rrnAB* (white) strains are shown for chemostat monocultures at slow (0.11 h^{-1}) and fast (0.56 h^{-1}) dilution rates. Error bars represent the standard error of the measurements of two independent cultures.

Figure 4.4 Relative fitness values for the control (black), Δ*rrnB* (dark grey), Δ*rrnA* (light grey), and Δ*rrnAB* (white) strains in batch culture competition experiments with the control strain. The value for the control represents the relative fitness of the Ara^+ versus the Ara^- control strain. Error bars represent standard errors of the measurements.

Figure 4.5 Relative fitness of each rRNA deletion strain in chemostat competition experiments with slow dilution rates (0.11 h^{-1}) is represented as the population ratio (vs. control) versus the number of population doublings. The data for the control represents the fitness of the Ara^+ strain relative to the Ara^- strain. Error bars represent the standard error of four independent cultures for each strain.

Figure 4.6 Empirical (solid lines with symbols) and simulated (dotted lines) relative fitness of Δ*rrnB* in fast (black) and slow (dark grey) chemostat competition experiments are represented as the population ratio (Δ*rrnB* vs.

control) versus the number of population doublings. Error bars indicate the standard error of four independent cultures.

Figure 4.7 Empirical (solid lines with symbols) and simulation (dotted lines) relative fitness of Δ*rrnA* in fast (black) and slow (dark grey) chemostat competition experiments are represented as the population ratio (Δ*rrnA* vs. control) versus the number of population doublings. Error bars represent the standard error of four independent cultures.

Figure 4.8 Empirical relative fitness values for the control (black), Δ*rrnB* (dark grey), Δ*rrnA* (light grey) and Δ*rrnAB* (white) strains in batch culture competition experiments, and relative fitness values based on simulations using all measured parameters or each parameter individually.

Figure 5.1 Map showing the relationship between stocks (□), converters (○), and flows (⊠⟹○) of the model programmed in the object-oriented language STELLA.

Figure 5.2 Batch culture sensitivity analyses. The population ratio (Population 1/Population 2) after 24 h simulations (labeled as Sensitivity) was plotted against the ratio of the tested parameters ($\mu_{MAX}1/\mu_{MAX}2$, lag2/lag1, and K_S2/K_S1).

Figure 5.3 Sensitivity analyses of chemostat simulations. The sensitivity (change in population ratio (Pop1/Pop2) per doubling) of model parameters under fast (0.81 h^{-1}) and slow (0.11 h^{-1}) chemostat dilution rates is plotted against the ratio of the parameters ($\mu_{MAX}1/\mu_{MAX}2$) and (K_S2/K_S1).

Figure 5.4 Batch culture verification data. The dynamics of the ancestor (left axis, solid line) and derived (left axis, dashed line) populations, and the concentration of glucose (right axis, dotted line), using the estimated parameters in (76) are shown.

Figure 5.5 Population density dynamics for chemostat verification simulations using parameters in Table 5.2 for experiment A, B, and C.

Figure 5.6 Validation of model performance under batch culture conditions. Empirical versus simulation relative fitness values are shown for the control (black), Δ*rrnB* (dark grey), Δ*rrnA* (light grey), and Δ*rrnAB* (white) strains.

Figure 5.7 Population ratio dynamics for slow chemostat validation simulations of direct competition experiments with (A) Δ*rrnB*, (B) Δ*rrnA*, and (C) Δ*rrnAB* strains vs. the control strain using parameters in Chapter 4.

Figure 5.8 Chemostat validation at fast dilution rates. Empirical and simulation data for (A) Δ*rrnB*/control and (B) Δ*rrnA*/control population ratio versus doublings during fast chemostat dilution rates (0.81 h^{-1})

CHAPTER 1

INTRODUCTION

1.1 Central observations

The rRNA genes can be found in multiple copies on a prokaryotic chromosome, whereas the majority of genes are present as single copies. The numbers of rRNA genes can vary widely between different prokaryotic species (Figure 1.1) (27, 69). Many species contain only one or a few copies of the rRNA genes, but some have up to 14 as in *Clostridium beijerinckii* (77). While the number of rRNA genes can vary between different prokaryotic species, among isolates of the same species the number of genes seems to be conserved (13). The research in this dissertation attempts to address why some prokaryotes contain multiple copies of the rRNA genes, and why the numbers of copies vary between different prokaryotic species.

Figure 1.1 Phylogenetic relationship and rRNA operon copy number of environmental isolates and representative prokaryotic species. Major phylogenetic groupings are indicated on the right. Figure taken from (46).

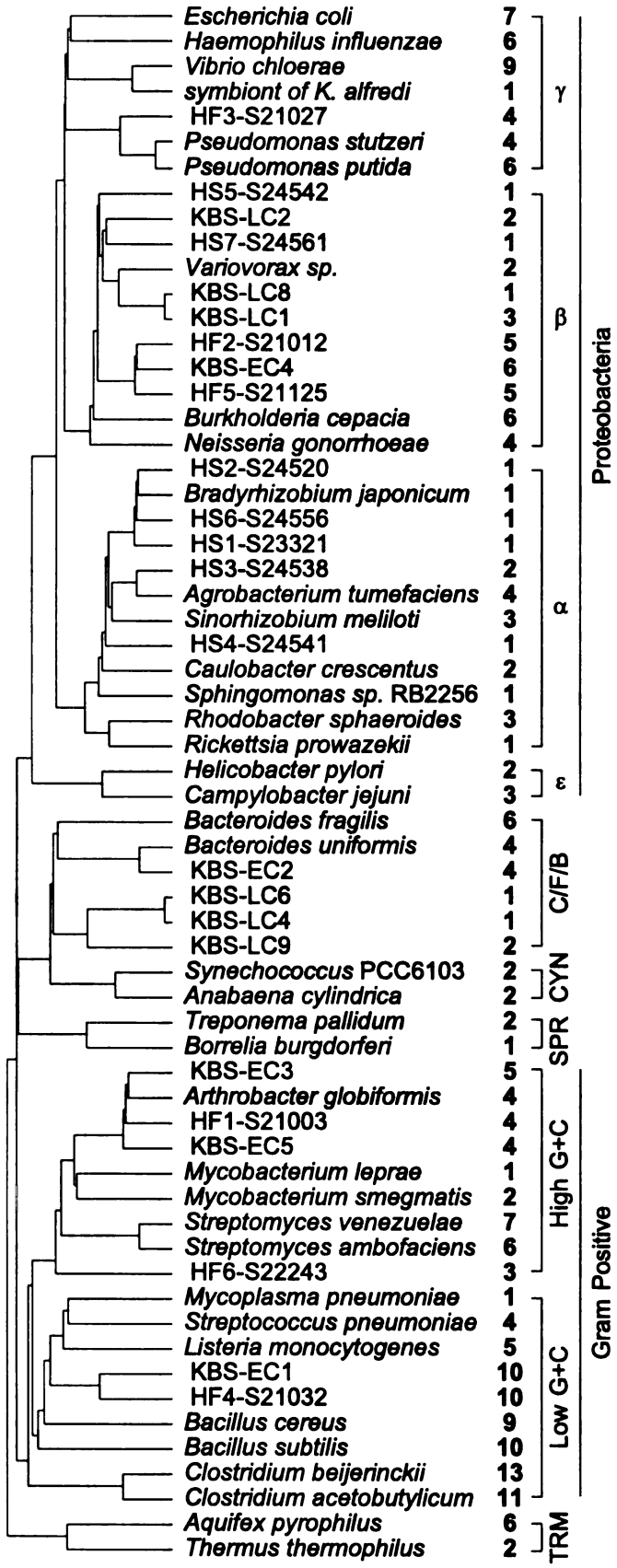
Escherichia coli 7
Haemophilus influenzae 6
Vibrio chloerae 9
symbiont of K. alfredi 1
HF3-S21027 4
Pseudomonas stutzeri 4
Pseudomonas putida 6
HS5-S24542 1
KBS-LC2 2
HS7-S24561 1
Variovorax sp. 2
KBS-LC8 1
KBS-LC1 3
HF2-S21012 5
KBS-EC4 6
HF5-S21125 5
Burkholderia cepacia 6
Neisseria gonorrhoeae 4
HS2-S24520 1
Bradyrhizobium japonicum 1
HS6-S24556 1
HS1-S23321 1
HS3-S24538 2
Agrobacterium tumefaciens 4
Sinorhizobium meliloti 3
HS4-S24541 1
Caulobacter crescentus 2
Sphingomonas sp. RB2256 1
Rhodobacter sphaeroides 3
Rickettsia prowazekii 1
Helicobacter pylori 2
Campylobacter jejuni 3
Bacteroides fragilis 6
Bacteroides uniformis 4
KBS-EC2 4
KBS-LC6 1
KBS-LC4 1
KBS-LC9 2
Synechococcus PCC6103 2
Anabaena cylindrica 2
Treponema pallidum 2
Borrelia burgdorferi 1
KBS-EC3 5
Arthrobacter globiformis 4
HF1-S21003 4
KBS-EC5 4
Mycobacterium leprae 1
Mycobacterium smegmatis 2
Streptomyces venezuelae 7
Streptomyces ambofaciens 6
HF6-S22243 3
Mycoplasma pneumoniae 1
Streptococcus pneumoniae 4
Listeria monocytogenes 5
KBS-EC1 10
HF4-S21032 10
Bacillus cereus 9
Bacillus subtilis 10
Clostridium beijerinckii 13
Clostridium acetobutylicum 11
Aquifex pyrophilus 6
Thermus thermophilus 2
γ
β
α
ε
Proteobacteria
C/F/B
CYN
SPR
High G+C
Low G+C
Gram Positive
TRM

Figure 1.1

1.2 The rRNA genes

DNA sequences within the rRNA genes are highly conserved among all organisms. The rRNA genes (in prokaryotes, 16S, 23S, and 5S rDNA) are expressed from strong promoters that are tightly regulated to coordinate the amount of rRNA (and therefore ribosomes) within the cell. Expression of the rRNA genes is controlled by the physiological condition of the cell. Many other genes involved in protein synthesis are controlled in connection with the expression of the rRNA genes. For instance, the binding of rRNA with ribosomal proteins (r-proteins) relieves the r-protein promoters from feedback inhibition. The rRNA genes are typically organized into operons that have one or more strong promoters, followed by the 16S rRNA gene, an internally transcribed spacer (ITS) region that may contain one or more tRNA genes, the 23S and 5S genes, and occasionally one or more distally-located tRNA genes followed by termination sequences (Figure 1.2). There are exceptions to this consensus, especially among some of the Archaea, in which the rRNA operons lack ITS tRNAs, or where one or all of the rRNA genes are distributed around the chromosome, behind their own promoters (as reviewed in 28).

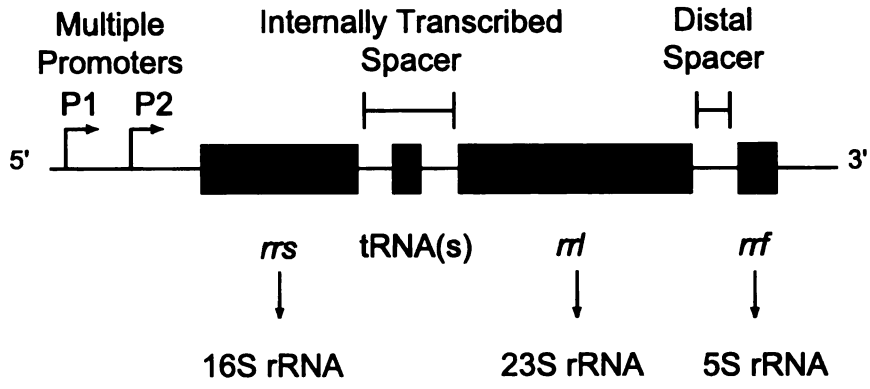

Figure 1.2 Typical organization of prokaryotic rRNA operon.

1.3 Non-adaptive explanations for multiple rRNA operons and their conservation

There are several possible non-adaptive explanations for the presence of multiple rRNA operons on a prokaryotic chromosome and the variation in rRNA operon copy number among different prokaryotes. Some of the explanations that have been explored suggest that rRNA operon copy number in prokaryotes may be related to genome size, the result of genetic drift, and/or largely determined by evolutionary history. Duplications of regions of the genome that include the rRNA genes could lead to larger genome sizes as well as an increase in number of rRNA operons. The rRNA genes themselves represent obvious sites where unequal recombination events could lead to the duplications mentioned above. The number of rRNA operons however, is not a function of genome size. Two recent studies have concluded that there is not a significant correlation between genome size and rRNA gene copy number (27, 46). Two examples that illustrate the poor correlation between rRNA gene copy number and genome size are *Bradyrhizobium japonicum*, which has a very large genome (~8.7 Mb) and one copy of the rRNA genes, and *Haemophilus influenzae*, which has a small genome (~1.8 Mb) but six copies of the rRNA genes (26, 50).

A lack of conservation in the sequence, organization, and number of rRNA operons might be expected if the operons were subject to considerable genetic drift. As discussed above however, large portions of the sequence and the overall organization of rRNA operons are generally conserved among all prokaryotic species. When many isolates of the same prokaryotic species have

been surveyed, the number of prokaryotic rRNA operons is highly conserved (e.g. 13). The number of rRNA operons might differ between certain serovars of *Vibrio cholerae* (43) or strains in *Salmonella typhimurium* (4), but in both of these cases the difference was by a single operon, constituting a small deviation in overall rRNA copy number. It is unlikely that genetic drift is the sole factor that determines the rRNA operon copy number of prokaryotic species.

Any comparative analysis must take into consideration the independence of each observation. It is therefore important to consider the impact of phylogeny on rRNA operon copy number. For example, a correlation between a high number of operons and a shared physiological trait might be used to argue a causative relationship. If all of the species that shared this physiological trait and the high rRNA operon copy number were also closely related, an equally compelling argument could be made that this correlation was due to their common ancestry. Also, if the rRNA operon copy number of a prokaryotic species were largely determined by evolutionary history, closely related species would be expected to have the same number of rRNA operons. To the extent that bacterial diversity has been studied however, phylogeny does not seem to play an obvious role in determining the number of rRNA operons in prokaryotes (Figure 1.1, (69)). There is no obvious link between phylogeny and rRNA operon copy number beyond the species level.

1.4 Multiple rRNA operons as an adaptation

The occurrence of multiple rRNA operons in prokaryotes could be the result of an adaptation to certain environmental conditions. Multiple rRNA operons could allow faster rates of rRNA synthesis, faster growth, and the ability to quickly respond to more favorable growth conditions. The rRNAs are the end product of the rRNA operons; and unlike other genes the rRNA gene products cannot be amplified through translation. Multiple rRNA operons on a chromosome can amplify rRNA synthesizing capacity by offering more sites for rRNA synthesis within the cell to meet the large demand for ribosomes under fast growth. The synthesis of rRNA constitutes over 50% of the transcriptional activity of a fast-growing *Escherichia coli* cell, and one rRNA operon would not be sufficient to supply all of the ribosomes needed at the fastest growth rates (11). Faster growth rates were therefore thought to be the main reason for the occurrence of multiple rRNA operons in *E. coli.*

Multiple rRNA operons do allow for higher rates of rRNA synthesis and growth, but recent evidence suggests that maximal growth rates may not be the main determinant of rRNA copy number (11, 16). Up to four of the seven rRNA operons in *E. coli* can be inactivated without significantly affecting the rate of total rRNA synthesis (16), suggesting that *E. coli* cells contain more rRNA operons than are needed at their maximal observed growth rates. This observation has been used to suggest that although multiple rRNA operons can support faster rates of rRNA synthesis, they increase the cell's ability to quickly respond to fluctuating nutrient conditions (17).

1.5 Role of rRNA operon copy number as a life history trait

The number of rRNA operons on the prokaryotic chromosome is well conserved among isolates of the same species (e.g. 13), but rRNA operon copy number is not necessarily conserved between even closely related species (Figure 1.1, and (69)). The conservation of rRNA operon copy number within a species but not between different species is a common life history pattern. The life history pattern of a species is a concept developed by macroecologists to describe the lifetime pattern of growth, differentiation, storage and, most importantly, reproduction. An observed life history is the result of long-term evolution, as well as the more immediate forces of the environment in which a species is and has been living (9). The number of rRNA operons could be a trait that has a major impact on the life history pattern of a species. The main goal of the work presented here was to investigate the mechanistic connection between the life history of an organism and its rRNA operon copy number.

The first hypothesis tested in this dissertation research stated that multiple rRNA operons are an advantage to an organism in environmental conditions defined by fluctuations in nutrient availability. Cells with more rRNA operons have more sites from which to synthesize rRNA after an influx of nutrients. Multiple rRNA operons can therefore result in faster growth rates, as well as provide the cell with a larger capacity for de novo ribosome synthesis following a shift to favorable growth conditions, such as an influx of nutrients.

The inactivation of rRNA operons in strains of *E. coli* may not significantly affect growth rate, but the time required for the cells to respond to nutrient fluctuations increases considerably (17). Additionally, *E. coli* cells growing at very slow rates accumulate excess ribosomes, which could offer the cell an advantage upon a shift to more favorable growth conditions (47). In Chapter 3, one or two rRNA operons were deleted in strains of *E. coli*. These deletions were unique from all previous manipulations of chromosomal rRNA operons (3, 5, 18, 23) because they did not introduce any additional marker genes and the tandem rRNA operon promoters were removed, causing them to be transcriptionally silent. These strains with 5 to 7 rRNA operons were used in Chapter 4 to study the impact of rRNA operon copy number on cell physiology and the strains' ability to compete in environments with frequent fluctuations in limited nutrient availability.

The second specific hypothesis tested addressed the potential trade-off for multiple rRNA operons. It stated that cells with fewer rRNA operons are at an advantage under conditions in which growth is controlled by stable, limiting nutrient concentrations. This hypothesis was based upon evidence that *E. coli* cells with multiple rRNA operons have excess ribosomes at very slow growth rates (47). These excess ribosomes are most likely the result of constitutive expression of the rRNA operons (68) and therefore; cells with fewer rRNA operons would contain fewer excess ribosomes at very slow growth rates. The excess ribosomes might be an advantage upon an influx of nutrients, but their synthesis also represents a large metabolic expense to cells under stable

conditions in which they will not be utilized (47). Cells with fewer rRNA operons that contain fewer excess ribosomes would not experience the same metabolic expense of diverting limited biosynthetic resources away from cell division. In Chapter 2, plasmid-borne rRNA operons were used to study the effect of additional rRNA operons on *E. coli* cells under various growth rates. Also, direct competition experiments between cells differing in rRNA operon copy number were run in chemostats with slow dilution rates in Chapter 4. These experiments were used to test for any competitive advantage that may exist in the rRNA deletion (Δ*rrn*) strains (Chapter 3), compared to the wild type control strain.

The empirical measurements of individual growth parameters and cumulative relative fitness (Chapter 4) of each strain developed in Chapter 3 were used in the computer model described in Chapter 5. This model was programmed to simulate the direct competition of two populations for a shared limiting nutrient in either batch or chemostat culture conditions. After programming and verifying the performance of the model, the individual growth parameters of each strain of *E. coli* were used to simulate the direct competition experiments. The simulation results were used as a validation of the model's ability to accurately simulate the dynamic changes in population density and nutrient concentration in direct competition experiments under both batch and chemostat culture conditions.

CHAPTER 2[a]

GROWTH RATE-DEPENDENT ACCUMULATION OF RNA FROM PLASMID-BORNE RIBOSOMAL RNA OPERONS IN *ESCHERICHIA COLI*

2.1 Introduction

Most prokaryotic genes are present as a single copy on the chromosome. Exceptions to this generality include the ribosomal RNA (rRNA) genes, which are frequently organized into an operon. The number of rRNA operons can range from one to as many as thirteen copies per chromosome (69). This variation and the absence of any obvious correlation between rRNA operon copy number and organismal phylogeny (69) led us to investigate the potential adaptive significance of rRNA operon copy number.

It has been assumed that the number of rRNA operons is directly proportional to maximal growth rates (42). Although an organism with one rRNA operon may not be able to achieve the maximum growth rates obtainable by an organism with a higher multiplicity of rRNA operons, deletion of one or two rRNA operons in *E. coli* has a marginal effect on maximal growth rate (16, 23). The inactivation of single or multiple rRNA operons in *E. coli* does, however, influence the time required to shift to faster growth rates upon encountering more favorable growth conditions (17). The enhanced capacity for a rapid response to favorable growth conditions suggests that multiple rRNA operons may be an evolutionary adaptation and advantage to organisms that experience fluctuating growth

[a] Stevenson and Schmidt 1998. J. Bacteriol. **180** (7): 1970-72

conditions (19, 69). A potential tradeoff for this enhanced capacity is the synthesis of superfluous rRNA and ribosomes under constant, slow growth conditions. While transcription of the rRNA operons is proportional to growth rate in moderate to fast growing cells, the same relationship does not exist at slow growth rates (19, 32, 69). Under slow growth conditions in a chemostat, the presence of "excess" ribosomes has been observed in populations of *E. coli* (47).

2.2 Materials and Methods

The potential disadvantages of multiple rRNA operons in *E. coli* were investigated in this study by increasing rRNA gene dosage using plasmid-borne rRNA operons. *E. coli* strain B/r which had been propagated for 10,000 generations in glucose minimal medium (56) was selected for this study to minimize changes in growth rate due to adaptation to laboratory growth conditions. Cells were transformed with plasmids derived from pKK3535, which contains the *rrnB* operon from *E. coli* (12). Plasmid pEZ211 contains the functional *rrnB* operon (Figure 2.1A) and was made by digesting pKK3535 with the restriction endonucleases *Sgr*AI and *Mun*I (Boehringer Mannheim, Indianapolis, IN) to remove the upstream λ promoter P_{L57} (44). Sequence determination of this region revealed a larger fragment of 1,756 bp was removed, apparently due to "star" or non-specific restriction activity of *Sgr*AI. This and subsequent digestions left overhanging ends which were polished with T4 DNA polymerase (New England Biolabs, Inc., Beverly, MA) and re-ligated using T4 DNA ligase (Boehringer Mannheim). Restriction, polymerase, and ligation

reactions were performed according to manufacturers' protocols. The rRNA promoters P1 and P2 were deleted in a second plasmid, pEZ200 by digesting pKK3535 with the restriction endonucleases *Sgr*AI and *Bgl*II (Figure 2.1B).

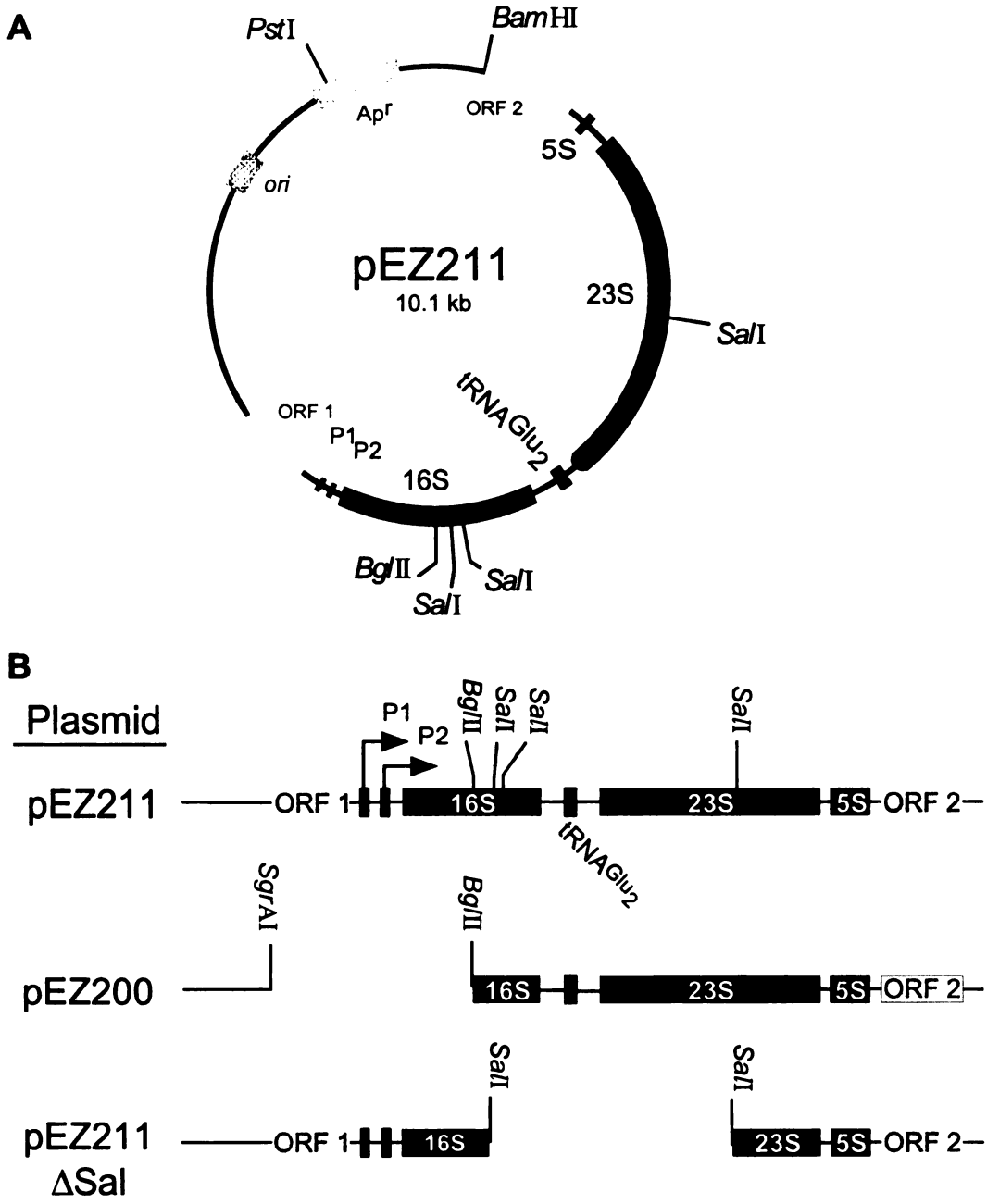

Figure 2.1 (A) Map of pEZ211 showing the 7.0 kb *rrn*B operon of *E. coli* cloned into pBR322 between the *Bam*HI and *Sgr*AI restriction sites. (B) Linearized representation of *rrnB* insert in pEZ211, removal of *rrn* promoters P1 and P2 in pEZ200, and internal deletion in pEZ211ΔSal.

Growth rates for each transformant were determined by measuring the change in optical density ($O.D._{600}$) as a function of time. Growth rate experiments were initiated by inoculating 5 ml of Luria broth (LB) (67) from culture stocks preserved at -80°C. Following overnight incubation at 37°C, triplicate conditioning cultures were inoculated (1:100) in 5 ml test medium. The test media consisted of modified Davis minimal medium (DM) (56) or LB. DM and LB were both amended with 200 μg/ml ampicillin when used to grow transformants. DM was further amended with either 1 mg/ml sodium acetate (Ac), sodium acetate plus 40 μg/ml each of 10 essential L-amino acids (Sigma Chemical Co., St. Louis, MO) (Ac-AA), 1 mg/ml glucose (Glc), or glucose plus amino acids (Glc-AA). LB was amended with 1 mg/ml glucose (LB-Glc). Aliquots (0.5 ml) of the conditioning cultures in mid-exponential growth phase were used to inoculate triplicate 50 ml cultures of specific test medium. All liquid cultures were aerated via vigorous shaking (≥200 rpm) at 37°C. To determine if differences in growth rates were correlated with the accumulation of RNA, concentrations of RNA were determined by a scaled-down orcinol assay (20) for at least three replicate cultures of the host strain and transformants carrying either pEZ200 or pEZ211 grown in each test medium. Since RNA concentrations are proportionate to growth rate (11), comparisons of RNA concentrations were made after normalizing the data to specific growth rate.

2.3 Results

Effects attributed to carriage of the pEZ plasmid backbone and promoter-less rRNA operon were assessed by comparing the growth of pEZ200 transformants with the host strain. There was no consistent difference between the growth rates of transformants carrying the control plasmid pEZ200 and the

host strain ($\bar{x}$ = 96%; Table 2.1). Similarly, the presence of pEZ200 had little effect on the concentration of RNA relative to the host strain on any medium ($\bar{x}$ = 95%; Table 2.2).

Table 2.1 Specific growth rates (μ) of the host strain and transformants carrying pEZ200 or pEZ211, grown in different media

Medium	Specific growth rate (μ)[a]			Relative growth rate[b]	
	host strain	pEZ200	pEZ211	pEZ200/ host strain	pEZ211/ pEZ200
Acetate	0.41 (0.01)	0.35 (0.02)	0.23 (0.01)	**85**	**66**
Acetate-AA	0.66 (0.01)	0.67 (0.04)	0.45 (0.00)	**102**	**67**
Glucose	1.09 (0.01)	0.99 (0.05)	0.66 (0.04)	**91**	**67**
Glucose-AA	1.19 (0.02)	1.15 (0.05)	0.98 (0.07)	**97**	**85**
LB-Glucose	1.60 (0.01)	1.71 (0.18)	1.45 (0.31)	**107**	**85**

[a] values are the sample mean of at least three replicate cultures, sample standard deviations are in parentheses.

[b] Relative growth rate is the ratio of specific growth rates depicted as % (i.e. multiplied by 100); slow growth values are grouped by dark shading, fast growth values are grouped by light shading.

Table 2.2 Concentration of RNA (fg/fl) of the host strain and transformants carrying pEZ200 or pEZ211, grown in different media.

	Concentration of RNA (fg/fl)[a]			Relative RNA conc. (normalized to μ)[b]	
Medium	host strain	pEZ200	pEZ211	pEZ200/ host strain	pEZ211/ pEZ200
Acetate	26.8 (2.1)	25.0 (1.7)	33.3 (3.9)	**109**	**202**
Acetate-AA	40.2 (4.9)	40.1 (3.4)	54.1 (8.7)	**98**	**201**
Glucose	56.2 (3.6)	44.8 (2.5)	74.0 (9.8)	**88**	**248**[c]
Glucose-AA	79.5 (8.1)	72.1 (5.8)	81.4 (5.8)	**94**	**132**
LB-Glucose	122.5 (2.8)	115.7 (5.6)	122.4 (3.4)	**88**	**125**

[a] values represent the sample mean of at least three replicate cultures, sample standard deviations are in parentheses; cell volumes (fl) of 5% formalin-fixed cells were determined using a Coulter Counter Channelizer (Coulter Electronics, Inc., Miami).

[b] ratio of normalized (divided by μ) RNA concentrations depicted as %; shading is as described in Table 2.1.

[c] normalized RNA concentration of transformants carrying pEZ211 was 218% that of the host strain, suggesting that the determination of RNA concentration for cells containing pEZ200 and growing on Glc, was anomolously low.

There was however, a dramatic effect on both growth rate and cellular RNA concentration when the rRNA promoters were present on the plasmid-borne rRNA operon (pEZ211). At slower growth rates (Ac, Ac-AA, and Glc), cells with pEZ211 grew an average of 33% slower than those with the control plasmid, pEZ200 (Table 2.1). Along with slower growth rates, extra rRNA operons resulted in normalized RNA concentrations, which were at least 100% higher than the control (Table 2.2). Transformants carrying pEZ211 not only had higher concentrations of RNA per unit volume (fg/fl), but also more RNA per cell (Figure 2.2).

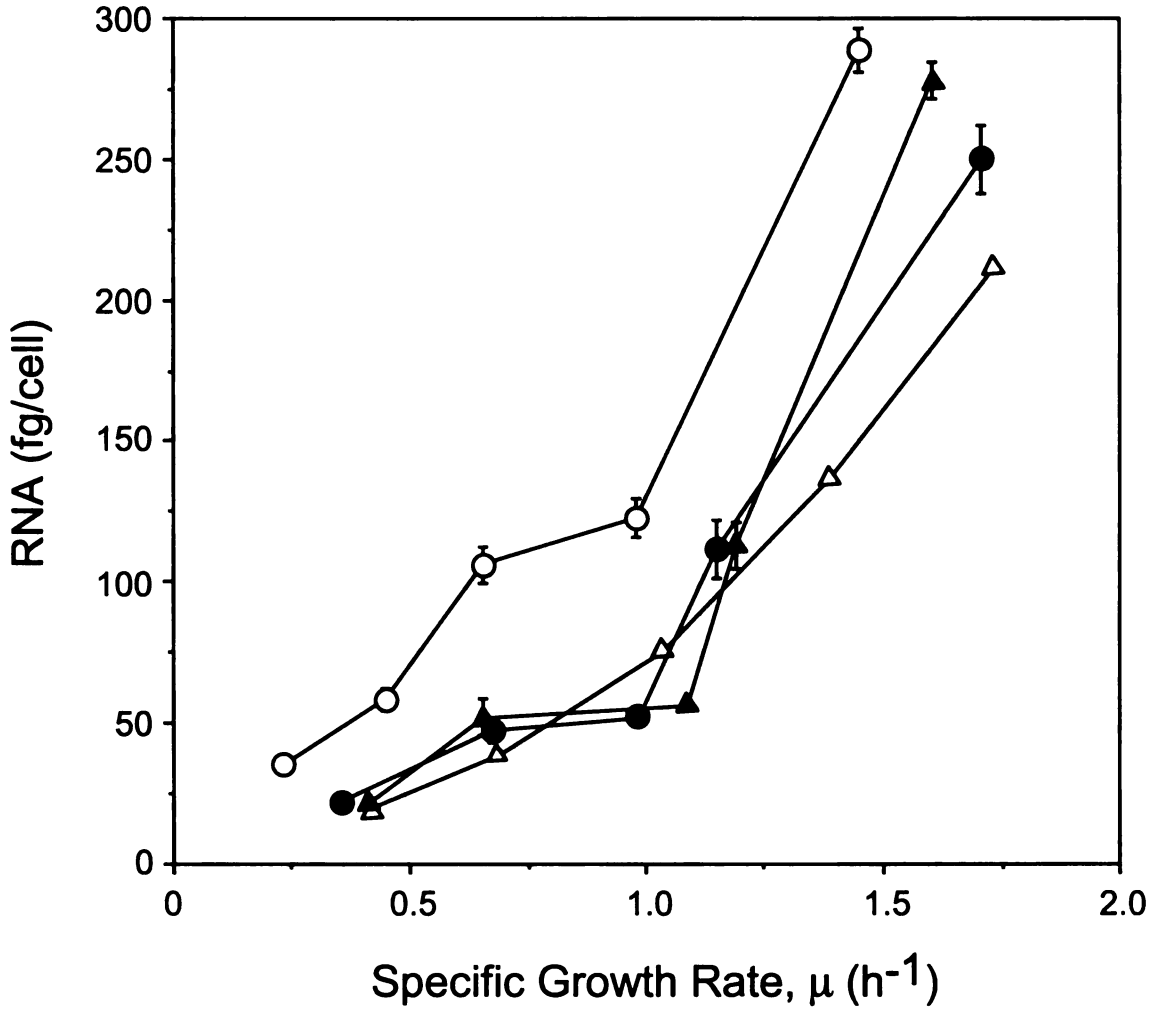

Figure 2.2 Cellular RNA content (fg/cell) as a function of growth rate, μ (h^{-1}) for the evolved host strain (▲), and transformants with pEZ200 (●) or pEZ211 (O) compared with previously published values for *E. coli* B (△; (11)). Error bars represent sample standard deviations.

The accumulation of RNA in slowly growing *E. coli* cells may be due to constitutive expression of the rRNA operons from the P2 rRNA promoter (9, 18). Since rRNA synthesis is linked to the expression of ribosomal proteins and other genes, the overproduction of rRNA would have the effect of diverting limiting resources to the production of unnecessary ribosomes, resulting in a decreased growth rate (32, 34, 41). The additional RNA in transformants carrying pEZ211 does not appear to be due to an increase in plasmid copy number because in comparable experiments with a slightly different host strain and rRNA operon-containing plasmid constructs, Baracchini and Bremer (8) reported a 41% decrease in growth rates and only slight differences in the plasmid copy number at various growth rates.

The effect of extra rRNA operons on both growth rate and cellular RNA concentration was diminished when cells were grown in media which led to faster growth rates (Glc-AA and LB-Glc). Transformants carrying pEZ211 grew 15% slower than those with pEZ200 (Table 2.1), and had an average of 29% more RNA per unit volume when normalized to specific growth rate (Table 2.2). The smaller difference between RNA concentrations of pEZ200 and pEZ211 transformants suggests a more effective means of compensation for the additional rRNA operons at higher growth rates. The mechanism of compensation is most likely transcriptional regulation of the operons (41).

Nomura and colleagues (41) made direct measurements of rRNA synthesis rates with similar plasmid constructs at faster growth rates and reported that cells were able to down regulate rRNA synthesis from all rRNA

operons within the cell as a result of feedback inhibition. The growth rate of these populations was reduced by 10%. This reduction was attributed to an imbalance in tRNA pools resulting from the increased expression of tRNAs located on the plasmid-borne operon. The rRNA synthesis rate in these cells was 19% higher than the control when normalized to growth rate (41), suggesting that modest RNA overproduction may have also contributed to the reduced growth rate.

A third plasmid (pEZ211ΔSal) was used to investigate the possibility that the observed changes in growth rate were due to the sequestration of RNA polymerase by the numerous promoters of the rRNA operons. The non-functional rRNA operon of pEZ211ΔSal was developed by digesting pEZ211 with *Sal*I which resulted in the deletion of a majority of the structural RNA genes (Figure 2.1B). There was no consistent deviation in the doubling times of cells expressing non-functional rRNA (pEZ211ΔSal transformants) relative to the control (Table 2.3) suggesting that the presence of the promoters alone is not sufficient to explain the changes in growth rate. Cells carrying pEZ211ΔSal were elongated, frequently occurred in chains, and tended to form aggregates at slower growth rates. Although the altered cell morphology had no obvious affect on growth rate estimation, cell enumeration was ineffective via particle counting or direct microscopy. As a result, the concentration of RNA could not be determined for cells with pEZ211ΔSal.

Table 2.3 Specific growth rate (μ) for pEZ211ΔSal transformants in different media.

	Specific growth rate (μ)[a]	Relative growth rate[b]
Medium	pEZ211ΔSal	pEZ211ΔSal/ pEZ200
Acetate	0.38 (0.04)	**108**
Acetate-AA	0.60 (0.05)	**88**
Glucose	0.82 (0.03)	**83**
Glucose-AA	1.14 (0.18)	**99**
LB-Glucose	1.62 (0.15)	**95**

[a,b] see Table 2.1, footnotes [a] and [b]

2.4 Conclusions

The presence of extra rRNA operons in a population of *E. coli* resulted in overproduction of RNA and decreased growth rates. These effects were exaggerated at slower growth rates, suggesting that regulation of rRNA synthesis was overwhelmed at slow growth rates. The metabolic expense associated with ribosome overproduction when nutrient availability is low may be compensated for by the capacity to rapidly shift up growth rate in response to an influx of nutrients. The potential advantage of a rapid shift in growth rate may seldom be realized in stable, low nutrient environments where the diversion of limited resources towards the production of excess ribosomes would clearly be disadvantageous. Understanding the advantages and disadvantages of multiple rRNA operons in different environmental conditions should provide insight into the selective pressures that influence rRNA copy number.

CHAPTER 3

REMOVAL OF RIBOSOMAL RNA OPERONS FROM THE *ESCHERICHIA COLI* CHROMOSOME

3.1 Introduction

The *Escherichia coli* chromosome has seven ribosomal RNA (rRNA) operons (45). The rRNA operons are located on the half of the chromosome closest to the origin of replication, which can further increase the number of rRNA operon copies in rapidly growing cells containing multiple replication forks (Figure 3.1, (7, 22)). Transcription of the rRNA operons is in the same direction as DNA replication, reducing the conflict between these two processes on the same region of the chromosome (11). All of the rRNA operons in *E. coli* (*rrnA, B, C, D, E, G,* and *H*) contain upstream activation sequences, strong tandem promoters, structural RNA genes (16S, 23S, and 5S), and some tRNA genes (Figure 3.2A, reviewed in (32)).

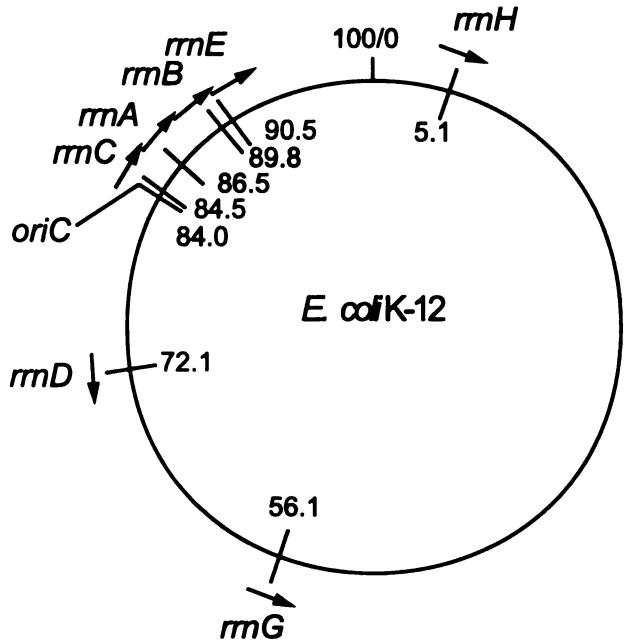

Figure 3.1 Location (in min) of the seven rRNA operons (*rrn*) and the origin of replication (*oriC*) on the *E. coli* K-12 chromosome (22). Arrows indicate the direction of rRNA operon transcription.

A

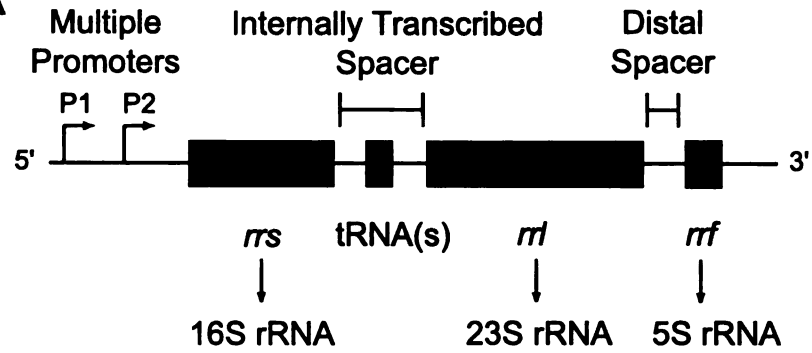

B

rrn Operon	ITS tRNA(s)	Distal tRNA(s)
B, E, G	Glu_2	-
C	Glu_2	Asp_1, Trp
A	Ile_1, Ala_{1B}	-
D	Ile_1, Ala_{1B}	Thr_1
H	Ile_1, Ala_{1B}	Asp_1

Figure 3.2 The (A) general organization (19), and (B) tRNA genes of the seven *E. coli* rRNA operons (61,62).

Sequence composition and organization of the seven rRNA operons is very similar yet, some differences do exist (7). Each rRNA operon has either the $tRNA^{Glu}_2$ gene (*rrnB, C, E,* and *G*), or the $tRNA^{Ile}_1$ and $tRNA^{Ala}_{1B}$ genes (*rrnA, D,* and *H*) in the internally transcribed spacer region (ITS) between the 16S and 23S genes, and a few also contain distally located tRNA genes (Figure 3.2B). The similarity between the rRNA operons on the same chromosome creates potential sites for homologous recombination, which could explain the maintenance of the highly conserved regions of each operon via gene conversion, and could also play a major role in genomic rearrangements (reviewed in (40)). The subtle sequence differences among the rRNA operons could also lead to differential expression of the operons or functional differences of their products (18).

Previous studies of rRNA operons and their function have been based on chromosomally located rRNA operons inactivated by either the insertion of marker genes (16-18), or deletion of part or all of an rRNA operon (3, 6, 23). These constructions are unsuitable for directly determining the specific effects of rRNA operon deletion because they result in the expression of additional marker genes, synthesis of truncated transcripts from intact rRNA promoters, or the deletion of adjacent genes. In contrast, the rRNA operon deletions reported here were designed to enable the direct determination of the ecological and physiological effects of rRNA operon copy number in *E. coli*. These deletions removed the majority of two *E. coli* rRNA operons (*rrnA* and *rrnB*) including their promoters, resulting in transcriptionally "silent" deletions.

3.2 Materials and Methods

Bacterial strains, plasmids, and phage

All bacterial strains and all plasmids and phage used or created in this study are listed in Tables 3.1 and 3.2. These tables list the names, relevant genotype or phenotypes, and the source for each entry. The rRNA operons were deleted from two isogenic strains of *E. coli* (REL 4548, and BS 4548) that come from the same line, which has evolved for 10,000 generations in glucose minimal medium batch cultures (56). The two strains differ only by a single point mutation, which is neutral and renders BS 4548 capable of utilizing the sugar arabinose (Ara^+), while the parental strain REL 4548 cannot (Ara^-). Both strains represent a well-studied line of *E. coli* with a stable genetic background.

Table 3.1 Bacterial strains

Strains	Relevant genotype or phenotype	Source
TOP10	Lac-, *recA, endA1*	Invitrogen, chemically competent cells
REL 4548	Ara$^-$	R.E. Lenski (56)
BS 4548	Ara$^+$	spontaneous Ara$^+$ mutant of REL 4548
D308	*recD*$^-$	F.W. Dahlquist (66)
DBS 222	*rrnB*$^-$, Suc^s, Kan^r	D308 linear transformant of pRB222, UpB:sacB-neo:DnB fragment
DAS 113	*rrnA*$^-$, Suc^s, Kan^r	D308 linear transformant of pRA113, UpA:sacB-neo:DnA fragment
BS 211	Ara$^+$, *rrnB*$^-$, Suc^s, Kan^r	P1 transduction of BS 4548 with DBS 222 lysate
BS 210	Ara$^-$, *rrnB*$^-$, Suc^s, Kan^r	P1 transduction of REL 4548 with DBS 222 lysate
BS 111	Ara$^+$, *rrnA*$^-$, Suc^s, Kan^r	P1 transduction of BS 4548 with DAS 113 lysate
BS 110	Ara$^-$, *rrnA*$^-$, Suc^s, Kan^r	P1 transduction of REL 4548 with DAS 113 lysate
BS 311	Ara$^+$, *rrnA*$^-$, Δ*rrnB*, Suc^s, Kan^r	P1 transduction of BS 111 with DAS 113 lysate
BS 310	Ara$^-$, *rrnA*$^-$, Δ*rrnB*, Suc^s, Kan^r	P1 transduction of BS 110 with DAS 113 lysate
BS 201 (Δ*rrnB*)	Ara$^+$, Δ*rrnB*	allelic exchange of UpB:sacB-neo:DnB in BS 211 with UpB:DnB from pKTS203
BS 200 (Δ*rrnB*)	Ara$^-$, Δ*rrnB*	allelic exchange of UpB:sacB-neo:DnB in BS 210 with UpB:DnB from pKTS203
BS 101 (Δ*rrnA*)	Ara$^+$, Δ*rrnA*	allelic exchange of UpA:sacB-neo:DnA in BS 111 with UpA:DnA from pKTS102
BS 100 (Δ*rrnA*)	Ara$^-$, Δ*rrnA*	allelic exchange of UpA:sacB-neo:DnA in BS 110 with UpA:DnA from pKTS102
BS 301 (Δ*rrnAB*)	Ara$^+$, Δ*rrnA*, Δ*rrnB*	allelic exchange of UpA:sacB-neo:DnA in BS 311 with UpA:DnA from pKTS102
BS 300 (Δ*rrnAB*)	Ara$^-$, Δ*rrnA*, Δ*rrnB*	allelic exchange of UpA:sacB-neo:DnA in REBS 310 with UpA:DnA from pKTS102

Table 3.2 Plasmids and Phage

Plasmids	Relevant genotype or phenotype	Source
pUC19	Amp^r, *lacZ'*	Pharmacia
pBR322	Amp^r, Tet^r,	Pharmacia
pCR 2.1-TOPO	Amp^r, Kan^r	Invitrogen
pKK3535	Amp^r, *rrnB* operon	J. Brosius
pC1	Amp^r, *rrnA* operon	C.L. Squires (18)
pIB279	Amp^r, *sacB-neo* cassette	I.C. Blomfield (10)
pMAK705	Cam^r, *rep^{ts}*, *lacZ*	C.M. Hamilton (36)
pUPB1	Amp^r, UpB	upstream-*rrnB* (UpB) fragment (*Nde*I and *Bam*HI, 817bp) cloned into pUC19
pUBD4	Amp^r, UpB:DnB	downstream-*rrnB* (DnB) fragment (*Bam*HI and *Xba*I, 991bp) cloned into pUPB1
pRB222	Amp^r, UpB:*sacB-neo* cassette:DnB	sacB-neo cassette (*Bam*HI, 3,825 bp) from pIB279 cloned into pUBD4
pKTS203	Cam^r, *rep^{ts}*, UpB:DnB	UpB:DnB fragment from pCR-UBD (*Hin*dIII and *Xba*I) cloned into pMAK705
pCR-UBD	Amp^r, Kan^r, UpB:DnB	Ligation of pCR 2.1-TOPO with UpB:DnB fragment (from pUBD4 plasmid DNA)
pCR-UpA	Amp^r, Kan^r, UpA	Ligation of pCR 2.1-TOPO with upstream-*rrnA* (UpA) fragment (from REL 4548 genomic DNA)
pCR-DnA	Amp^r, Kan^r, DnA	Ligation of pCR 2.1-TOPO with downstream-*rrnA* (DnA) fragment (from pC1 plasmid DNA)
pUPA2	Amp^r, UpA	UpA fragment (*Nde*I and *Kpn*I, 1667bp) from pCR-UpA cloned into pUC19
pUAD11	Amp^r, UpA:DnA	DnA fragment (*Kpn*I and *Xba*I, 941 bp) from pCR-DnA cloned into pUPA2
pRA113	Amp^r, Kan^r, sucrose^s, UpA:*sacB:neo* cassette:DnA	sacB:neo cassette (*Bam*HI, 3,825 bp) cloned into *Kpn*I restriction site of pUAD11 via blunt-ended ligation
pCR-UAD	Amp^r, Kan^r, UpA:DnA	Ligation of pCR 2.1-TOPO with UpA:DnA fragment (from pUAD11)
pKTS102	Cam^r, *rep^{ts}*, UpA:DnA	UpA:DnA (*Xba*I, 2,609 bp) fragment from pCR-UAD cloned into pMAK705
Phage P1*vir*	Vir$^-$	L. Snyder (72)

Bacterial growth conditions, media

Liquid broth cultures were grown in 16 x 100 mm culture tubes, shaking at 225 rpm and 37°C unless otherwise specified. The liquid medium used was Luria-Bertani (LB) broth (67), sometimes containing one or more of the following antibiotics [Amp, ampicillin (100 mg/ml); Kan, kanamycin (50 mg/ml); or Cam, chloramphenicol (30 mg/ml)]. Solid agar medium most commonly used was LB with 1.5% (w/v) Bacto agar (Difco Laboratories; Detroit, MI) added. Antibiotics were present in the concentrations listed above when specified. The other solid agar medium used (LB_{Suc}) was LB agar lacking NaCl but containing 6% (w/v) sucrose. The soft agar medium used in the generalized transduction procedure below was LB containing 0.75% (w/v) Bacto agar.

General cloning procedures

Plasmid and genomic DNA were digested with restriction endonucleases according to manufacturer protocols (NEB; New England Biolabs Inc.; Beverly MA). DNA fragments with either blunt ends or cohesive ends were ligated using the Prime Efficiency blunt-ended DNA ligation kit (Eppendorf-5 Prime Inc.; Boulder, CO). Plasmid and genomic DNA were harvested from cells using the Wizard S/V Plasmid DNA Purification Kit (Promega Corp.; Madison, WI), and the Tissue DNA Purification Kit (Qiagen Inc.; Valencia, CA), respectively. When necessary, electrophoresis in agarose gels (0.6 – 1.0% agarose in 0.5x TBE) was used to isolate DNA fragments after restriction digestion. Once isolated, DNA fragments of the correct size were cut out of the agarose gel, and DNA was recovered using the Qiaex II DNA recovery kit (Qiagen Inc.).

DNA was transformed into either One Shot TOP10 chemically competent *E. coli* cells (Invitrogen; Calsbad, CA) according to manufacturer's protocols, or cells of other *E. coli* strains made chemically competent using a protocol found in the Transformer Site-Directed Mutagenesis Kit product protocol (PT1130-1; Clonetech Laboratories; Palo Alto, CA).

Generalized transduction was carried out with a virulent mutant of phage P1 (P1*vir*). The protocol used varied from most common ones (59, 64) in that the lysate was prepared on LB agar plates with a LB soft agar overlay (Appendix A) to obtain a higher titer (usually 10^9 to 10^{10} PFU/ml).

PCR and XL PCR amplification

DNA fragments under 4 kb were PCR amplified using Biolase DNA polymerase (ISC; Intermountain Scientific Corporation; Kaysville, UT) in the following reaction conditions [1x reaction buffer (ISC), 2 mM MgCl2, 2.5 mM each dNTP, ~200 ng template DNA, 7.5 µM each primer, 25 or 100 µl final reaction volume]. A Perkin Elmer GeneAmp PCR System 9600 thermal cycler (PE Biosystems; Norwalk, CT) was used for these reactions with the following temperature regime: 95°C for 3 min, 30 cycles of (94°C for 30 sec, 60°C for 30 sec, and 72°C for 45 sec), 72°C for 10 min, and hold at 4°C indefinitely. When potentially larger DNA fragments (>4 kb) were to be PCR amplified, the GeneAmp XL PCR kit (PE Biosystems) was used, which utilizes the proofreading *Tth* DNA polymerase. Reactions were set up according to the manufacturer's protocols except that total reaction volumes of 25 µl were sometimes used, and

colony material was occasionally used as the template. The temperature regime used was the same as above except that each cycle was kept at 72°C for 10 min.

Visualization of rRNA operons using southern hybridization

Southern hybridization was used to visualize rRNA operons of each strain of *E. coli* (Appendix B). Genomic DNA was digested with *Pvu*II, separated according to size via electrophoresis in agarose gels (0.6% agarose in 0.5x TBE buffer), and transferred to Magnacharge nylon transfer membranes (Micron Separations Inc.; Westborough, MA) using the VacuGene XL Vacuum Blotting System (Amersham Pharmacia Biotech; Piscataway, NJ). After cross-linking the DNA to the membrane with the Stratlinker UV Crosslinker (Stratagene; La Jolla, CA), a digoxigenen-dUTP labeled probe (DIG High Prime labeling and detection kit; Boehringer Mannheim Corporation (BMB); Indianapolis, IN) specific for a conserved region (positions 8-356) of the *E. coli* 16S rDNA gene, was hybridized to the immobilized fragments of genomic DNA containing an rRNA operon. After hybridization, the membrane was washed and hybridized probe was detected according to the manufacturer's protocol (BMB). Each rRNA operon was visualized by the hybridized probe and identified by its unique fragment size. Genomic DNA from cells that contained modified rRNA operons or rRNA operons replaced by marker alleles or deletions, either showed altered fragment sizes or no corresponding fragment.

Deletion of the *rrnB* operon

The first step in the procedure used for deleting the *rrnB* operon (outlined in Figure 3.3) from the genomes of REL 4548 (Ara^-) and BS 4548 (Ara^+) was to construct a marker allele for the *rrnB* operon. Two fragments of sequence (UpB and DnB, Figure 3.4) that flanked the *rrnB* operon were amplified from the REL 4548 genome using the UpB and DnB primers in Figure 3.5. The UpB fragment contained sequence only found at one site on the chromosome. The downstream (DnB) fragment included the 3' end of the *rrnB* operon, most of which was conserved among the other rRNA operons. The UpB fragment was cloned into pUC19 (pUPB1, Table 3.1), and then the DnB fragment was cloned into pUPB1 adjacent to UpB, to form pUBD4 (Figure 3.3). This plasmid was used in creating the marker allele and served as the source of the deletion allele (UpB and DnB) used in the final step of the *rrnB* deletion, discussed below.

A marker cassette containing both selectable and counter-selectable markers (*sacB:neo*) from pIB279 (10), was cloned in between UpB and DnB on pUBD4 creating the *rrnB*-specific marker allele UpB:*sacB:neo*:DnB on the plasmid pRB222 (Figure 3.3). The selectable marker gene (*neo*) encodes for resistance to neomycin and kanamycin, which was used as the selective agent. The counter-selectable marker gene (*sacB*) encodes for the exoenzyme levansucrase in *Bacillus subtilis* (30). Expression of this gene in *E. coli* and other Gram-negative prokaryotes is lethal when the cell is grown in the presence of sucrose (29).

Intermediate strains of REL 4548 and BS 4548 were then constructed (BS 210 and BS 211, respectively; Figure 3.3), in which the marker allele replaced the *rrnB* operon. First, a linear fragment of DNA containing the marker allele was used to transform strain D308, a *recD* mutant strain of *E. coli* (66). The resulting transformant (DBS 222) was kanamycin resistant (Kan^r) and sucrose sensitive (Suc^s) due to the marker allele that had replaced the wild type *rrnB* operon. Generalized transduction (59, 64) with phage P1 *vir* was then used to move the marker allele into both REL 4548 and BS 4548, creating the intermediate strains of each neutral marker type (Ara^- and Ara^+, respectively).

The plasmid pKTS203 was constructed by cloning the UpB:DnB deletion allele from pUBD4 into the temperature sensitive plasmid pMAK705 (36) (Figure 3.3). The intermediate strains were transformed with pKTS203 at the permissive temperature (30^oC). Transformant colonies were grown in LB_{KanCam} at the non-permissive temperature (44^oC), selecting for cells with the plasmid integrated into the chromosome at the marker allele via recombination between the homologous UpB or DnB sequences. Transferring these cultures to fresh LB without antibiotics at 44^oC selected for cells in which a second recombination event occurred, liberating the plasmid from the chromosome. If the second recombination event occurred between the region of homology opposite from where integration occurred (UpB or DnB), the deletion allele was exchanged with the marker allele, and the resulting free plasmid contained the marker allele (shown in Figure 3.3, (as discussed in 10, 36)). Suc^r cells were isolated on LB_{Suc} agar; these cells had exchanged the marker allele with the deletion allele on the

plasmid, subsequently lost the plasmid, and therefore contained no markers (Δ*rrnB* in Figure 3.3). Screening of these isolates for the Suc^r Kan^s Cam^s phenotype, XL PCR amplification of the deletion region, and southern hybridization of the remaining rRNA operons confirmed the deletion of the *rrnB* operon.

Figure 3.3 Steps used to delete the *rrnB* operon from the REL 4548 and BS 4548 genome, creating the BS 200 and BS 201 (Δ*rrnB*) strains .

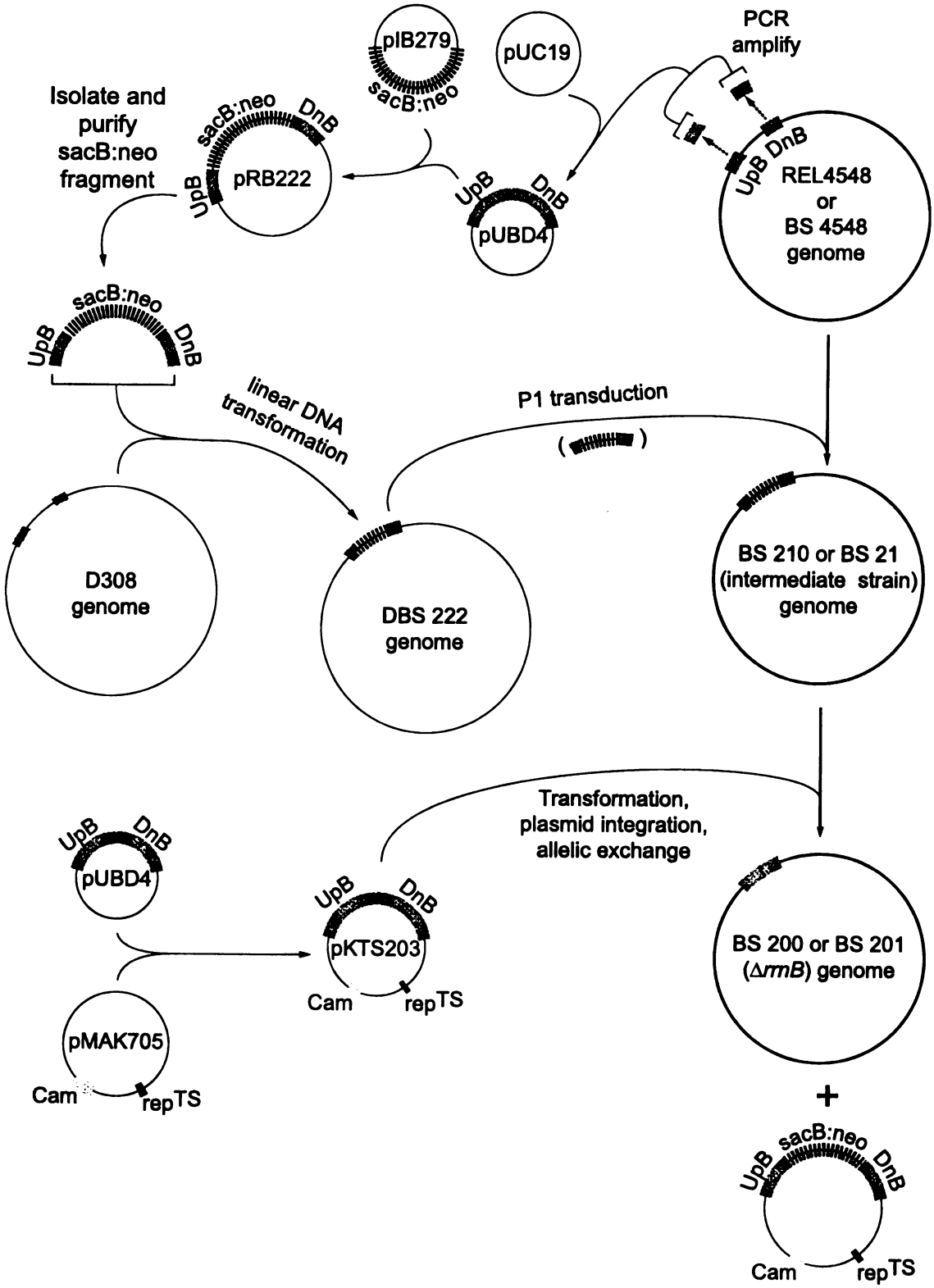
pIB279
sacB:neo
pUC19
PCR
amplify
Isolate and
purify
sacB:neo
fragment
sacB:neo
UpB
DnB
pRB222
UpB
DnB
pUBD4
UpB DnB
REL4548
or
BS 4548
genome
sacB:neo
UpB
DnB
linear DNA
transformation
P1 transduction
(
)
D308
genome
DBS 222
genome
BS 210 or BS 21
(intermediate strain)
genome
Transformation,
plasmid integration,
allelic exchange
UpB
DnB
pUBD4
UpB
DnB
pKTS203
Cam
repTS
BS 200 or BS 201
(ΔrmB) genome
pMAK705
Cam
repTS
+
UpB
sacB:neo
DnB
Cam
repTS

Figure 3.3

Deletion of the *rrnA* operon

The *rrnA* operon was deleted from the genome of REL 4548, BS 4548, and both Δ*rrnB* strains in the same manner in which the *rrnB* operon was deleted above. Regions upstream (UpA) and downstream (DnA) of the *rrnA* operon (Figure 3.4) were amplified using *rrnA*-specific primers (Figure 3.5), and cloned adjacent to one another on pUC19 to form pUAD11. A marker allele (UpA:sacB:neo:DnA) was constructed as above, on pRA113, and its linear DNA fragment was used to transform D308 *E. coli* cells. These transformants (DAS 113) served as the donor strain to transduce the marker allele into REL 4548, BS 4548, and both Δ*rrnB* strains, forming intermediate strains. The UpA:DnA deletion allele from pCR-UAD (Table 3.1) was cloned into the pMAK705 plasmid backbone, forming pKTS102. This plasmid was used to transform the intermediate strains at the permissive temperature ($30^{O}C$). After growth in LB with, and then without antibiotics at $44^{O}C$, cells that had exchanged the marker allele for the deletion allele and lost the resulting plasmid were isolated on LB_{Suc} agar. These cells were screened for the Suc^{r} Kan^{s} Cam^{s} phenotype, the *rrnA* and *rrnB* regions were amplified, the remaining rRNA operons were visualized through southern hybridization to confirm the rRNA operon deletions. The strains that contained the *rrnA* deletion were designated Δ*rrnA* and the strain with both the *rrnA* and *rrnB* deletions was designated Δ*rrnAB*.

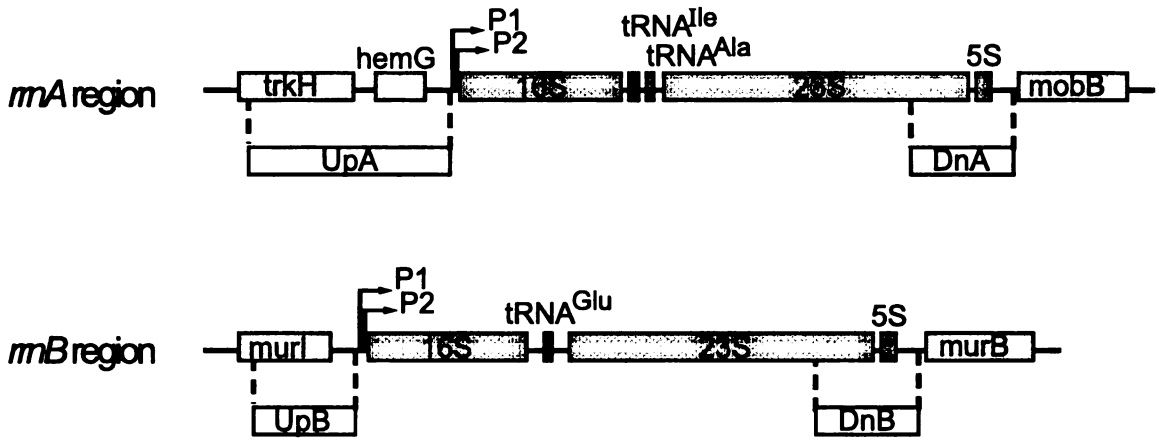

Figure 3.4 Regions of *E. coli* chromosome containing the *rrnA* and *rrnB* operons, showing the amplified flanking regions (UpA, DnA, UpB, and DnB; white boxes), structural rRNA genes (16S, 23S, and 5S;dark grey boxes), tRNA genes ($tRNA^{Ile}$, $tRNA^{Ala}$, and $tRNA^{Glu}$; dark grey boxes), and adjacent genes (*trkH, hemG, mobB, murI, murB*; light grey boxes) are shown.

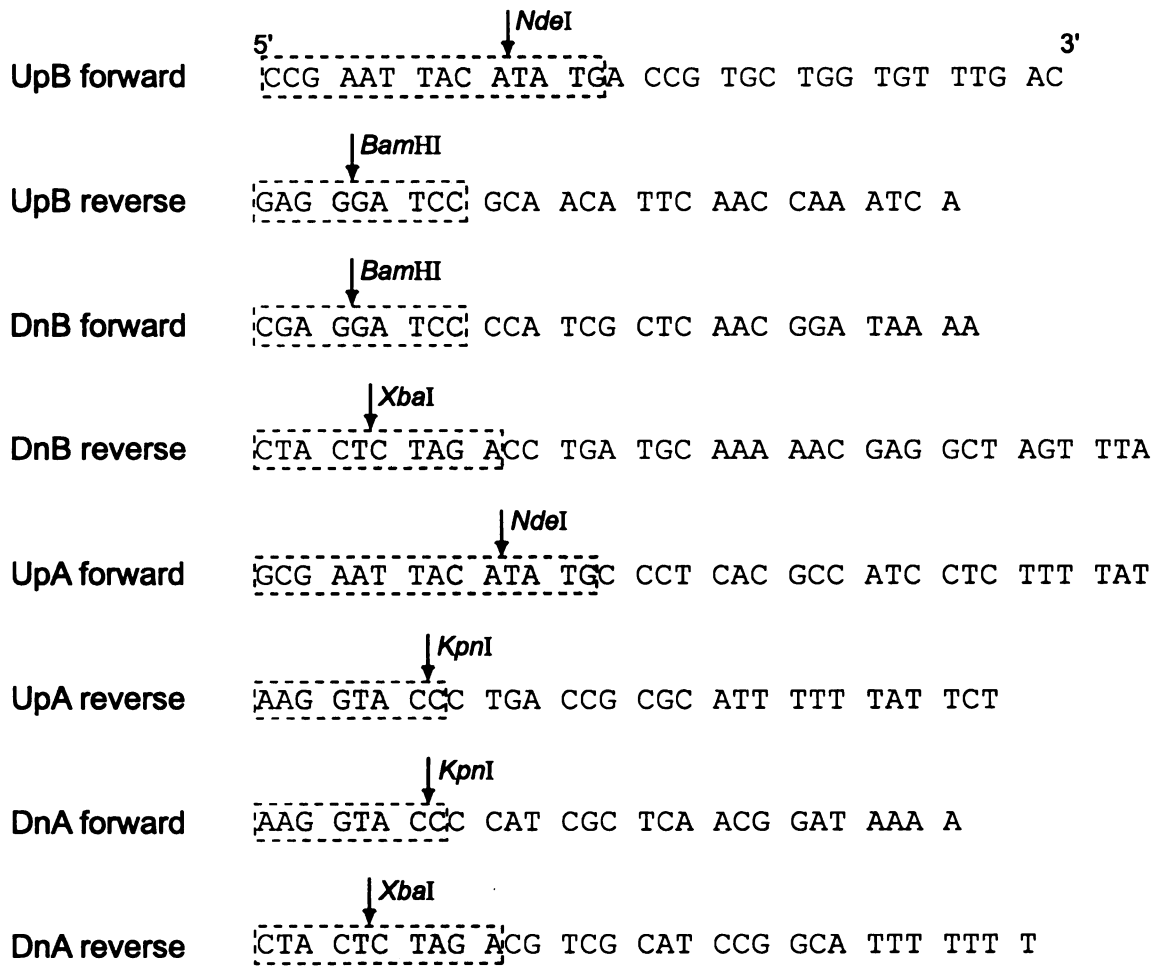

Figure 3.5 Oligonucleotide primers used throughout rRNA operon deletion procedure. The non-target specific tails at the 5' end of each primer are shown in boxes, the recognition sequences of restriction endonucleases are labeled and shown in the shaded area of each box, and the arrows indicate restriction sites.

3.3 Results

The deletion of the *rrnB* and *rrnA* operons outlined above, relied on the use of homologous sequence which flanked the regions being deleted (Figure 3.4). In the case of *rrnB*, the region upstream of the deletion (UpB) included the 3' end of the gene *murI* and all sequence directly upstream of the *rrnB* promoters P1 and P2. The region of homologous sequence upstream of *rrnA* (UpA) included most of the *trkH* gene from the 3' end, all of the *hemG* gene, and ended directly upstream of the *rrnA* P1 and P2 promoters. The DNA sequence in these upstream regions is found nowhere else on the chromosome. The downstream regions used for *rrnB* (DnB) and *rrnA* (DnA) included the 3' end of each 23S gene, the entire 5S gene, and ended just upstream of the *murB* gene in the case of *rrnB*, and upstream of the *mobB* gene in the *rrnA* deletion. The majority of the sequence in the downstream regions includes sequences from the 23S and 5S rRNA genes, which are conserved among all seven rRNA operons.

The majority of the *rrnB* and *rrnA* operons, including the promoter sequences were deleted. Upon deletion, the sequence remaining at the *rrnB* site included only the UpB and DnB regions adjacent to each other. The intervening sequence that was removed included the *rrnB* promoters P1 and P2, the entire 16S rRNA gene, the ITS region including the $tRNA^{Glu}_2$ gene, and the 5' end of the 23S gene. The deletion of *rrnB* from the chromosomes of both REL 4548 and BS 4548 (Ara^- and Ara^+, respectively) resulted in the strains designated as BS 200 and BS 201 (Δ*rrnB* for short). Southern hybridization showed that the genomic DNA from the Δ*rrnB* strain lacks the *rrnB*-specific fragment seen in the

control strain REL 4548 (Figure 3.6). The *rrnB* operon deletion was further verified by amplifying the *rrnB* region of the chromosome using genomic DNA from Δ*rrnB*, and the primers UpB forward and DnB reverse (Figure 3.5) in an XL PCR reaction. The size of the resulting fragment (1.9 kb, lanes 8-16, Figure 3.7) corresponded to the size of the deletion allele amplified from pUBD4 (lane7), and was easily distinguishable from the wild type *rrnB* operon (lane 5, 6.1 kb) or the marker allele (lane 6, 5.4 kb). By removing the *rrnB* promoters, no transcription of the remaining *rrnB* sequence should occur.

The deletion of *rrnA* from the chromosomes of REL 4548, BS 4548, and the Δ*rrnB* strains resulted the strains designated as BS 100 and BS 101 (Δ*rrnA* for short) and BS 300 and BS301 (Δ*rrnAB* for short). The sequence that was deleted from *rrnA* included the *rrnA* promoters P1 and P2, the entire 16S gene, the ITS region with the $tRNA^{Ile}_{1}$ and $tRNA^{Ala}_{1B}$ genes, and most of the 23S gene at the 5' end. Genomic DNA from Δ*rrnA* and Δ*rrnAB* lacks the *rrnA*-specific fragment in the southern hybridization (Figure 3.6). As with the Δ*rrnB* strains above, the deletion of *rrnA* was verified in Δ*rrnA* and Δ*rrnAB* by amplifying the *rrnA* region of the chromosome with the primers UpA forward and DnA reverse (Figure 3.5). The *rrnA* regions amplified from Δ*rrnA* (2.6 kb, lane 4, Figure 3.8) and Δ*rrnAB* (2.6 kb, lanes 5-9) genomic DNA are easily distinguished from the wild type *rrnA* operon (7.4 kb, lane 2) and the *rrnA*-specific marker allele (6.4 kb, lane 3). Also, the *rrnB* regions amplified from Δ*rrnAB* as above (1.9 kb, lanes 13-17) are easily distinguished as deletions compared to the wild type *rrnB* operon

(6.1 kb, lane 11). As with the deletion of *rrnB*, the *rrnA* deletions left no promoters or additional marker genes, and did not affect adjacent genes.

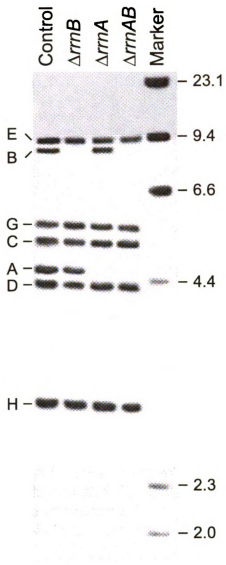

Figure 3.6 Southern hybridiztion of genomic DNA of each strain digested with *Pvu*II and hybridized with a 16S DIG-labelled probe. Hybridized bands corresponding to each of the seven rRNA operons in the control strain are labeled on the left. Sizes (kb) of each band of the λ *Hin*dIII DNA marker are labeled on the right.

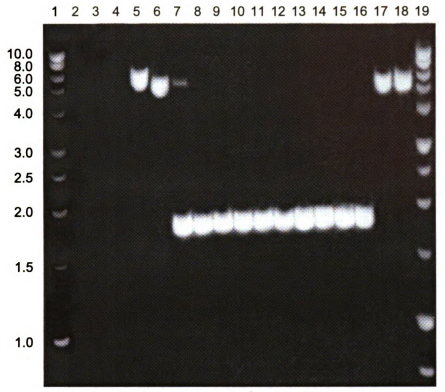

Figure 3.7 XL PCR amplification of the wild type *rrnB* operon (lane 5, 6.1 kb), *rrnB*-specific marker allele (lane6, 5.4 kb), plasmid-borne UpB:DnB deletion fragment (lane 7, 1.8 kb), and chromosomal *rrnB* deletions (lanes 9-16, 1.8 kb). Fragments sizes of a 1 kb DNA ladder in lanes 1 and 19 are marked to the left of lane 1.

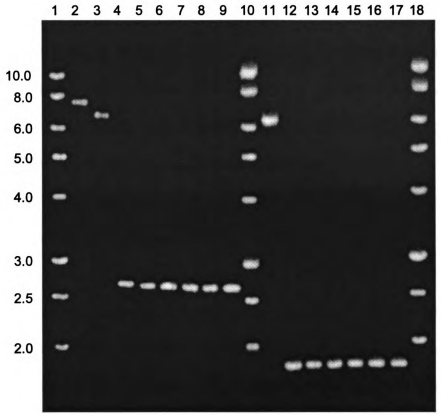

Figure 3.8 XL PCR amplification of wild type *rrnA* (lane 2) and *rrnB* (lane 11) operons, intermediate *rrnA*-specific marker allele (lane 3), *rrnA* deletion in BS 101 (lane 4), *rrnB* deletion from BS 201 (lane 12), and both *rrnA* and *rrnB* deletions from BS 301 strain isolates (lanes 5-9 and 13-17 respectively). Fragment sizes of a 1 kb DNA ladder (lanes 1, 10, and 18) are marked to the left of lane 1.

3.4 Discussion

Deletion of rRNA operons

This study outlines the genetic techniques needed for the deletion of rRNA operons. The difficulty in manipulating genes that are present in multiple copies on the same chromosome lies in the cell's ability to repair these genes through gene conversion. It was essential that regions of sequence were used, which unlike the rRNA operons were present in a single copy on the chromosome to ensure that recombination occurred with the target operon and not with any of the other rRNA operons.

Previous studies deleting rRNA operons have used inserted marker genes (3, 18), deleted only part of the rRNA operon leaving the rRNA promoters intact (3, 6, 18), or altered adjacent genes in the deletion process (23). The cells from these constructions express additional marker phenotypes, produce truncated rRNA transcripts from the still-active rRNA promoters, or have adjacent genes that are also altered, all which may have affects not specifically attributable to the deletion of rRNA operons. The rRNA operon deletions in this study do not involve the addition of marker genes, lack active promoters, and adjacent genes are not affected, making the resulting strains useful for directly determining the specific fitness or physiological effects of deleting rRNA operons from the chromosome.

Care was taken in choosing which rRNA operons were deleted to minimize the perturbation to the tRNA gene pool. *rrnA* and *rrnB* each represent one of the two groups of *E. coli* rRNA operons with respect to the tRNA genes

located in their ITS regions. The ITS regions of *rrnA, D,* and *H* operons have the $tRNA^{Ile}_1$ and $tRNA^{Ala}_{1B}$ genes, whereas the ITS regions of the *rrnB, C, E,* and *G* operons have the $tRNA^{Glu}_2$ gene. Unlike the *rrnC, D,* and *H* operons on the *E. coli* chromosome, neither *rrnA* nor *rrnB* has tRNA genes located distal to the operon. The *rrnA* and *rrnB* operons are also located close to each other on the chromosome, which should reduce the difference in gene dosage when the cell is dividing faster than DNA replication and has multiple copies of the chromosome within the cell (11).

The procedure used to delete the *rrnB* and *rrnA* operons was complex but precise, with strong selection provided for each step. An essential step in the deletion of each rRNA operon was the construction of an intermediate strain in which a marker allele has replaced the wild type rRNA operon that is to be deleted. To get the marker allele to replace the target rRNA operon on the chromosome, a *recD* strain of *E. coli* (D308) was transformed with linear DNA (66). Linear DNA transformants were selected for the Suc^s and Kan^r phenotypes. These cells had the wild type rRNA operon replaced by the marker allele through recombination with the homologous sequence flanking the marker genes. The upstream homologous sequence allowed for rRNA-specific recombination and prevented the cell from repairing the mutation with one of the other rRNA operons (discussed below). The region of sequence used upstream of the rRNA operon promoters was not part of the operon and therefore was unique to that location on the chromosome. Generalized transduction with phage P1 *vir* was used to move the marker allele from the chromosome of transformed

recD cells into a strain of *E. coli* that has evolved in glucose minimal medium for 10,000 generations (56), thereby producing intermediate strains. The potential limitation caused by the P1 transduction of DNA from the *recD* cells (derived from *E. coli* strain K-12, (66)) into the evolved strains of *E. coli* (derived from *E. coli* strain B, (51, 56)) is discussed below.

The intermediate strains were transformed with a temperature sensitive plasmid containing the deletion allele, which consisted of the rRNA operon-specific upstream and downstream regions. Growing these transformants at non-permissive temperatures with, and then without antibiotics promoted an exchange of the deletion allele with the marker allele between the plasmid and the chromosome. The counter-selectable marker *sacB* simplified the isolation of cells that had undergone an allelic exchange and lost the resulting plasmid, therefore containing a deleted rRNA operon and no markers. It was possible however, to find cells that apparently had a mutation in the *sacB* gene and were able to grow on LB_{Suc} agar. Further screening for Kan^S allowed for the identification of cells that had indeed undergone the allelic exchange among those that still had the marker allele (Kan^r) but could somehow grow on LB_{Suc} agar. The use of markers that provide strong selection along with the temperature sensitive plasmid was essential in facilitating the allelic exchange between the marker allele and the deletion fragment.

Conclusion

Further studies of the strains with Δ*rrnB*, Δ*rrnA*, and Δ*rrnAB* have shown that these deletions are stable for many generations. These strains have differences in several growth parameters as will be discussed in another chapter, but overall they are robust and grow well under all tested conditions. This alone is evidence that neither *rrnB*, *rrnA*, nor *rrnB* and *A* together are essential for the growth of *E. coli*.

3.5 Lessons learned during construction of rRNA deletion strains

Generalized transduction between strains of *E. coli*

Generalized transduction was used to move the marker alleles from the constructed *recD*⁻ strains to the intermediate strains. The *recD* strains were derived from an *E. coli* K-12 strain (66), whereas the REL 4548 and BS 4548 strains and their derivatives are from an *E. coli* B strain (51, 56). Furthermore, the REL 4548 and BS 4548 strains have been evolved for 10,000 generations under specific conditions (56). These two different strains of *E. coli* are relatively closely related within one subgroup of *E. coli* strains based on a study of sequence divergence of 20 enzyme-encoding loci (38). There are some known regions of sequence differences between their genomes as well as in their restriction modification systems (71). When phage P1 is used in transduction, between 91 and 100 kb of donor DNA typically enters the recipient cell (64). Only one known region of intraspecific sequence divergence (the *phn* operon) is located anywhere near 100 kb upstream or downstream of the *rrnA* and *rrnB*

operons. Based on the location of the known regions of high intraspecific sequence divergence, the region of the chromosome that contains the *rrnC, A, B* and *E* operons appears to be well conserved among different strains of *E. coli* (58).

The fact that genomic DNA from *E. coli* K-12 was used to transduce this evolved line of *E. coli* B raises the question as to what other donor DNA could have been incorporated into the recipient B strain of *E. coli* along with the rRNA operon marker alleles. The effect of incorporating this additional donor DNA on the ecological and physiological properties measured in these rRNA operon deletion strains must be considered. In order fully to address this question, a control strain must be "reconstructed" from the same intermediate strains that were used to delete the rRNA operons. Transforming these intermediate strains with a temperature sensitive plasmid that contains the full rRNA operon and isolating those cells that have replaced the marker allele with the full operon could accomplish this. Only these reconstructed controls can be considered to be otherwise isogenic to the rRNA operon deletion strains, and are currently under construction.

Gene conversion

Gene conversion apparently took place in an earlier attempt to delete *rrnB*, where a marker allele was constructed by inserting the *sacB* and *neo* marker genes into the 16S rDNA gene of a cloned *rrnB* operon. The resulting construction had the marker genes flanked by 16S rDNA sequence (704 bp

upstream and 837 bp downstream) that were conserved among all the other rRNA operons. A temperature sensitive plasmid carrying the marker allele was used to promote an exchange of the marker allele with the wild type *rrnB* operon. Once the marker allele was present on the chromosome, any of the other six rRNA operons were available to repair this mutation through a non-reciprocal recombination event. The occurrence of this event was only caught by virtue of which rRNA operon was used to repair the mutation. If *rrnG*, *E*, or *C* were used, the repaired operon did not appear any different from the wild type *rrnB* operon when visualized by southern hybridization (Figure 3.8). If however, the repair of the marker *rrnB* allele was facilitated by recombination with *rrnA*, *D*, or *H*, the repaired operon resulted in a band that was a different size and did not correspond with the size of either the wild type *rrnB* operon or the *rrnB* marker allele.

The difference in size of these repaired operons appeared because they were hybrids with regards to their ITS region. An extra *Pvu*II restriction site in the ITS regions of *rrnA, D, and H* resulted in a fragment of unique size. The hybrid fragments were smaller than they would be if they had been repaired back to *rrnB*-like sequence through recombination with *rrnG*, *E*, or *C*, but larger than the marker allele (Figure 3.9). This self-repair phenomenon illustrates the importance of flanking homologous sequence in permitting gene conversion among the rRNA operons.

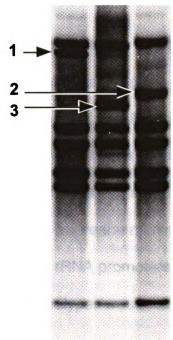

Figure 3.9 Southern hybridization of a repaired chromosomal *rrnB* operon. Hybridized DNA fragments that correspond with the wild type *rrnB* operon (1), the marker *rrnB* allele (2), and the hybrid *rrnB* operon (3) are labeled with arrows.

Marker gene orientation

Another lesson that was learned in earlier attempts to delete the *rrnB* operon is that the orientation of a marker gene has a great impact on the marker phenotype when it is downstream of the rRNA promoters. When marker genes were inserted into the 16S gene of a cloned *rrnB* operon (discussed above), markers were only weakly expressed if their orientation was opposite of rRNA transcription. In constructions where the markers were in the same orientation of the rRNA operon, or when the rRNA promoters P1 and P2 were not present, expression of the marker phenotypes was robust (data not shown).

Temperature sensitive plasmid

The temperature sensitive replication of the plasmid used for allelic exchange between the marker allele and the rRNA deletion fragment enabled the selection of cells that had integrated the plasmid into the chromosome, but it was still possible to isolate cells that contained free plasmid. The temperature sensitivity of the plasmid pMAK705 and its derivatives was therefore not absolute when grown at non-permissive temperatures. This plasmid was still a good vehicle for allelic exchange when the proper selectable and counter-selectable markers were used, as noted by Blomfield et al (10).

CHAPTER 4

EFFECT OF DELETING RIBOSOMAL RNA OPERONS FROM THE *ESCHERICHIA COLI* CHROMOSOME

4.1 Introduction

The research in this chapter investigates the potential connection between the number of rRNA operons on the *Escherichia coli* chromosome and its life history. As discussed in Chapter 1, the number of rRNA operons on the chromosome of a prokaryotic species may be an adaptation to the environmental conditions in which that species has evolved, and a component of the life history of that species.

The first hypothesis that was tested states that multiple rRNA operons are an advantage in environments defined by fluctuations in nutrient availability. Cells with a higher number of rRNA operons could have a higher capacity for de novo ribosome synthesis upon an influx of nutrients, or excess protein synthesizing capacity prior to an influx of nutrients. The rate-limiting step in the production of ribosomes is the synthesis of rRNA, which is controlled at the level of transcription. Furthermore, the rRNAs are the end product of the rRNA genes. Multiple rRNA operons are an obvious way for a cell to increase rRNA synthesizing capacity.

The second hypothesis that was tested represents the potential tradeoff for having multiple rRNA operons, stating that fewer rRNA operons are an advantage in environments defined by the stable and limiting availability of

nutrients. *E. coli* cells growing very slowly ($\mu \leq 0.2\ h^{-1}$) contain excess ribosomes believed to be the result of constitutive expression of the seven rRNA operons (47). If the number of excess ribosomes were proportional to the number of rRNA operons, then cells with fewer rRNA operons would be expected to have fewer excess ribosomes. The expression of excess rRNA would represent a metabolic expense to cells in stable, slow growth conditions. If the expression of excess rRNA resulted in excess ribosomes, the metabolic expense would be compounded by the cost of synthesizing the rest of the protein synthesizing machinery, which is regulated with the transcription of rRNA. The diversion of limited resources towards the production of excess ribosomes would be a disadvantage to a cell if that cell did not encounter the influx in nutrients needed to utilize the higher protein synthesizing capacity.

Previous work attempting to study the relationship between rRNA operon copy number and cell physiology was based upon strains of *E. coli* with altered numbers of rRNA operons. The rRNA operon copy number was altered in these strains through the addition of plasmid-borne operons ((33, 74), Chapter 2) or by the inactivation (18) or deletion (3, 5, 23) of operons on the chromosome. The studies using plasmid-borne rRNA operons were limited by unknown or varying plasmid copy number and could only add rRNA operons to the genome of the cells. The previous constructions, in which rRNA operons on the chromosome were either inactivated or deleted, were also unsuitable for the experiments outlined in this study. It was not possible to discern the effect of rRNA operon manipulations in these previous constructions from the effects of deleting

adjacent genes (23), the expression of truncated rRNA transcripts from intact rRNA promoters (3, 5), or the additional expression of marker genes (18). New strains in which the rRNA operons *rrnA* and *rrnB* were each or both deleted were constructed with these requirements in mind (as discussed in Chapter 3) and used in the experiments described below. The deletions included the rRNA promoters and a large portion of the operon, but not adjacent genes on the chromosome. These rRNA operon deletion strains were designed to be more suitable than the previous rRNA operon deletions in determining the direct effect of rRNA operon deletion on physiological traits and competitive ability of *E. coli*.

To test the hypotheses discussed above, strains of *E. coli* containing either 6 or 5 rRNA operons (Δ*rrnA*, Δ*rrnB*, or Δ*rrnAB*) were used in mixed culture competition experiments with a wild type control (7 rRNA operons). These culture conditions resulted in direct competition for a shared nutrient with fluctuating or constant availability, and gave a direct measurement of the competitive ability of each strain relative to the control. To determine which growth parameters contributed to any measurable difference in competitive ability, the parameters lag time, maximal growth rate, K_S, and death rate were individually measured for each strain in batch monocultures. Additionally, cell yield and cell volume were measured to better understand what physiological traits might be impacted by the deletion of rRNA operons.

4.2 Materials and Methods

Bacterial strains

The bacterial strains used in this study are thoroughly described in Chapter 3. All strains come from the same line of *E. coli* that has evolved for 10,000 generations under batch culture conditions in glucose minimal medium (56). These strains are isogenic except for any rRNA deletion and a neutral point mutation rendering reciprocal strains able to utilize the sugar arabinose (Ara^+), where as the parental line cannot (Ara^-). The Ara^- and Ara^+ strains form red and white colonies, respectively, when grown on tetrazolium arabinose indicator agar (TA), enabling the identification and enumeration of colonies from each population in mixed cultures during direct competition experiments (57).

Strains with the *rrnA*, *rrnB*, and both *rrnA* and *B* operons deleted are designated as Δ*rrnA*, Δ*rrnB*, and Δ*rrnAB*, respectively. Deleting the same rRNA operons from strains of each marker type (Ara^+ and Ara^-) allowed for reciprocal competition experiments. The promoters and all but the end of the 23S gene and the 5S gene were deleted from the targeted rRNA operon on the chromosome (described in Chapter 3).

Media and culture conditions

Luria Bertani (LB) broth (67) was used when growing cells from glycerol stocks stored at –80°C. These cultures were grown in 3 ml volumes, sterile 16 x 100 mm culture tubes, and incubated at 37°C, shaking at 225 rpm overnight. The liquid medium used for all growth and competition experiments was Davis

Minimal broth (DM) (15) supplemented with 2.0 mg/L thiamine hydrochloride. Glucose was added (0.1, 25, or 1000 mg/L) as the limited nutrient. The specific concentrations of glucose used are indicated with each experiment below (e.g. DM+1000 refers to 1000 mg/L glucose). The solid agar medium used was either LB agar (LB broth with 1.5% [wt/vol] agar added) or tetrazolium arabinose (TA) indicator agar (57).

Batch cultures were grown in 10 or 50 ml volumes in 50 or 250 ml Erlenmeyer flasks, respectively, incubated at 37°C, and shaking at 225 rpm for complete aeration. For all experiments, cultures were first grown in LB from –80°C glycerol stocks, and then used to inoculate a DM conditioning culture with a specific concentration of glucose and incubated for exactly 24 hours, shaking at 37°C. The inoculum for the conditioning culture was approximately 1:100 of the population density achieved at the specific glucose concentration. This conditioning culture was then used to inoculate (1:100) fresh DM medium for the experiment performed.

Chemostat cultures were inoculated with conditioning batch cultures and grown in 65 ml volumes in 8 parallel 3 x 20 cm glass vessels that were enclosed with a #8 rubber stopper and submersed in a 37°C water bath (Figure 4.1). The chemostat vessels received medium and air through a thin glass tube that ran through the top of the vessel and down to 1 cm above the bottom. The sterile medium (DM+25) was delivered from up to 4 parallel reservoirs (10 liters each) to the inflow tube by a variable speed peristaltic pump. Air was also pulled in through the inflow tube and a 0.45 μm HEPA filter, providing ample aeration and

mixing. A second glass tube that was connected to a vacuum, entered through the top of the vessel and extended approximately halfway to the bottom of the vessel. This outflow tube removed culture medium and cells, maintained the volume of the culture, and provided the negative pressure that pulled in the air for aeration and mixing. A sampling port was located on the side of the vessel and above the level of the culture. This port was fitted with a rubber septum and was used to aseptically inoculate and sample the chemostat vessel. Sterile, 5 ml syringes fitted with 5/8 inch, 23 gauge needles were used to inoculate the vessels, and sterile 1 ml syringes fitted with sterile, 9 inch, 23 gauge, stainless steel, non-coring needles were used to sample the cultures.

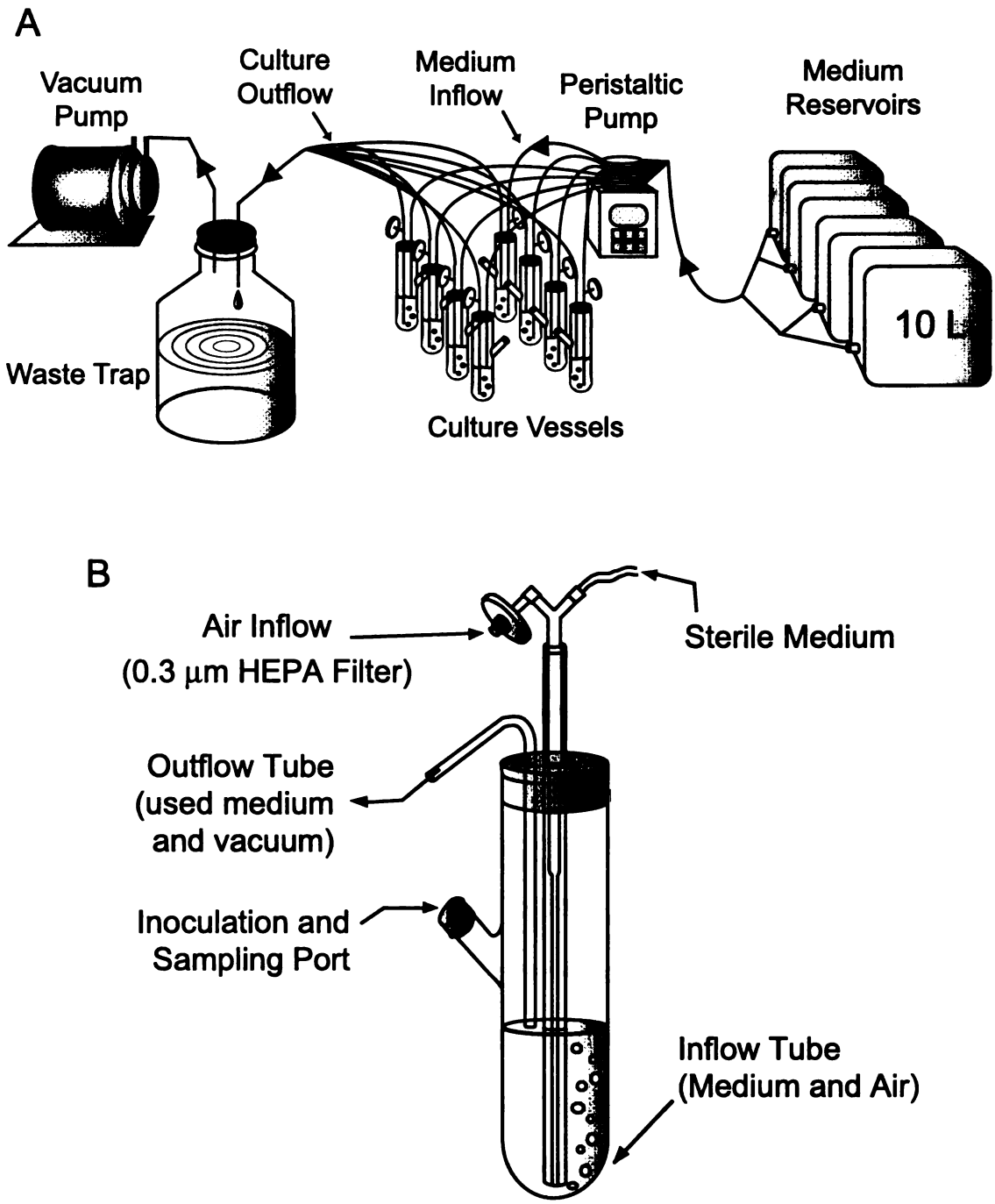

Figure 4.1 (A) Diagram of chemostat culture system. (B) Sideview of individual chemostat culture vessel.

Measurement of specific growth parameters

Lag time

The amount of time (h) required for a culture to enter exponential growth after a 1:100 inoculation with stationary phase cells was estimated and referred to as lag time. The cultures were treated identically to those in batch culture competition experiments (described below), and all inoculations and samplings of cultures were staggered by 15 min intervals to insure precise timing. Each conditioning culture was used to inoculate 10 ml of fresh DM+25 medium. Immediately after inoculation and mixing (time, t = 0 hours), a sample of each culture (approx. 3.5×10^5 CFU/ml) was diluted and an aliquot was spread onto 4 replicate LB agar plates. The cultures were incubated for exactly 4 hours (t = 4), and another sample of each culture was taken, serially diluted, and an aliquot was spread onto 4 replicate LB agar plates. The time point of 4 h represented a convenient time to sample each culture during mid-exponential growth. The agar plates were incubated overnight and the CFU/ml of culture was determined.

The duration of lag time for each culture was estimated similarly as described in (55). Exponential growth was extrapolated from the population density at t = 4, back in time until the extrapolated CFU/ml intersected the initial CFU/ml at t = 0 h that was actually measured. The point of intersection represents the elapsed time (lag) after inoculation, before the culture reached exponential growth, assuming the initiation of exponential growth was instantaneous. The lag time for each strain (control, Δ*rrnA*, Δ*rrnB*, and Δ*rrnAB*) was represented as the mean of 4 cultures (2 Ara^+ and 2 Ara^- cultures).

Maximal growth rate

The maximal growth rate (μ_{MAX}) of each strain in DM+1000 medium, and under the batch culture conditions described above, was estimated by calculating the slope of the linear regression of natural log-transformed population density values ($O.D._{600}$) versus time during exponential growth. The concentration of 1000 mg/L glucose in DM+1000 was used to achieve cultures with sufficient optical densities for accurate measurement with a Lambda 3 UV-Vis spectrophotometer (PE Applied Biosystems). Cultures with larger volumes (50 ml) than the competition experiments were also used to enable the many samplings needed for spectrophotometric measurement and minimize the impact upon the entire culture volume.

K_S

The parameter K_S represents the concentration of a growth-limiting substrate at which a culture grows at half the maximal specific growth rate. This parameter is a component of the Monod equation, which represents the relationship between specific growth rate (μ) and substrate concentration (S) as follows;

$$\mu = S \bullet \mu_{MAX}/(S + K_S).$$

The K_S for each strain was calculated using the estimated specific growth rate (μ) of each strain growing on DM+0.1; a concentration of glucose (0.1 mg/L) very near K_S for the control strain (76). The glucose concentration (S), the

specific growth rate (μ), and μ_{MAX} (determined as described above) were used in the above equation rearranged to solve for K_S as follows;

$$K_S = S\,[(\mu_{MAX}/\mu) - 1].$$

K_S estimates were calculated for three replicate cultures of each strain.

As described above, LB cultures were inoculated from –80°C glycerol stocks for each strain and incubated overnight at 37°C, shaking at 225 rpm. The final population density obtainable on DM+0.1 was much lower than the final population density of the LB overnight cultures. The LB overnight cultures were therefore serially diluted 1:10^4 before they were used to inoculate the 50 ml of DM+0.1 medium used for the conditioning cultures. Aliquots of the conditioning culture were transferred to fresh DM+0.1 medium. Dilutions of the freshly inoculated test cultures were spread onto triplicate LB agar plates for enumeration at time points equaling 0, 2, and then every hour up to 12 hours after inoculation. The mean CFU/ml values for each culture were Ln-transformed and plotted versus time. The specific growth rate of each culture was estimated as the mean slope of these linear regressions, and used with glucose concentration and μ_{MAX} to calculate K_S as described above.

Death rate

The death rate of each strain during stationary phase was estimated as the rate of decrease in population density between 12 and 24 hours. This measurement was modeled after those in (76). Triplicate 10 ml DM+25 medium flasks were inoculated (1:100) from conditioning cultures as described above,

and dilutions of each culture were spread onto triplicate LB agar plates every hour after inoculation between 12 and 24 hours. The mean CFU/ml for each culture at each timepoint was Ln-transformed and plotted versus time. The regression was assumed to be linear, and the inverse slope was reported as death rate (i.e. a positive death rate represented a decrease in population density). Monitoring of the change in CFU/ml of each strain was continued up to 197 hours after inoculation.

Measurement of other physiological traits

Cell yield

The cell yield that is reported was measured as the number of cells produced per μg of glucose in chemostat monocultures (equilibrium population density), and assumes that the utilization of glucose in each culture is equal. This was measured for each strain by determining the equilibrium population density (cells/ml) in two independent chemostat monocultures at slow (0.11 h^{-1}) and fast (0.56 h^{-1}) dilution rates, and dividing by the concentration of glucose in the medium (25 μg/ml). Population density was determined for 4 aliquots of each culture by direct enumeration of the fixed cells using a Coulter Counter particle analyzer (Beckman Coulter, Inc., Fullerton, CA), and subtracting "background" particles measured in a sample of sterile medium.

Cell volume

The mean cell volume (fl) of each strain was also measured using the same samples used to determine cell yield, and the Coulter Counter particle analyzer (Beckman Coulter Electronics).

Batch culture competition experiments

The relative fitness of each strain was measured in mixed batch culture competition experiments with the control strain (as described in 54). Each competing strain with opposite marker type (Ara^+ and Ara^-) was grown from stocks and conditioned for 24 hours in DM+25 (described above). The conditioning cultures of each competitor were used to inoculate four replicate culture flasks containing 10 ml DM+25 with each population at 1:200, for an initial population ratio of 1:1. Each mixed culture was then sampled at time (t) = 0 h and 24 h, where an aliquot of each culture was diluted when necessary and spread onto TA agar to enumerate each population. Also after 24 h, a 100 μl aliquot of each culture was transferred to fresh DM+25 medium. Again after 24 h, these competition cultures were sampled to enumerate each population and used to inoculate fresh medium. Each competition culture was transferred to fresh DM+25 at least 4 times. During each period of competition, the cultures underwent lag phase, exponential growth, and at least 10 hours of stationary phase before an aliquot was used to inoculate fresh DM+25 to repeat the growth phase cycle (about 6.6 doublings).

The relative fitness of each strain was calculated as the number of population doublings relative to the control. The initial densities of the Ara^+ and Ara^- competitors, can be represented as $N_1(0)$ and $N_2(0)$, respectively; where $N_1(1)$ and $N_2(1)$ refer to their corresponding densities after 24 hours. The average rate of increase, or Malthusian parameter (m), for each competitor during each 24-hour interval (1 d) was estimated as;

$$m_1 = \ln [N_1(1)/N_1(0)]/(1\ d),$$

where m_1 has units of d^{-1}, and the mean of these estimates was used for each strain. The fitness of one strain relative to another, $W_{1:2}$, was estimated as the ratio of the number of doublings of the two competitors, which is identical to the ratio of their Malthusian parameters (52);

$$W_{1:2} = m_1/m_2.$$

All statistical inferences about relative fitness values were based on at least 4 independent replicate estimates of relative fitness for the same strain.

Chemostat culture competition experiments

Relative fitness was also measured for each strain based upon population dynamics in mixed chemostat competition cultures with the control strain. At equilibrium, the ratio of population densities will not change if the competing populations have the same competitive ability. The ratio of population densities however, will change over time in favor of any population with a higher competitive ability than the other competing population. The difference in

competitive ability of one population relative to the other (relative fitness) is represented by the rate at which the ratio of population densities changes.

The entire chemostat system (8 parallel culture vessels, medium (DM+25) reservoirs, and all tubing) was assembled, clamped, and autoclaved as a closed system. After autoclaving, the culture vessels were placed in a water bath, the tubing was attached to the peristaltic pump, and the vacuum pump and waste trap were connected to the outflow tubes (Figure 4.1). The peristaltic and vacuum pumps were then turned on to fill the culture vessels. Once filled to the level of the outflow tube and at a constant temperature of 37°C, each culture vessel was inoculated (1:200) with conditioning cultures of each competing population of opposite marker (Ara^+ and Ara^-). This inoculation was performed by first mixing the populations in a 5 ml syringe and injecting the inoculum into the culture vessel through the sampling port.

Upon inoculation, the peristaltic pump was stopped for 6 – 12 hours until the cultures had reached early stationary phase in the culture vessels. At that point, the peristaltic pump was turned on at the desired rate and the culture was sampled (t = 0). A dilution of these samples was spread onto triplicate TA agar plates to enumerate each competing population. The chemostat cultures were assumed to have reached equilibrium when the total population density did not change significantly for at least 3 volume changes. The competition cultures were sampled periodically (based upon flow rate) to monitor changes in the ratio of population densities.

Calculation of chemostat-specific growth parameters

Using the growth parameters K_S and μ_{MAX}, the *J* parameter of each strain was calculated for the slow (0.11 h^{-1}) and fast (0.81 h^{-1}) dilution rates used in the mixed culture chemostat competition experiments. Bacterial populations present in chemostats at equilibrium grow at the same rate as the dilution rate (*D*) and reduce the concentration of nutrients to the lowest amount needed to grow at that rate. According to chemostat theory, this nutrient concentration (*J*) can be determined using the equation:

$$J = K_S\,(D/r),$$

where $r = (\mu_{MAX} - D) > 0$, the intrinsic rate of increase of a particular species (37). For a population to exist in a chemostat at equilibrium its maximal specific growth rate must be faster than the dilution rate ($D < \mu_{MAX}$) and the input concentration of the limiting nutrient (S_0) must be greater than *J* ($S_0 > J$). Also according to theory, the population with the lowest *J* parameter will competitively exclude all other species with higher *J* values. The *J* values for each strain at both dilution rates were used to predict the outcome of the mixed chemostat culture competition experiments.

4.3 Results

Specific growth parameters

The mean values of lag time, maximal growth rate, and K_S for each strain are given in Table 4.1. A set of planned comparisons was used to calculate which differences between the mean values for each strain were statistically

significant (73) (same comparisons as in Appendix C). The effect on lag time and maximal growth rate was directly correlated with the number of rRNA operons in each strain. Compared to the control, the mean lag time estimates of both Δ*rrnA* and Δ*rrnB* were about 4% (2.4 min) longer than the control, whereas the lag time of the Δ*rrnAB* strains was about 20% (12 min) longer. Wild type *E. coli* cells are therefore about 1/3 of a doubling ahead of cells with only 5 rRNA operons inoculated at the same time, in the same medium, and under batch culture conditions. Maximal growth rates of the rRNA deletion strains were slightly slower than the control, and also correlated with the number of deleted rRNA operons. Opposed to lag times and maximal growth rates, the differences in K_S values for each strain were not correlated with the number of deleted rRNA operons. The Δ*rrnB* strain showed a slightly lower K_S than the control, but the K_S of both the Δ*rrnA* and Δ*rrnAB* strains increased significantly (29.7 and 26.2%, respectively) relative to the control.

Table 4.1 Growth parameters measured for each strain[a]

Strain	Lag (h)[b]	μ_{MAX} (h^{-1})[c]	K_S (μg/ml)[d]
Control	1.43 ± 0.039	1.03 ± 0.011	0.118 ± 0.0035
Δ*rrnB*	1.48 ± 0.091	1.00 ± 0.012	0.111 ± 0.0025
Δ*rrnA*	1.48 ± 0.076	1.00 ± 0.016	0.153 ± 0.0047
Δ*rrnAB*	1.71 ± 0.070	0.99 ± 0.014	0.149 ± 0.0116

[a] values are means of at least three measurements ± standard errors of the measurements

[b] planned comparisons show that only Δ*rrnAB* mean is significantly different from the control ($F_{1,28} = 7.37$, $P < 0.05$) and both Δ*rrnA* and Δ*rrnB* ($F_{1,28} = 6.54$, $P < 0.05$)

[c] planned comparisons show that Δ*rrnB* and Δ*rrnA* means are significantly different from the control ($F_{1,44} = 3.09$, $P < 0.10$), and Δ*rrnAB* mean is significantly different from the control ($F_{1,44} = 4.84$, $P < 0.05$) but not Δ*rrnA* and Δ*rrnB*.

[d] planned comparisons show that Δ*rrnA* and Δ*rrnAB* means are not different from each other but are significantly different from Δ*rrnB* ($F_{1,3} = 20.12$, $P < 0.05$) and the control ($F_{1,3} = 11.50$, $P < 0.05$), which are also not different from each other

There was no appreciable death rate measured for any of the strains between 12 and 24 hours after inoculation (Figure 4.2). The population densities of these cultures did not change significantly [paired *t* test ($P_3 > 0.05$)] until after 48 hours, when the number of viable cells dropped rapidly (data not shown). There was also no discernable difference between the strains in their long-term survival under these conditions.

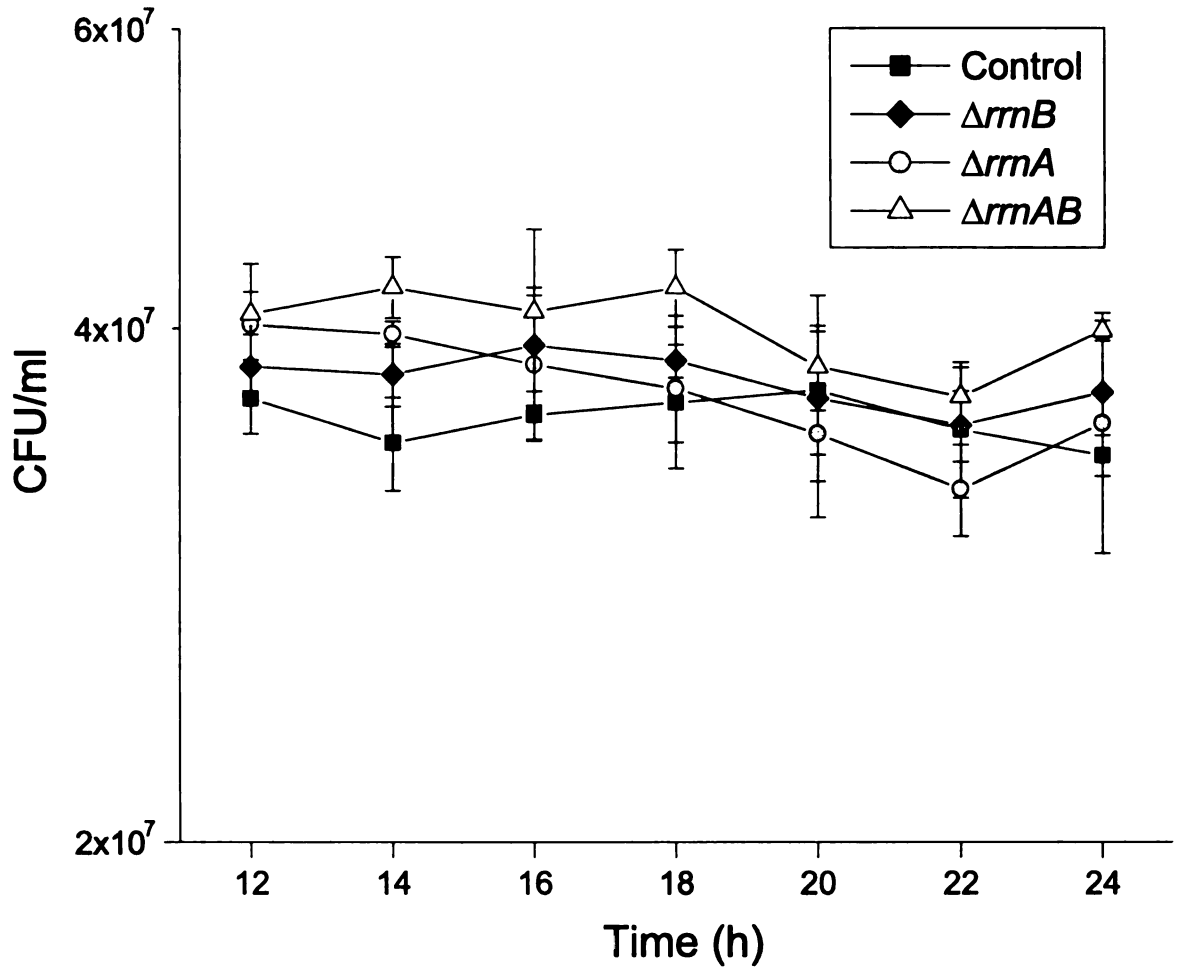

Figure 4.2 The death rate is shown as the change in population density (CFU/ml) of each strain in batch monocultures from 12 to 24 hours.

Measured physiological traits

Cell yield

The mean cell yield of each strain is shown in Figure 4.3A. These data seems to coincide with the K_S data in that strains with a deleted *rrnA* operon are affected to a larger extent than strains with the *rrnB* deletion. In slow dilution rate chemostat cultures (0.11 h^{-1}) the cell yield of Δ*rrnB* is similar to the control strain, whereas the cell yield of Δ*rrnA* and Δ*rrnAB* are 39% and 42% lower ($F_{1,3}$ = 910.25, $P < 0.05$), respectively. In faster dilution rate chemostat cultures (0.56 h^{-1}), no significant difference was measured between the cell yield of all strains based on planned comparisons.

Cell volume

The mean cell volume of each strain during slow (0.11 h^{-1}) and fast (0.56 h^{-1}) dilution rate chemostat conditions is shown in Figure 4.3B. These data suggests an inverse relationship to cell yield in slow chemostat conditions because the mean cell volume of both Δ*rrnA* and Δ*rrnAB* cells is larger than the control and Δ*rrnB*. Based on planned comparisons, the only significant difference between mean cell volumes was between Δ*rrnAB* and the control under fast chemostat conditions ($F_{1,3}$ = 10.83, $P < 0.05$).

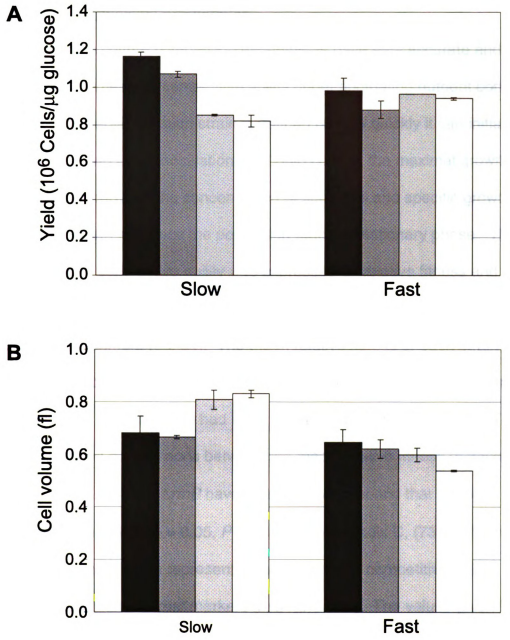

Figure 4.3 (A) Cell yield (10^6 cells/μg glucose), and (B) cell volume (fl) for the control (black), Δ*rrnB* (dark grey), Δ*rrnA* (light grey), and Δ*rrnAB* (white) strains are shown for chemostat monocultures at slow (0.11 h^{-1}) and fast (0.56 h^{-1}) dilution rates. Error bars represent the standard error of the measurements of two independent cultures.

Batch culture competition experiments

The batch culture competition experiments gave very accurate and precise measurements of competitive ability under fluctuating nutrient conditions. The competitive ability of each strain is defined by how quickly it can initiate exponential growth upon inoculation into liquid culture, the maximal growth rate, the relationship between the concentration of substrate and specific growth rate (K_S), and the death rate once the population reaches stationary phase. The measurement of competitive ability was expressed as relative fitness and refers to the increase in population density relative to a competing population in a direct competition experiment (53, 54). The mean relative fitness of each strain was directly related to the number of rRNA operons in that strain, in that the strains with fewer rRNA operons were had lower a relative fitness (Figure 4.4). The results of planned comparisons between the mean relative fitness of each strain show that only Δ*rrnA* and Δ*rrnB* have relative fitness means that are not significantly different ($F_{1,24} = 0.05$, $P > 0.10$; see Appendix C, (73)). The value given for the control strain represents the difference in competitive ability between strains with different markers (Ara^+ and Ara^-). The values given for each of the deletion strains is the mean of relative fitness values for strains of both marker types.

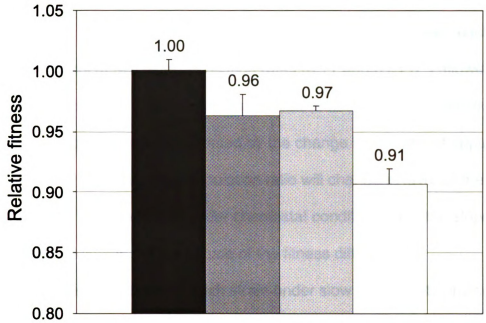

Figure 4.4 Relative fitness values for the control (black), Δ*rrnB* (dark grey), Δ*rrnA* (light grey), and Δ*rrnAB* (white) strains in batch culture competition experiments with the control strain. The value for the control represents the relative fitness of the Ara^+ versus the Ara^- control strain. Error bars represent standard errors of the measurements.

Chemostat competition experiments

Mixed culture chemostat competition experiments between each strain and the control at two different dilution rates (0.11 and 0.81 h^{-1}) allowed for the direct measurement of relative fitness. Relative fitness under equilibrium chemostat conditions is represented by the change in the ratio of population densities per doubling. The population ratio will change in favor of the population with a higher relative fitness under chemostat conditions, and the slope of this regression indicates the magnitude of the fitness difference.

The relative fitness of each strain under slow chemostat conditions is shown as the ratio (vs. the control strain) of the population densities versus the number of doublings in Figure 4.5. The data shown for the control strain represents the relative fitness for the Ara^+ control strain in competition experiments with the Ara^- control strain. The stability of the population ratio in the control strain competition experiments illustrates the neutrality of the marker phenotype. The competitive ability of Δ*rrnB* is also very much the same as that shown for the control strain. The Δ*rrnA* and Δ*rrnAB* strains, however, have a much lower competitive ability in the slow chemostat relative to the control strain. The relative fitness of Δ*rrnB* (Figure 4.6) and Δ*rrnA* (Figure 4.7) was also measured in chemostats with faster dilution rates (0.81 h^{-1}). The relative fitness of Δ*rrnB* at faster dilution rates was not discernable from that in chemostats with slower dilution rates. Δ*rrnA* still had a negative relative fitness at fast dilution rates, but it had a higher relative fitness than at slow dilution rates.

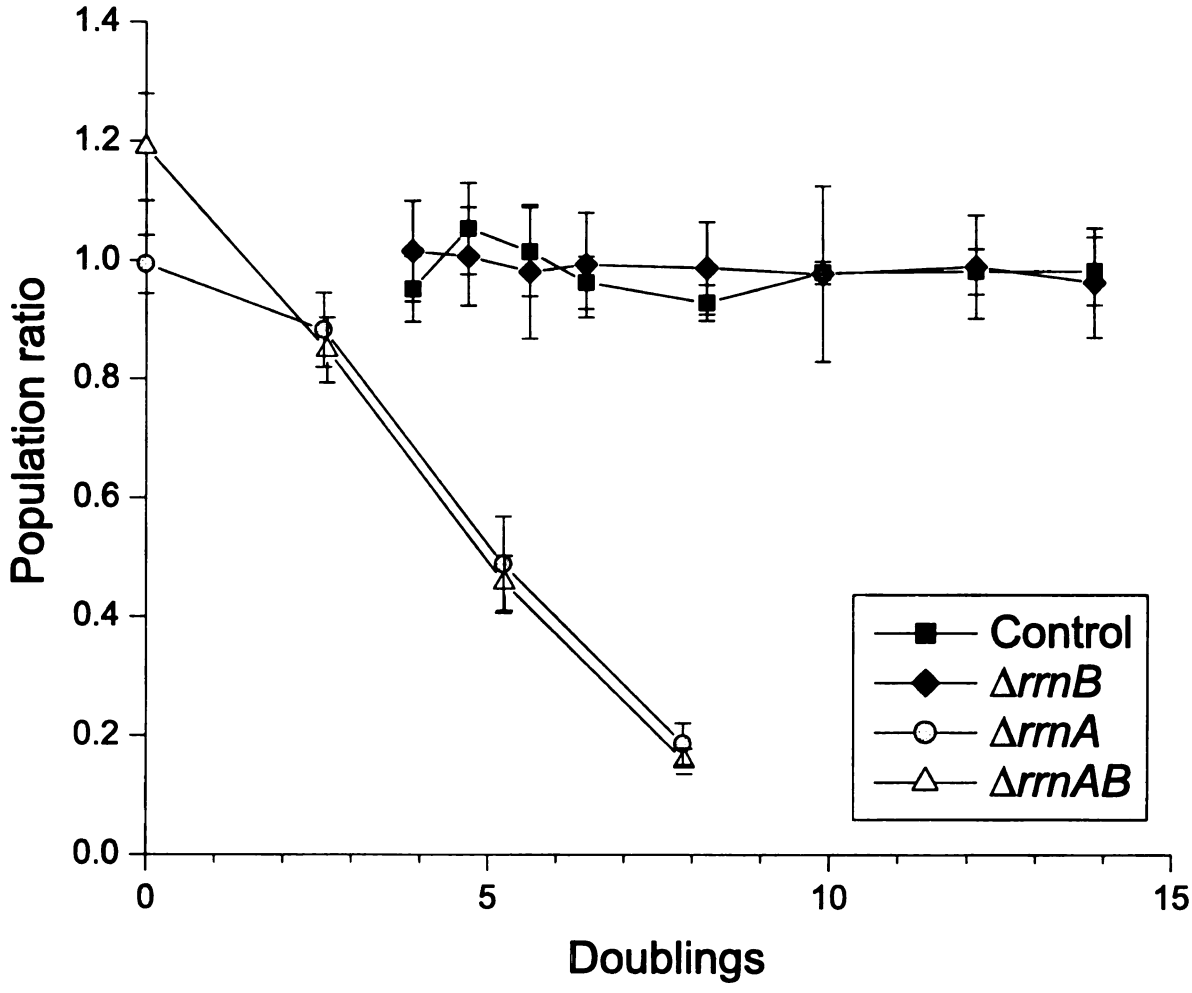

Figure 4.5 Relative fitness of each rRNA deletion strain in chemostat competition experiments with slow dilution rates (0.11 h^{-1}) is represented as the population ratio (vs. control) versus the number of population doublings. The data for the control represents the fitness of the Ara^+ strain relative to the Ara^- strain. Error bars represent the standard error of four independent cultures for each strain.

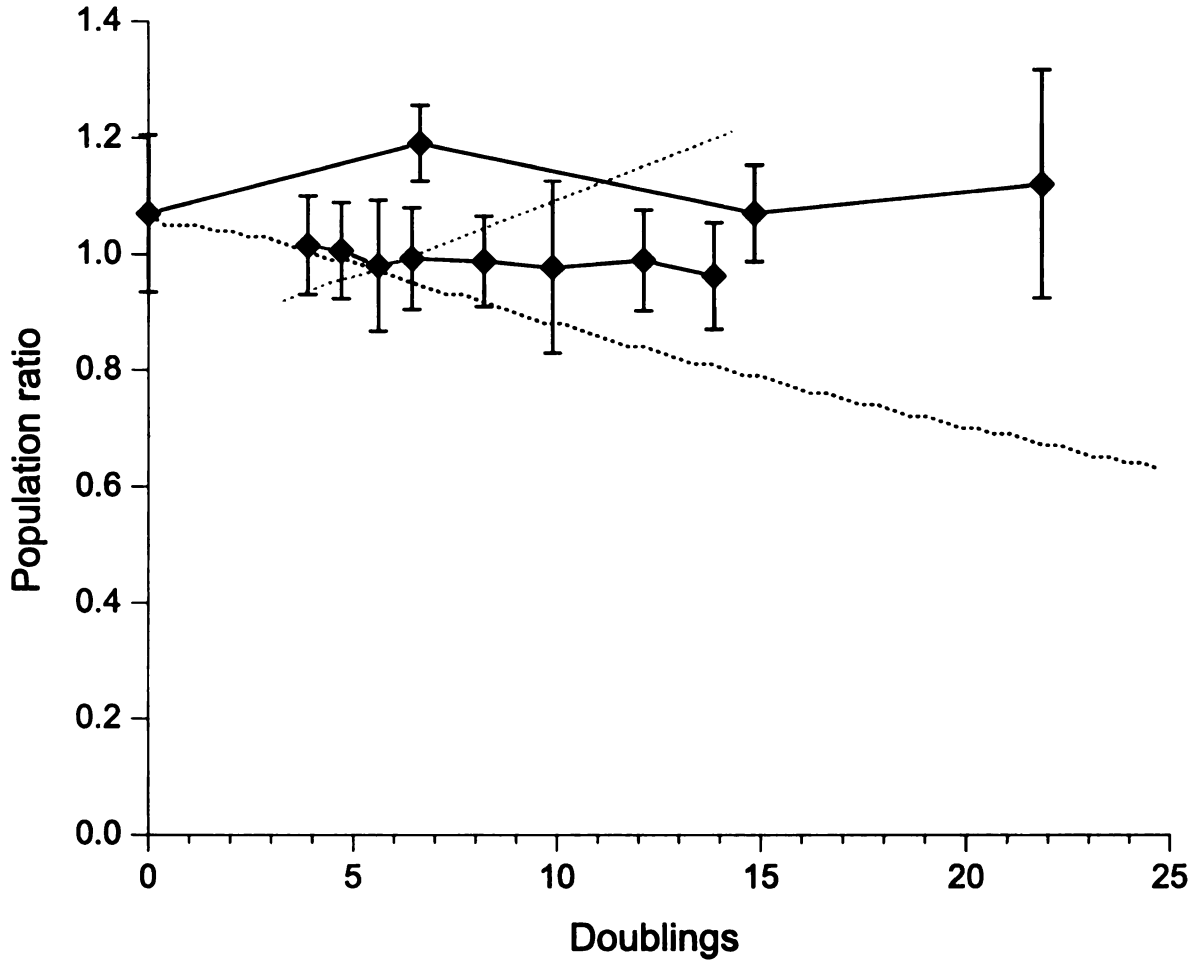

Figure 4.6 Empirical (solid lines with symbols) and simulated (dotted lines) relative fitness of Δ*rrnB* in fast (black) and slow (dark grey) chemostat competition experiments are represented as the population ratio (Δ*rrnB* vs. control) versus the number of population doublings. Error bars indicate the standard error of four independent cultures.

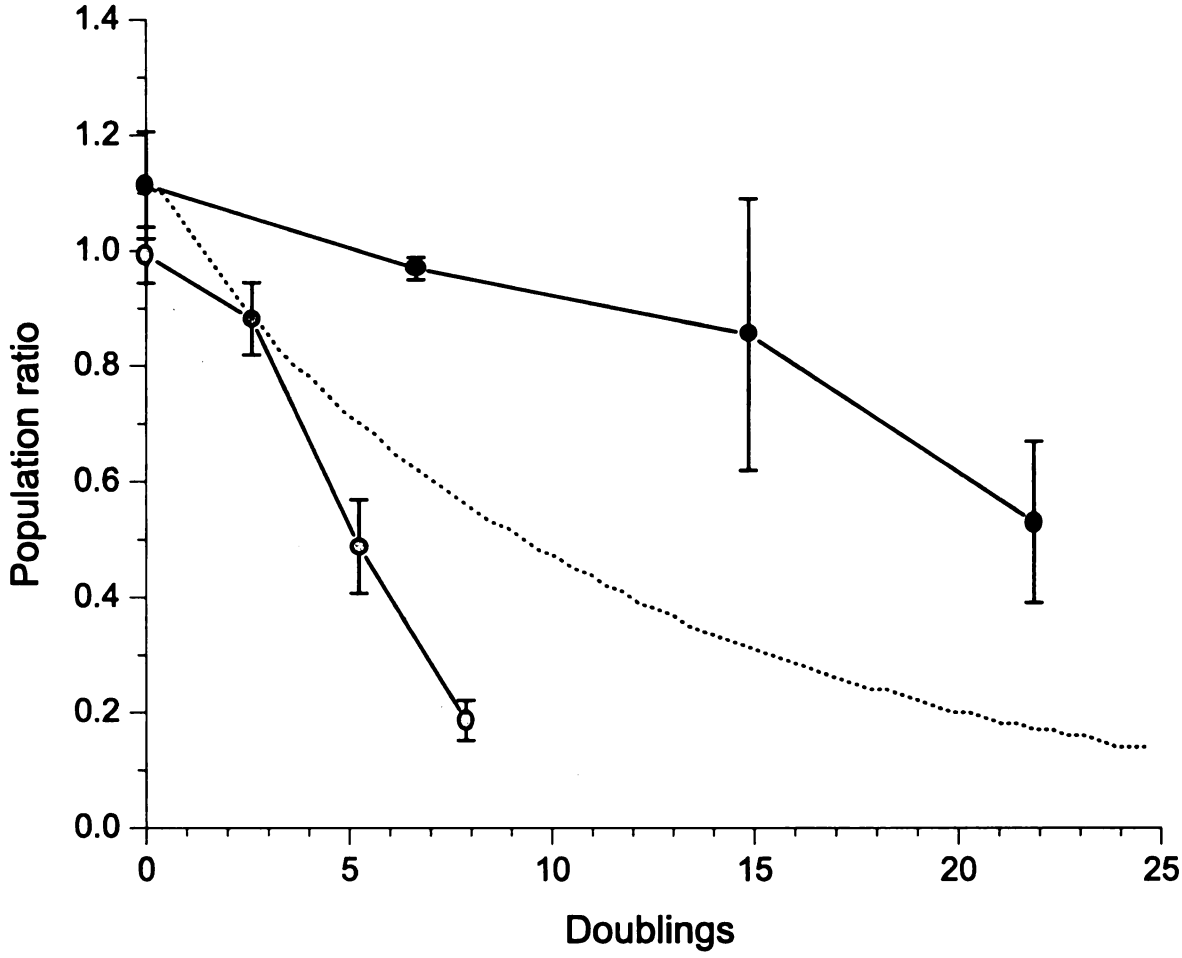

Figure 4.7 Empirical (solid lines with symbols) and and simulation (dotted lines) relative fitness of Δ*rrnA* in fast (black) and slow (light grey) chemostat competition experiments are represented as the population ratio (Δ*rrnA* vs. control) versus the number of population doublings. Error bars represent the standard error of four independent cultures.

Calculated chemostat-specific growth parameters

The *J* parameters calculated for each strain at each dilution rate correlate with the outcome of each chemostat competition experiment described above except for Δ*rrnB* at slow dilution rates. According to the calculated *J* parameter Δ*rrnB* would have a higher competitive ability compared to the control strain at slow dilution rates, which did not occur. It is important to point out however, that the calculations of *J* parameters used the means for K_S and μ_{MAX} reported in Table 4.1. Not all of the differences between these means were statistically significant. Therefore, only the differences in *J* parameters of strains with a deleted *rrnA* operon (Δ*rrnA* and Δ*rrnAB*) with those with a functional *rrnA* operon (control and Δ*rrnB*) should be considered significant, as with the K_S values for each strain (Table 4.1).

Table 4.2 Chemostat-specific growth parameters

Strains	*J* (μg/ml)[a]	
	D[b] = 0.11	*D* = 0.81
Control	0.0141	0.434
Δ*rrnB*	0.0137	0.473
Δ*rrnA*	0.0189	0.652
Δ*rrnAB*	0.0186	0.671

[a] $J = K_S \bullet (D/\mu_{MAX} - D)$ as described in (37).
[b] D = dilution rate (h^{-1})

4.4 Discussion

This study used strains of *E. coli* to test the assertion that the rRNA operon copy number of a prokaryotic species represents an adaptation to

environmental conditions, with respect to the pattern of nutrient availability. One of the basic tenets of bacterial physiology is that macromolecular content (e.g. RNA concentration) changes with growth rate. The synthesis of rRNA, which is regulated at the transcriptional level, is the rate-limiting step in ribosome synthesis and therefore can limit growth. Multiple rRNA operons are an effective way to increase the cell's capacity to synthesize rRNA by effectively increasing rRNA gene dosage.

It has been postulated that a culture of *E. coli* responds quickly to nutrient influxes with rapid growth as a result of the seven rRNA operons on the *E. coli* chromosome (1, 47). Previous work studying the connection between the number of functional rRNA operons on the chromosome and cell physiology (5, 17, 23) have used strains in which the effect on rRNA operon copy number could not be discerned from secondary effects of the rRNA operon manipulations. The research reported here was based on strains of *E. coli* containing rRNA operon deletions, which were designed to eliminate the shortcomings of previously used rRNA operon deletion strains by removing the majority of the targeted rRNA operons (including the promoters) but leave all other genes intact. These strains were therefore used to investigate the connection between rRNA operon copy number, individual growth parameters, and cumulative competitive ability under different nutrient availability regimes.

Effect of rRNA copy number on relative fitness in fluctuating nutrient conditions

The results of the batch culture competition experiments support the hypothesis that multiple rRNA operons are an advantage under culture conditions that are defined by fluctuating nutrient availability. This was evident when strains with either one or two deleted rRNA operons were competing with the control strain for limited nutrients in batch cultures, where nutrient availability fluctuates with each transfer to fresh medium. There was a direct correlation between the number of rRNA operons in the cells and relative fitness under batch culture conditions in glucose minimal medium (Figure 4.4).

The overall relative fitness in batch culture of each competing population was comprised of a collection of individually measured growth parameters (Table 4.1). The impact of each growth parameter on relative fitness was tested using the computer model described in Chapter 5 by simulating competition experiments in which only one, or all of the measured growth parameters differed between the two competing populations (Figure 4.8). Although the differences between individual growth parameter means were not always statistically significant, the cumulative differences between all growth parameters of each strain significantly effected overall relative fitness (Figure 4.4, Appendix C) and were accurately depicted in the model simulation results. The simulation data shows that the decrease in maximum growth rate and increase in lag time contribute similarly to the decreased relative fitness of strains with 6 rRNA operons (Δ*rrnA* and Δ*rrnB* in Figure 4.8). When a second rRNA operon was deleted, the increase in lag time of the resulting strain (Δ*rrnAB*) had a larger

impact on relative fitness than maximum growth rate. The amount of time needed for a stationary phase culture to reach exponential growth upon inoculation into fresh medium (lag time) increased about 4% relative to the control strain in Δ*rrnB* or Δ*rrnA*, whereas the lag time of Δ*rrnAB* was about 20% longer than the control strain. This amount of time (0.28 h) is appreciable when one considers that during that time, the control strain is growing exponentially and beginning to remove the limited amount of nutrients.

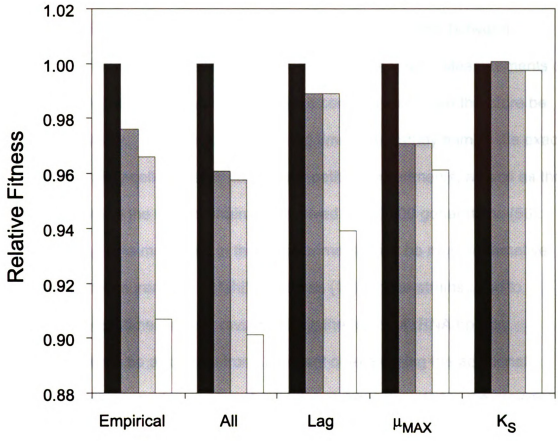

Figure 4.8 Empirical relative fitness values for the control (black), Δ*rrnB* (dark grey), Δ*rrnA* (light grey) and Δ*rrnAB* (white) strains in batch culture competition experiments, and relative fitness values based on simulations using all measured parameters or each parameter individually.

Populations of *E. coli* have evolved under environmental conditions that are best described as feast and famine, referring to the disparity between fluctuations in nutrient availability inside animal intestines (63). Measurements of lag time depend heavily upon previous culture conditions and can therefore be somewhat arbitrary. The measurement of lag time in this study mimics the exact conditions faced by cells in batch culture competition experiments, as well as the conditions in which the control strain had evolved for 10,000 generations (56). Additionally, lag time measured in these experiments may be more informative than previous measurements of "shift-up" times (17). In the strains used to measure "shift-up" times in the previous study, the effect of rRNA operon inactivation cannot be discerned from the effect of expressing the additional antibiotic resistance markers. Also, the "shift-up" times reported in the previous study reflect the amount of time needed to shift from one exponential growth rate to a higher growth rate. The measured lag times in the present study however, not only reflect the time needed to make additional protein-synthesizing machinery (i.e. ribosomes) for growth under the more favorable growth condition, but to do this starting from a "non-growing" physiological state.

Effect of rRNA operon copy number on relative fitness in stable nutrient conditions

The second hypothesis states that cells with fewer rRNA operons are at an advantage under stable, nutrient limiting growth conditions. Although the amount of ribosomes is closely regulated with growth rate in *E. coli* cells growing

at moderate to fast rates (11), *E. coli* cells maintain excess protein synthesizing capacity under very slow growth conditions ($\mu \leq 0.2\ h^{-1}$) (47). It was suggested that these "excess" ribosomes might offer the cell an advantage upon an influx of nutrients. In the absence of a fluctuation in nutrient availability however, the synthesis of excess ribosomes under slow growth rates might be a metabolic expense that cells with fewer rRNA operons would not experience. Cells with fewer rRNA operons would therefore be at an advantage under slow, stable, limiting nutrient conditions where there were no sudden influxes of nutrients. According to the hypothesis stated above, a negative correlation between relative fitness and rRNA operon copy number was expected in chemostat competition experiments. This hypothesis however, was not supported by the experimental data, and there was no correlation with rRNA operon copy number (Figures 4.5-4.7).

The rRNA deletion strain Δ*rrnB* had a slightly lower mean K_S value (Table 4.1). When the mean growth parameter values were used (regardless of significance) to simulate chemostat competition experiments (grey dotted line, Figure 4.6), or determine *J* parameters (Table 4.2) at slow dilution rates, Δ*rrnB* was predicted to have a higher competitive ability than the control strain. There was no measurable difference however, in the relative fitness of Δ*rrnB* in chemostat competition experiments with slow dilution rates ($0.11\ h^{-1}$). The population ratio of Δ*rrnB* versus the control did not change under equilibrium chemostat conditions for nearly 15 doublings of the total population. The disparity between the simulated and empirical competition outcomes indicates

the limit of precision in measuring K_S and the sensitivity of relative fitness to seemingly small differences in K_S at slow dilution rates. The model simulations and *J* parameter determinations more accurately depicted the outcome of chemostat competition experiments with fast dilution rates between Δ*rrnB* and the control strain (black dotted line, Figure 4.6), where the impact of K_S on relative fitness is smaller.

Concomitant with model simulations and *J* parameter calculations, the Δ*rrnA* and Δ*rrnAB* strains were considerably less fit than the control strain under slow chemostat conditions (Figure 4.5, Table 4.2). Their population ratios were less than 1:10 versus the control in about 10 doublings of the total population. The low relative fitness of both strains coincided with their increased K_S values, which were close to 30% higher than either the control strain or Δ*rrnB*. Chemostat competition experiments at fast dilution rates showed that although Δ*rrnA* still had a higher *J* parameter and therefore was less fit than the control strain, the relative fitness of the Δ*rrnA* strain was much improved relative to that in slow chemostat competition experiments (Figure 4.7). Based on chemostat theory and previously reported data (70), chemostats with faster dilution rates have higher residual concentrations of the limiting nutrient. The relative fitness of a strain is less sensitive to differences in K_S under these conditions, which explains the data above.

Possible impact of tRNA imbalance

The differential effect of deleting the *rrnA* or *rrnB* operon may be linked to some of their known differences. It is possible that the sequence divergence between the *rrnA* and *rrnB* operons (as with all of the operons) might lead to differential expression, or result in ribosomes with different properties. Alternatively, the differential phenotypes could be related to the different tRNA genes in the internally transcribed spacer (ITS) regions of *rrnA* and *rrnB*. The *rrnA, D,* and *H* operons have the Ile and Ala_{1B} tRNA genes in their ITS regions, whereas the *rrnB, C, G,* and *E* operons have only the Glu_2 tRNA gene. These tRNA genes are only represented in the rRNA operon ITS regions, whereas other tRNA genes are present in multiple copies elsewhere on the chromosome. It was originally thought that deleting the *rrnA* and *rrnB* operons would minimize the disruption of the tRNA gene pool because they represent one of the two groups of rRNA operons in *E. coli,* with respect to their ITS tRNA genes, and neither operon has any distal tRNA genes. It was hoped that the effect of deleting the tRNA genes present in the rRNA operons would be minimal as long as several intact copies were present in the remaining rRNA operons.

The deletion of a tRNA gene present in multiple copies may have a larger detrimental effect on competitive ability than anticipated, especially at slower growth rates. The tRNA genes that are present as multiple copies on the chromosome (including those in the rRNA operon ITS region) represent those tRNAs that are relatively more abundant in the pool of tRNAs in the cell, and

whose codons are used more frequently as growth rate increases (21). These properties suggest that those tRNA genes present in multiple copies, and their abundance relative to other tRNA genes, could be important to the efficient growth of a cell.

It is not possible to discern the effect of deleting rRNA genes from deleting tRNA genes present on the rRNA operons. None of the experimental results reported above can be excluded unequivocally from being partially, if not entirely, a consequence of deleting the tRNA genes along with the *rrnA* and *rrnB* operons. Furthermore, the differential effect of deleting the *rrnA* versus the *rrnB* operon might simply be the result of deleting the two tRNA genes in *rrnA* instead of one tRNA gene in the *rrnB* ITS region.

Proposed explanation of cumulative results

With the considerations stated above, a possible explanation is presented that could tie the results of batch culture and chemostat cultures together with the result of deleting rRNA and tRNA genes. This explanation is intended to illustrate the possibilities of extending this current line of research. The inability to discern the effect of deleting rRNA genes from deleting tRNA genes on an rRNA operon illustrates the need to investigate the impact of both rRNA and tRNA gene copy number on cell physiology and competitive ability under fluctuating and stable nutrient conditions.

The effect of deleting rRNA genes from the chromosome of a cell could impact the cell's ability to respond to fluctuations in nutrient availability by

increasing the amount of time needed for de novo ribosome synthesis. This impact is supported by the increase in lag time and decrease in relative fitness of rRNA operon deletion strains in batch culture. During steady state growth however, the cell might compensate for the deleted rRNA genes by increasing the amount of synthesis from the remaining copies. The deletion of tRNA genes however, causes an imbalance in the tRNA gene pool that is not corrected by increased rRNA synthesis from the remaining rRNA operons; the resulting proportion of tRNAs is still unbalanced with respect to the deleted tRNA gene. Compared to deleting the *rrnB* operon, deleting the *rrnA* operon might result in a greater impact on the tRNA gene pool because there are two tRNA genes in the *rrnA* ITS region ($tRNA^{Ile}$ and $tRNA^{Ala}_{1B}$) and only two other rRNA operons (*rrnD* and *H*) from which to make these tRNAs. The impact of an imbalance of tRNAs could result in decreased translational efficiency, as more time is required for the affected tRNAs to come into contact with the ribosome. One possible response to a decrease in translational efficiency could be the increase in production of ribosomes. A cell that needs more ribosomes for the same translational capacity would therefore require more metabolic energy per doubling event. The requirement of more metabolic energy would have its largest impact at the lowest concentration of nutrients.

There is an interesting correlation between the cell yield and cell volume of the Δ*rrnA* and Δ*rrnAB* strains and their relative fitness in chemostats with slow dilution rates, which supports the explanation above. The cells of the Δ*rrnA* and Δ*rrnAB* strains are larger and have a lower cell yield than those of the control and

Δ*rrnB* strains (Figure 4.3). At faster dilution rates (0.56 h^{-1}) however, the difference in either trait between all strains is greatly reduced. This suggests that cells with a deleted *rrnA* operon are somehow physiologically different at slow dilution rates, resulting in larger cells and decreased cell yields. Although cell yield is not a component of competitive ability in unstructured environments, there is likely some relationship between the cell yields, cell volumes, K_S and ultimately, relative fitness of the strains with a deleted *rrnA* operon.

The difference in K_S values, cell yield, and cell volume between Δ*rrnA* and Δ*rrnB* coincides with relative fitness differences observed in chemostat competition experiments. It does not however, explain how the deletion of an rRNA operon affects the cell or why there was a differential effect between the deletion of *rrnA* and *rrnB*. Work is currently ongoing to confirm these observations and address these questions. The *rrnA* operon will be replaced in Δ*rrnAB* to test for the "rescue" of the Δ*rrnA* phenotype, and then smaller fragments of the *rrnA* operon will be deleted in an attempt to identify the specific region of the operon that is responsible for the phenotype.

Potential limitations of comparing rRNA deletion strains to control strains

As discussed in Chapter 3, part of the procedure used in deleting the rRNA operons from the *E. coli* chromosome included the generalized transduction of genomic DNA from a *recD* mutant strain of *E. coli* K-12 into the *E. coli* B evolved strains used in this study. It is likely that other regions of the donor strain's genomic DNA, including the rRNA operon, also recombined into the

genome of the recipient strain. What is not known is if any of these potential regions of donor DNA is responsible for the effects observed in the rRNA operon deletion strains.

The *E. coli* K-12 and B strains are relatively closely related, falling within the same subgroup of *E. coli* strains based on 20 enzyme-encoding loci. Only one of these loci (*phn* operon) is even close to within 100 kb of the *rrnA* or *rrnB* operons and therefore possibly co-transduced using phage P1. Nonetheless, it will be important for control strains to be "reconstructed" from the intermediate strains by replacing the marker alleles with the entire rRNA operon instead of the deleted operon as in the deletion procedure (Chapter 3). Any effect caused by collateral transduction of genes other than the rRNA operon marker alleles will remain in these reconstructed control strains, which will have the rRNA operon replaced at the site of the marker allele. The control strains used in this study have not been transduced with any of the *recD* donor strain DNA and therefore do not represent controls that could be nearly as isogenic as the reconstructed control strains.

Conclusion

The work reported here supports the hypothesis that multiple rRNA operons are an advantage to an organism under fluctuating nutrient conditions. Further experimentation is needed however, in order to separate the effect of rRNA gene copy number from the tRNA genes that were also deleted as well as any effect caused by the transduction of *E. coli* K-12 DNA into the *E. coli* B strain

used in this study. No trade-off for the maintenance of multiple rRNA operons was measured in this study. Cells with fewer rRNA operons were not at an advantage in slow, stable, nutrient conditions. Additionally, the deletion of the *rrnA* operon caused a marked decrease in relative fitness under chemostat conditions that was attributable to an increased K_S parameter. Either the *rrnA* operon or its tRNA genes were somehow essential for comparable relative fitness under nutrient limiting growth. This attribute was previously unknown for any of the rRNA operons and raises many new questions about the differential properties of the multiple rRNA operons and their tRNA genes in *E. coli*.

CHAPTER 5

DEVELOPMENT OF A COMPUTER MODEL TO SIMULATE THE DYNAMICS OF TWO POPULATIONS COMPETING FOR A LIMITING NUTRIENT

5.1 Introduction

In natural ecosystems, a multitude of physicochemical influences as well as the activities of other microorganisms within the same environment influence microbial populations. A common goal of microbial ecologists is to understand how microbial populations interact with each other and their environment, and how these interactions affect the abundance and distribution of these populations. A fundamental interaction that drives many of these factors is the availability of nutrients for growth and proliferation of a population. When two or more populations within a microbial community vie for one or more of the same resources, the ultimate result can be inhibition of growth and/or survival of some of these competing populations. This competition for limiting resources is probably the most common type of interspecies interaction.

Mathematical models are powerful tools that can be used in investigating the impact of nutrient availability on population dynamics. Over fifty years ago, Monod derived equations that describe the relationship between the concentration of a limiting nutrient and the specific growth rate of a microbial population (60). Relevant parameters of microbial growth include; lag time, maximum specific growth rate, Monod half-velocity coefficient (K_S), death rate,

and yield. Many other equations have been developed to define substrate-specific growth rates more accurately, however most fit the available data just as well as the Monod equation, or contain biologically indefinable components (48). The close fit, extensive testing, and mathematical simplicity of the Monod equation justifies its use under many circumstances.

In the study reported here, the Monod equation was incorporated into a computer-based model that was programmed to simulate the dynamic relationships between microbial populations and the availability of the limiting nutrients. An object-oriented software package was used to program the model, which makes it easy to expand and use to simulate the direct competition between populations in which the limiting nutrients are supplied in a batch, continuous, or pulsed manner. All of the individual growth parameters mentioned above are incorporated into the model and can be set to match those of any competing population, as well as the beginning densities of those populations.

This chapter describes the computer model mentioned above, its behavior, verification, and validation. After programming the model, its behavior was studied to insure that it correctly simulated the relationships between nutrient concentration and population growth described in the Monod equation. The results from previously reported simulations and empirical competition experiments (37, 76) were compared with simulations using the model reported here in order to verify the performance of the model. Comparing simulations of competition experiments described in Chapter 4 with the empirical data further validated the performance of the model. This model does not incorporate any

new definitions of microbial growth, but it does provide an easy way to portray how individual growth parameters affect the competitive ability of a bacterial population under fluctuating and stable nutrient conditions. Additionally, the model represents an easy to use tool to further study the interactions between well-defined microbial populations competing for the same limiting nutrients.

5.2 Methods

Identification of variables

The model (Figure 5.1) is a three-compartment system composed of the limiting nutrient (glucose ($g \bullet L^{-1}$)), and two competing populations (Population 1 and Population 2, (cells $\bullet L^{-1}$)). The concentration of limiting nutrient in the culture vessel is the central state variable of the system. Dynamics of this variable are determined by the flows; 'flow in' from the reservoir, 'flow out' from overflow, and from the 'utilization' of each population. The physical 'flow in' and 'flow out' of the culture vessel are determined by the reservoir concentration multiplied by the dilution rate D (h^{-1}), which represents the number of volumes that are cycled per hour. The growth (cells•(L•h)-1) divided by the yield (cells•g-1) of each population determines the removal of glucose from the system due to utilization (g•(L•h)-1) by each population.

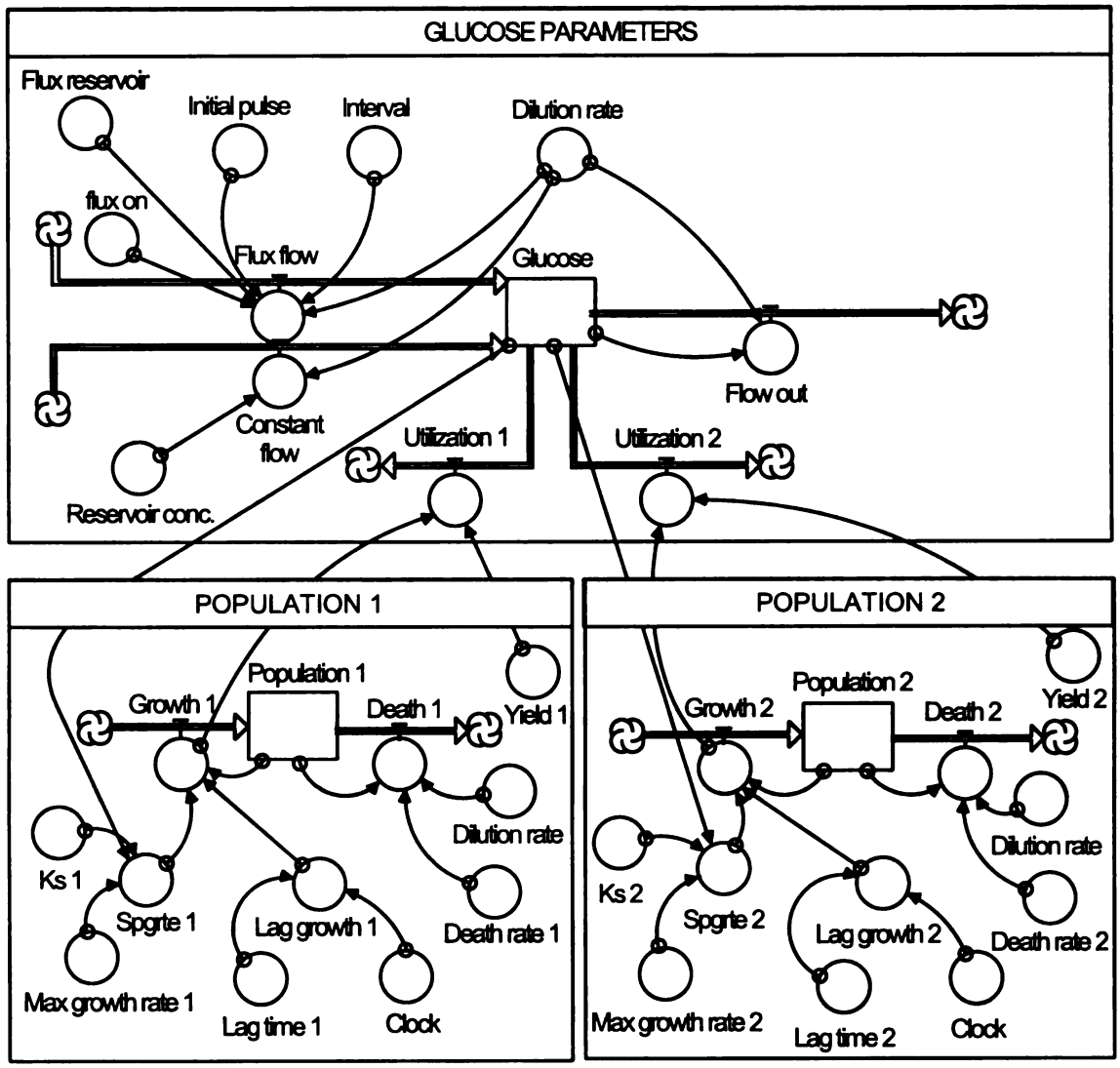

Figure 5.1 Map showing the relationship between stocks (○), converters (□), and flows (⊶) of the model programmed in the object-oriented language STELLA.

An additional flow into the glucose stock was programmed into the model to facilitate simulations of fluctuations in the amount of glucose entering the system. This flow 'flux flow' represents a second reservoir ('flux reservoir') of limiting nutrient that can be added to the total flow into the glucose stock. The 'flux flow' is controlled by the function (PULSE), which pulses an input of a specified size. In this case the pulse input is the 'dilution rate' multiplied by the 'flux reservoir' concentration of limiting nutrient ($g \bullet L^{-1}$). In using the PULSE function, the user has the option of setting the time at which the PULSE will first fire ('initial pulse') as well as the interval between subsequent PULSEs ('interval').

The flows, 'growth' and 'death' determine the dynamics of each population. The rate of growth of each population follows the Monod equation (60) as follows,

$$\mu = \mu_{MAX} \bullet [S]/K_S+[S], \qquad (1)$$

where μ is the specific growth rate, μ_{MAX} is the maximum growth rate, [S] is the substrate concentration, and K_S is the Monod half-velocity coefficient ([S] where μ is equal to $\mu_{MAX}/2$). Equation (1) defines the relationship between the specific growth rate of a population relative to the concentration of a limiting nutrient. In addition to the above parameters, lag time acts to delay the growth of a population at the beginning of a simulation, for the duration of the 'lag time' (h), and is programmed using logic statements. The 'lag growth' converter returns a value of zero growth for the specified duration of 'lag growth'.

The flow 'death' represents the overall death rate of the population. During batch culture simulations the 'dilution rate' is set = 0, and therefore the flow 'death' is equal to the parameter 'death rate'. Under continuous culture conditions the 'dilution rate' is set > 0, and 'death' is equal to the dilution rate multiplied by the population density and represents the washout of cells from the chemostat.

Parameterization

The parameterization of the model for each simulation was performed using the "Control Panel" interface. Here, the values for initial population size, K_S, maximum growth rate, lag time, and death rate can be set for each population. Parameters defining the reservoir and initial vessel concentrations of glucose, dilution rate, and the flux flow can also be set in the control panel. Other controls present in the control panel interface and other locations throughout the model include navigation and simulation controls. These controls allow the user to navigate quickly from one location to another, specify the step times and duration of simulations, and run, stop, or pause a simulation.

Modeling method

This deterministic model was programmed with STELLA® Research 5.1.1 software. The intuitiveness of this object-oriented modeling language allows the user to easily understand and program the relationships between the system components, and make additions or amendments to the model. Data generated

during simulations was exported to spreadsheets in Microsoft Excel ®, and Microcal Origin ® for further statistical and graphical analysis. The data exchange was made possible via the dynamic data-exporting feature of the modeling software. Another benefit of the STELLA software package is cross compatibility, allowing any model to be used on several computing platforms.

All simulations were run using the Euler's method of derivation with a step time of 0.00625 h (delta time, DT = 0.00625). This "optimum" DT was determined by sequentially decreasing the step time from 1.0 h by ½ until the simulation resulted in no quantitative change in population densities and no additional dampening of oscillations occurred. The "1/2 test" was used as suggested by the STELLA technical documentation because of the binary arithmetic the computer uses for calculation (39). At the DT = 0.00625, any further ½ decreases did not affect the outcome of the simulations, but chemostat simulations could not be run longer than 200 hours before the limit of maximum step times was reached. There is an internal limit of ~32,767 step times set within the software. If this limit would be exceeded, a warning message will appear suggesting a larger DT or shorter simulation.

Sensitivity analyses

The model was tested for sensitivity to changes in the parameters; μ_{MAX}, lag time, and K_S. Sensitivity was determined during batch and chemostat culture conditions by simulating competitions between populations that were identical except for the parameter being tested. Under batch culture conditions,

the sensitivity of the system to changes in the ratio of parameter values (e.g. $\mu_{MAX}1/\mu_{MAX}2$) was determined as the effect on the ratio of population densities (Pop 1/Pop 2) after 24 hours. Under chemostat conditions, the sensitivity of the system was measured as the change in the population ratio per doubling at fast (0.81 h^{-1}) and slow (0.11 h^{-1}) dilution rates.

Verification of model performance

The behavior of the model was verified using data that was previously modeled with Monod kinetics (76). When a batch culture competition was simulated, both experimental and theoretical data (Table 5.1) (76) were compared to simulation results (Table 5.1, Figure 5.4). Quantitative comparison was performed using empirically and mathematically derived values of relative fitness (*W*) (54, also described in Chapter 4).

In the case of continuous culture simulations, the model was parameterized with data for three experiments from Hansen and Hubbell (37) (Table 5.2). Their empirical and simulation data were compared to simulation results (Figure 5.6). In these simulations, the relative change in population densities indicates relative fitness and represents the rate at which one competitor excludes another. Quantitative comparison of simulation results was also made on the basis of the *J* parameter for each population (37, also described in Chapter 4). The *J* parameter represents the subsistence concentration of the limiting resource for a population at equilibrium. The

population with the lowest *J* value will competitively exclude all others with higher *J* values.

Validation of model performance

Simulations of competition experiments described in Chapter 4 were run using independently measured growth parameters for each strain (Table 4.1), and the specific population densities and nutrient parameters of the direct competition experiments that were simulated. The simulation results were compared to relative fitness values calculated for batch culture and the population ratio dynamics for chemostat competition experiments in order to validate the model performance.

5.3 Results

Sensitivity analyses

Under batch culture conditions, the outcome of the simulation was most sensitive to μ_{MAX} (Figure 5.2). As the μ_{MAX} of Population 1 was increased relative to Population 2 (a higher μ_{max} ratio), the population ratio (Pop 1/Pop 2) increased proportionately in favor of the population with the higher μ_{MAX}. The model was slightly less sensitive to changes in lag time, and rather insensitive to changes in K_S. As predicted by the Monod equation, increases in either lag time or K_S had a negative effect on relative fitness. For the purpose of comparing absolute model sensitivity, the effect on population ratio (Pop1/Pop2) was plotted against increases in lag time and K_S of Population 2 relative to Population 1. The

sensitivity of these parameters was as expected and indicates proper model behavior.

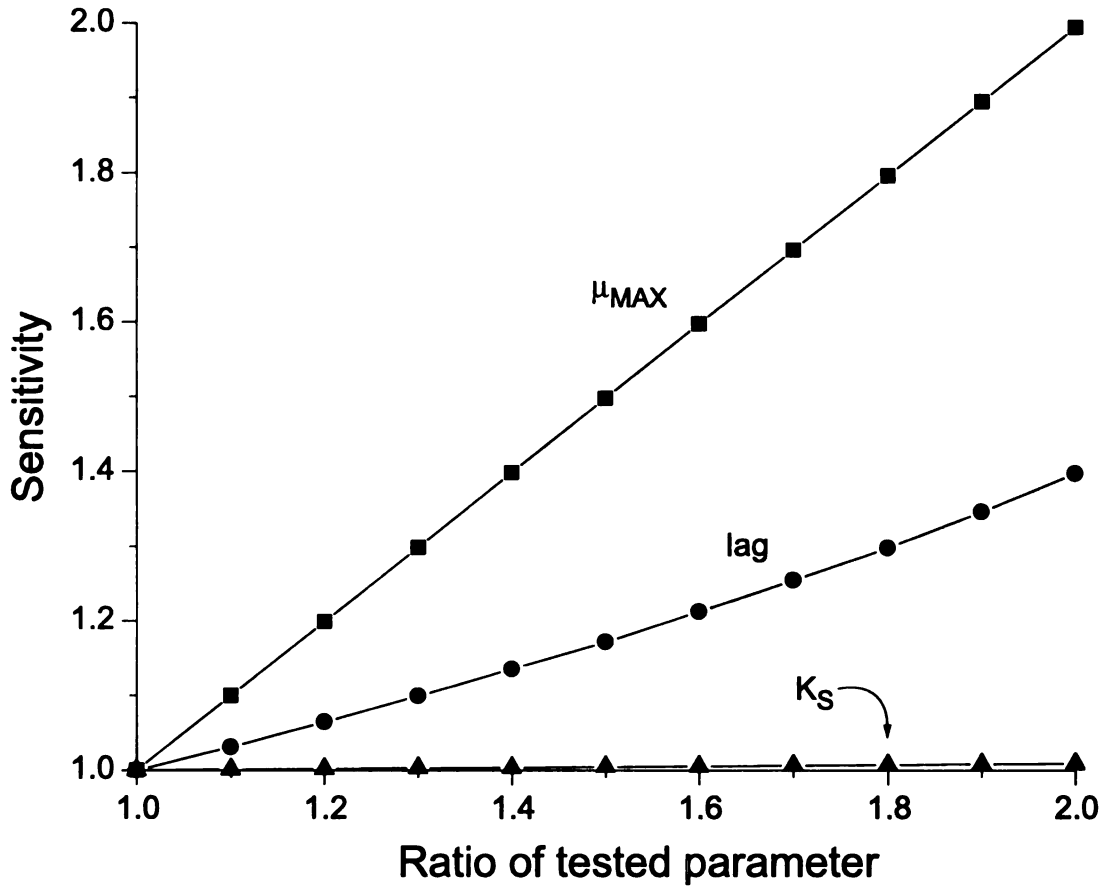

Figure 5.2. Batch culture sensitivity analyses. The population ratio (Population 1/Population 2) after 24 h simulations (labeled as Sensitivity) was plotted against the ratio of the tested parameters ($\mu_{MAX}1/\mu_{MAX}2$, lag2/lag1, and K_S2/K_S1).

The model was sensitive to changes in μ_{MAX} under chemostat culture conditions in a similar manner as in batch culture conditions (Figure 5.3). Unlike batch culture conditions however, the model was also sensitive to changes in K_S. The model was more sensitive to K_S at slow dilution rates (0.11 h^{-1}) than at fast dilution rates (0.81 h^{-1}). As the K_S of a population decreased (K_S2/K_S1 increases in Figure 5.3), the population ratio increases in favor of the population with the smaller K_S value. Under chemostat conditions, the sensitivity of the model to differences in lag time was not relevant because chemostats represent equilibrium conditions in which the cells are in steady state growth.

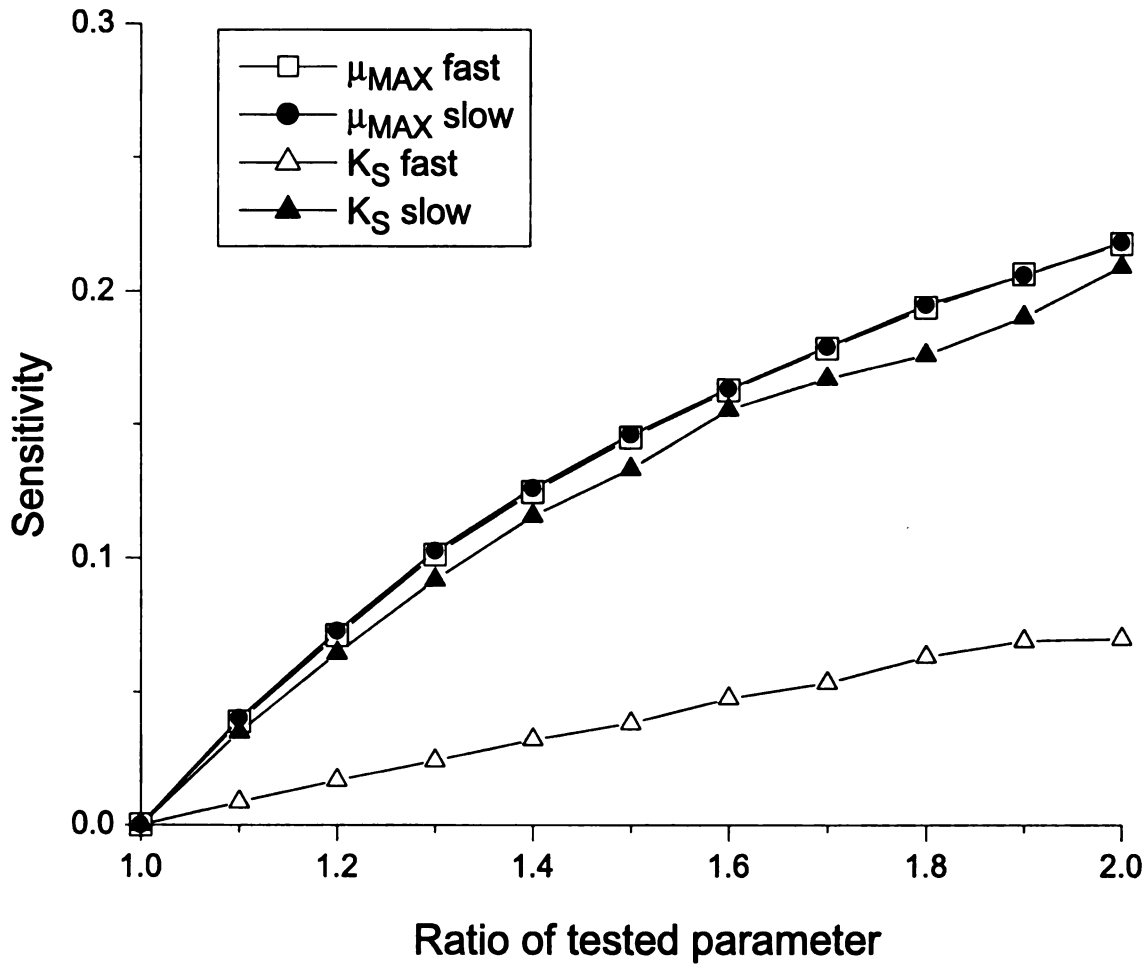

Figure 5.3 Sensitivity analyses of chemostat simulations. The sensitivity (change in population ratio (Pop1/Pop2) per doubling) of model parameters under fast (0.81 h^{-1}) and slow (0.11 h^{-1}) chemostat dilution rates is plotted against the ratio of the parameters ($\mu_{MAX}1/\mu_{MAX}2$) and (K_S2/K_S1).

Model Verification

Overall model behavior during batch culture simulations was correct in that the growth of each population was delayed for the amount of lag time given, followed by a period of exponential growth at the specified maximal growth rates (Figure 5.4). Following with Monod's equation, growth was limited by nutrient availability. The model behavior was further verified by comparison of simulation and empirical data from Vasi et al. (76) to the simulation results (Table 5.1). When relative fitness values were calculated with the simulation data, the model was able to account for 90% of the empirical relative fitness reported for the derived strain (Table 5.1). As was the case for Vasi et al (76), this only represents 60% of the actual gain in relative fitness of the derived strain. They went on to show that this discrepancy was best explained by an under-estimation of maximum growth rate based on the increase in biovolume versus cell numbers. When biovolume was accounted for in the adjusted maximal growth rate, the simulation results were not different than experimental data. With the same considerations, this would show a satisfactory verification of the model behavior and performance under batch culture conditions.

Table 5.1. Parameter values and results for a simulation of previously published batch culture competition experiments (76)

	Organism	
Fitness components	parental	derived
Lag time (h)	1.5264	1.2470
μ_{max} (h^{-1})	0.7726	0.8887
K_S (10^{-5} g•liter^{-1})	7.27	8.80
Other parameters of simulation		
Glucose (g•L^{-1})	0.25	0.25
Initial population (10^8 cells•L^{-1})	5.00	5.00
Yield (10^{12} cells•g^{-1})	2.6352	1.8386
Relative fitness (W)		
empirical	(1)	1.3486
simulation	(1)	1.21
simulation [a]	(1)	1.21

[a] all other values are from (76).

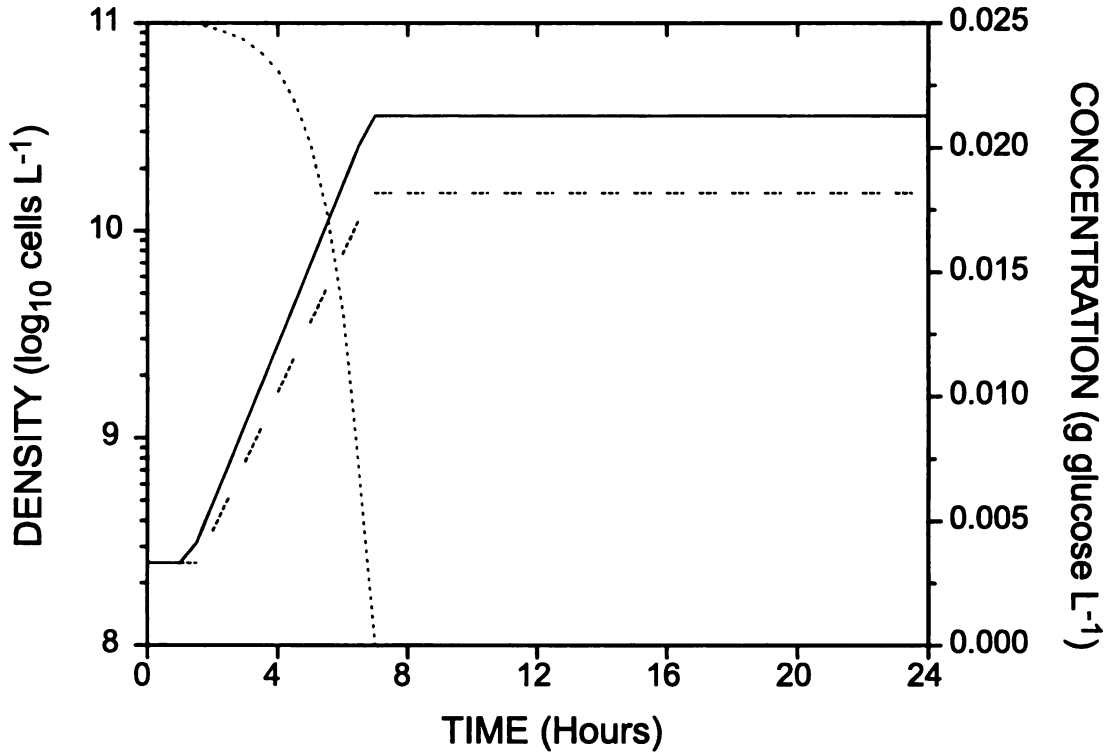

Figure 5.4 Batch culture verification data. The dynamics of the ancestor (left axis, solid line) and derived (left axis, dashed line) populations, and the concentration of glucose (right axis, dotted line), using the estimated parameters in (76) are shown.

The model was also run as a chemostat using data from Hansen and Hubbell (37) (Table 5.2). Each of the competition experiments reported in their study was simulated, and the results were compared to their simulation and empirical data. This represents a qualitative verification of the model under these conditions since no exact data for population densities were given in the published study. The population dynamics in model simulations (Figure 5.5) corresponded to those reported by Hansen and Hubbell, and the *J* values calculated for each population were identical to reported values (Table 5.3).

Table 5.2. Parameter values for simulations of previously published chemostat culture competition experiments (37)

Experiment	Bacterial strains	Populations				Cultures	
		Initial population (cells•L^{-1})	Yield (10^{10} cells•g^{-1})	K_S (g•L^{-1})	μ (h^{-1})	S_0 (g•L^{-1})	D (10^{-2} h^{-1})
A	C-8	5×10^{2}	2.5	3.0×10^{-6}	0.81	1×10^{-4}	6.0
	PAO283	8×10^{4}	3.8	3.1×10^{-4}	0.91		
B	C-8 $nal^r spec^s$	2×10^{5}	6.3	1.6×10^{-6}	0.68	5×10^{-6}	7.5
	C-8 $nal^s spec^r$	2×10^{3}	6.2	1.6×10^{-6}	0.96		
C	C-8 $nal^r spec^s$	8×10^{2}	6.3	1.6×10^{-6}	0.68	5×10^{-6}	7.5
	C-8 $nal^s spec^r$	4×10^{2}	6.2	0.9×10^{-6}	0.41		

Figure 5.5 Population density dynamics for chemostat verification simulations using parameters in Table 5.2 for experiment A, B, and C.

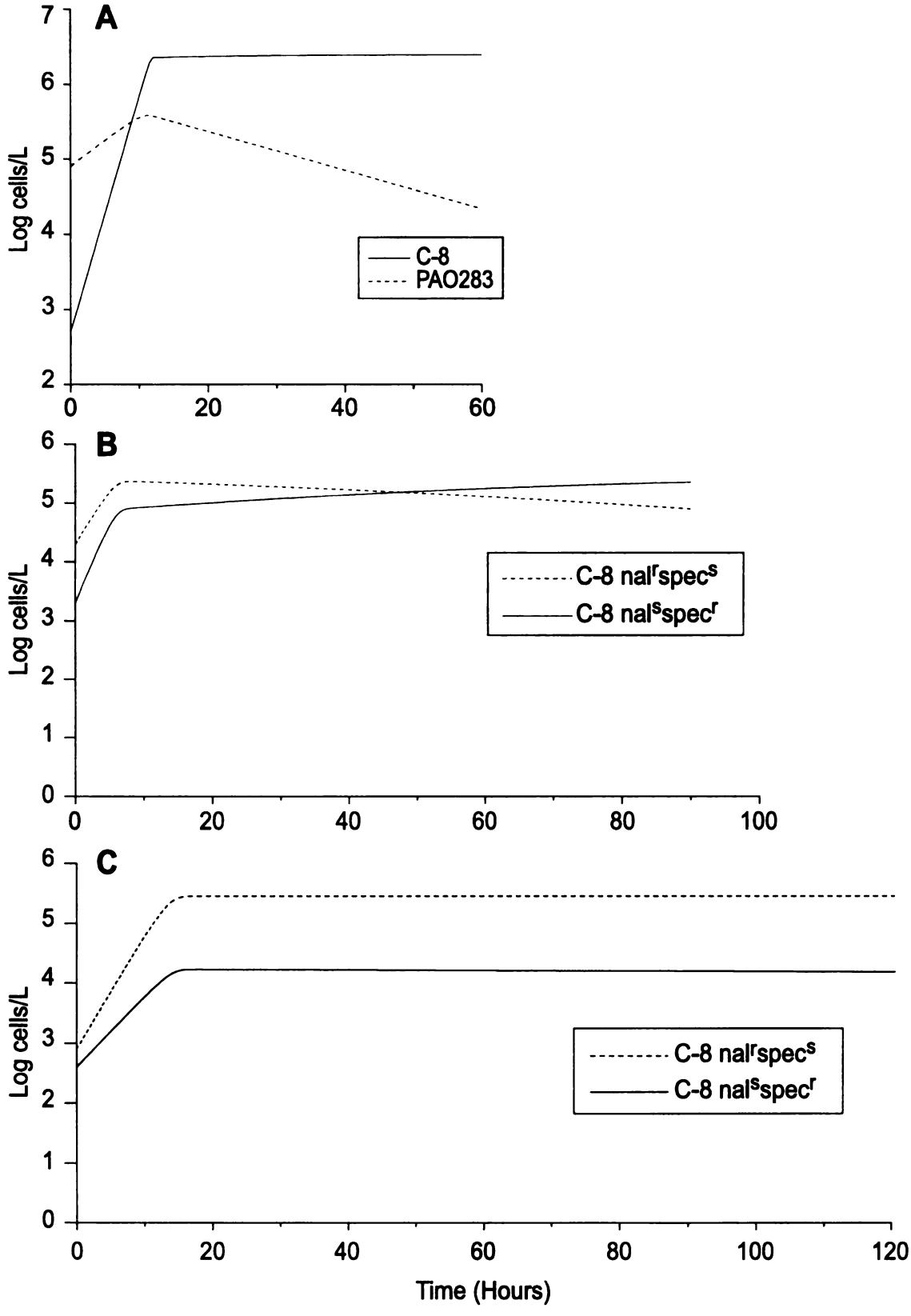
A
Log cells/L
C-8
PAO283
B
Log cells/L
C-8 nal^{r}spec^s
C-8 nal^{s}spec^r
C
Log cells/L
C-8 nal^{r}spec^s
C-8 nal^{s}spec^r
Time (Hours)

Figure 5.5

Table 5.3 Comparison of reported and calculated *J* parameters for chemostat model verification

	Strain	*J* parameter ($g \cdot L^{-1}$)[a]	
		Reported[b]	Calculated
A[c]	C-8	2.40×10^{-7}	2.40×10^{-7}
	PAO283	2.19×10^{-5}	2.18×10^{-5}
B	C-8 $nal^r spec^s$	1.98×10^{-7}	1.98×10^{-7}
	C-8 $nal^s spec^r$	1.35×10^{-7}	1.36×10^{-7}
C	C-8 $nal^r spec^s$	1.98×10^{-7}	1.98×10^{-7}
	C-8 $nal^s spec^r$	2.01×10^{-7}[d]	2.01×10^{-7}

[a] *J* parameter was calculated as follows; $J = K_S \bullet (D/r)$, where $r = \mu_{MAX} - D$.

[b] values taken from (37).

[c] letters correspond to panel labels for verification simulations represented in Figure 5.5

[d] this value represents *J* calculated from reported K_S, D, and μ_{MAX} values. A *J* value of 1.99×10^{-7} $g \bullet L^{-1}$ was reported (37).

Model Validation

Model validation is based on the ability to simulate the modeled system using independent empirical data. Using all parameters measured for each population (Table 5.4), the model was able to simulate the relative fitness of each strain very closely (Figure 5.6), thus validating its performance under batch culture conditions. When run as a chemostat, the model also closely simulated empirical competition results (Figures 5.7 and 5.8), except in the case of Δ*rrnB* at slow dilution rates (0.11 h^{-1}). The calculated *J* parameters and simulation data predicted that Δ*rrnB* would be more fit than the control strain at slow dilution rates. This discrepancy and its possible implications are discussed below. These simulations were very dependent upon the proper parameterization of initial population ratios. The exact initial population of each empirical competition was used for the simulations instead of an assumed 1:1 ratio.

Table 5.4 Calculated *J* parameters for chemostat model validation at different dilution rates (*D*)

	J parameter ($g \cdot L^{-1}$)[a]	
Strain	*D* = 0.11 h^{-1}	0.81 h^{-1}
Control	1.41×10^{-2}	4.39×10^{-1}
Δ*rrnB*	1.38×10^{-2}	4.79×10^{-1}
Δ*rrnA*	1.90×10^{-2}	6.58×10^{-1}
Δ*rrnAB*	1.88×10^{-2}	6.89×10^{-1}

[a] *J* parameter was calculated as follows; $J = K_S \cdot (D/r)$, where $r = \mu_{MAX} - D$.

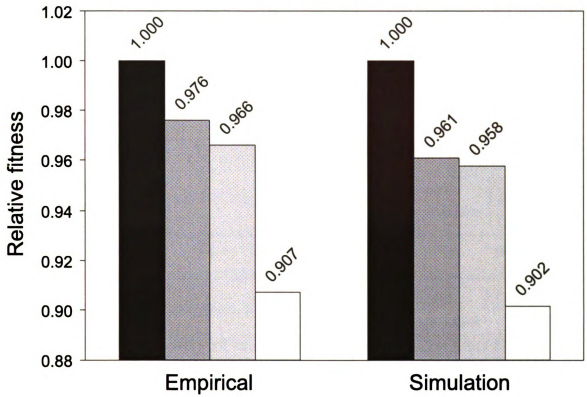

Figure 5.6 Validation of model performance under batch culture conditions. Empirical versus simulation relative fitness values for the control (black), Δ*rrnB* (dark grey), Δ*rrnA* (light grey), and Δ*rrnAB* (white) strains.

Figure 5.7 Population ratio dynamics for slow chemostat validation simulations of direct competition experiments with (A) Δ*rrnB*, (B) Δ*rrnA*, and (C) Δ*rrnAB* strains vs. the control strain using parameters in Chapter 4.

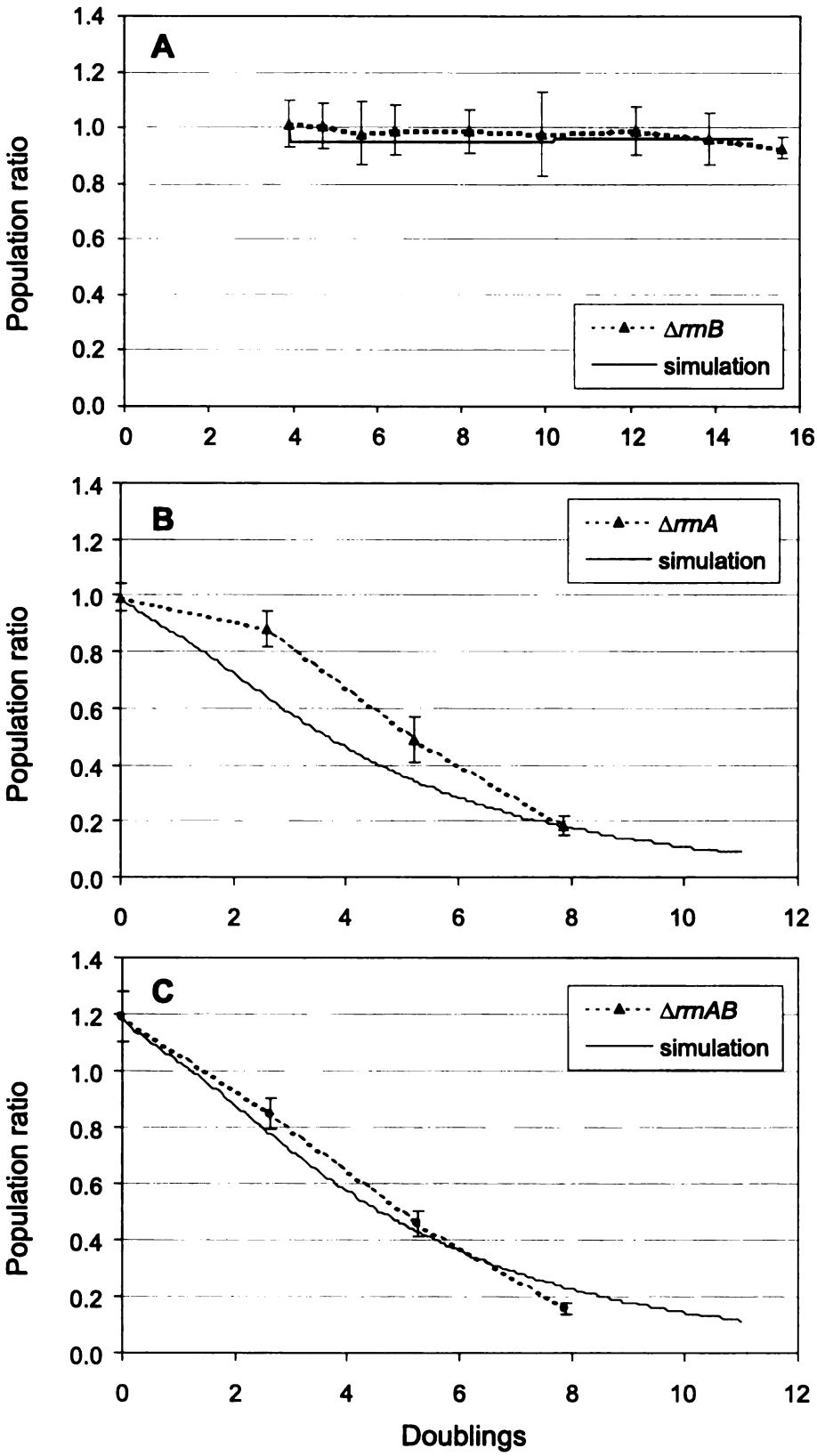
A
B
C
Population ratio
Doublings
ΔrrnB
ΔrrnA
ΔrrnAB
simulation
0.0
0.2
0.4
0.6
0.8
1.0
1.2
1.4
0
2
4
6
8
10
12
14
16

Figure 5.7

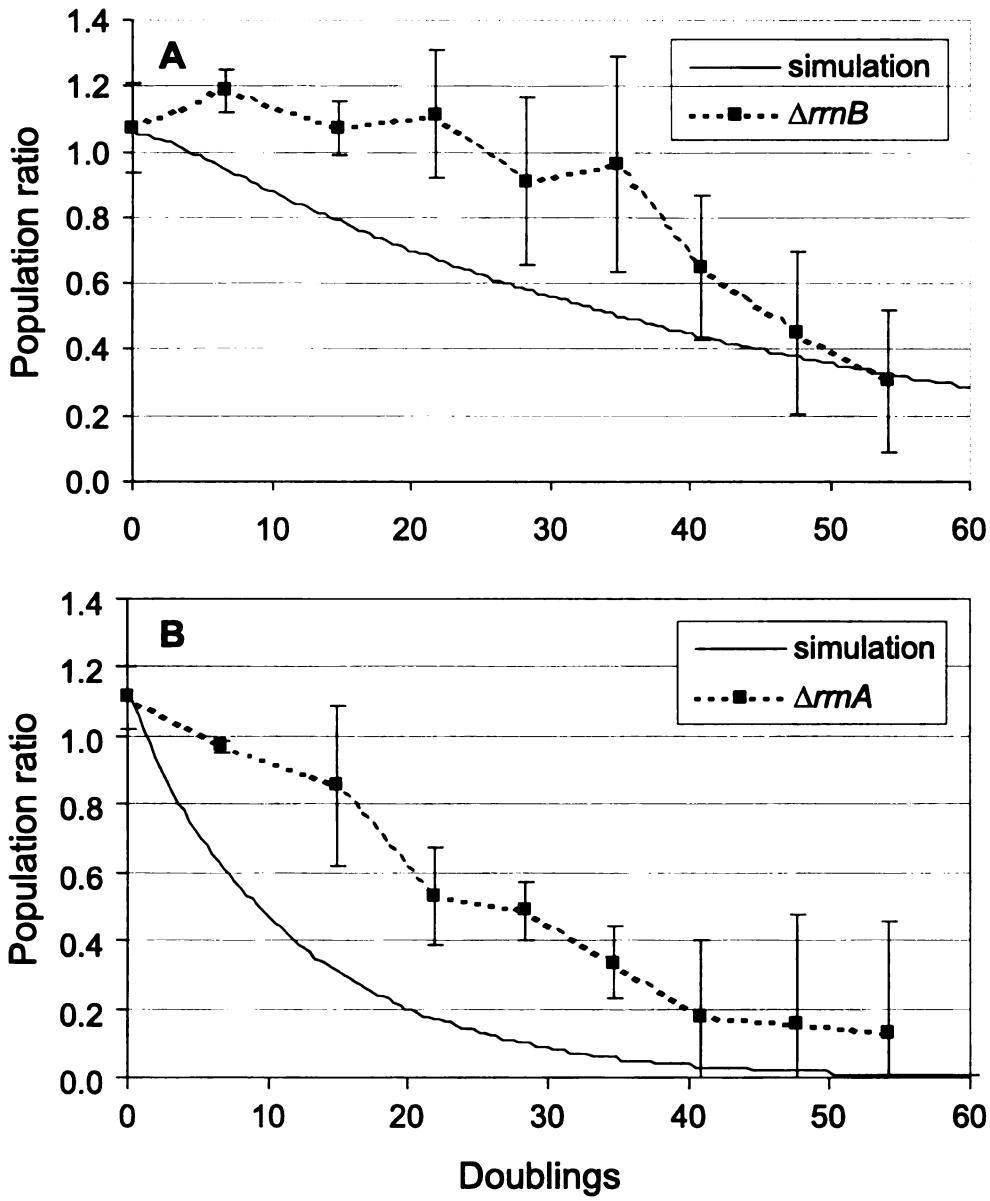

Figure 5.8 Chemostat validation at fast dilution rates. Empirical and simulation data for (A) Δ*rrnB*/Control and (B) Δ*rrnA*/Control population ratio versus doublings during fast chemostat dilution rates (0.81 h^{-1})

5.4 Discussion

The computer model reported here was designed to simulate the dynamics of two populations that are competing for a shared limiting nutrient. This model incorporated the dynamic changes in population growth and nutrient availability based upon the Monod equation, which describes the relationship between limiting nutrient concentration and specific growth rates of bacterial populations (60). The Monod equation was used because it is mathematically simple and accurately describes the relationship between nutrient concentration and growth rates under most conditions (14, 48). An object-oriented programming language and its supporting software package (STELLA, High Performance Systems, Inc.) were used to program this three-component model and all of the underlying relationships. An advantage to using this approach was the ease with which the model could be changed, expanded, and used.

A major problem in modeling is the balance of sufficient realism with complexity. If a model does not contain at least the most important mechanisms, it does not describe reality; whereas if a model is too complex, it is almost impossible to test experimentally (24, 65). No matter how complex a model may be, it is still a simplification of the more complex system being modeled. This simplification allows the most important interactions within a system to be understood, even without knowing all of the components or interactions within a system. Interactions that are incorrectly represented in the design of a model are often identified by its performance. Assumptions are made in the design of any

model, and those that are inappropriate also affect model performance. Two possible limitations of the model presented here stem from the use of the Monod equation to define the growth of a population and the accurate measurement of the growth parameters for each competing population. Specific assumptions of this computer model are that the environment is homogenous and there are no direct interactions between populations (e.g. inhibition, predation, synergism). There was also no allowance in the model for the internal storage of nutrients or the requirement of nutrients for the maintenance of viability between nutrient pulses. The above assumptions and omissions do not substantially affect the accuracy of the simulation data discussed below.

The model correctly predicted the population dynamics in both batch and chemostat culture conditions, which was evident in the nature and degree that model outcomes were sensitive to changes between the various growth parameters of each population. In batch culture conditions, there was a linear relationship between maximum specific growth rate and gains in relative fitness of a population, but smaller gains in relative fitness resulted from similar decreases in lag time (Figure 5.2). Unlike maximum growth rate and lag time, only very large changes in K_S (orders of magnitude) could result in comparable relative fitness gains. This was predictable since populations growing in batch cultures experience very low nutrient concentrations (where K_S has the largest effect on growth rate) for only a small period of time before entering stationary phase. When chemostat cultures were simulated, the sensitivity of relative fitness to changes in growth parameters was different in several ways.

Populations that are maintained in chemostat cultures are in steady state growth, and therefore lag times are no longer relevant. The relative fitness of a population was still very dependent upon maximal growth rates, regardless of dilution rates (assuming $D \leq \mu_{MAX}$) (Figure 5.3). K_S however, played a much larger role in determining relative fitness in chemostats than in batch culture conditions. Relative fitness in chemostat conditions was more sensitive to changes in K_S because populations growing in chemostats consistently experience very low concentrations of nutrients. The concentration of limiting nutrient in a chemostat vessel decreases with the dilution rate (70). At slower dilution rates therefore, relative fitness is more sensitive to differences in K_S.

The accurate simulation of competition experiments using growth parameter data from parental and evolved strains of *E. coli* (Figure 5.4 and Table 5.1) verified the performance of the model under batch culture conditions. The discrepancy between the simulation and empirical relative fitness values from Vasi et al. (76) was due to an over estimation of yield. When this was accounted for, there was no longer a difference between simulation and empirical values (76). The performance of the model under batch culture conditions was further validated by the accurate simulation of competition experiments between several strains of *E. coli* described in Chapter 4 (Table 4.1). The simulations of batch culture competition experiments that were based upon data from Chapter 4 accurately measured the relative fitness of each strain compared to empirical values (Figure 5.6).

The performance of the model was also tested under chemostat conditions by its accurate simulation of competition experiments using data from Hansen and Hubbell (37). The foremost predictive parameter for the outcome of competition under continuous culture conditions is based upon chemostat kinetics and the Monod equation. This parameter, *J* (37), represents the concentration of limiting nutrient on which a population can subsist in continuous culture at a given dilution rate. According to chemostat theory, the population with the lowest *J* value will out-compete all others with higher *J* values (37, 75). Two populations with equal *J* values are predicted to coexist, even if they have different values for μ_{MAX} and K_S (37). The model successfully predicted all of the above-mentioned outcomes (Table 5.2, Figure 5.5). The model performance under chemostat conditions was validated by its ability to accurately predict the outcome of all the chemostat competition experiments described in Chapter 4, with the possible exception of Δ*rrnB* versus the control strain at a slow dilution rate (Table 5.3, Figure 5.7 and 5.8).

Unlike the Δ*rrnA* and Δ*rrnAB* strains, the measured K_S of Δ*rrnB* was conspicuously lower than the control strain. Comparison of the model simulations with the empirical competition experiments suggests that the K_S is higher for Δ*rrnB* or lower for the control than measured. The compliance of batch culture and fast chemostat simulations to empirical results suggests that measurements of maximum growth rate and lag time are accurate for Δ*rrnB*. Based upon its measured K_S value, Δ*rrnB* is predicted to outcompete the control strain at slow dilution rates (Table 5.3, Figure 5.7A), where K_S has a larger effect

on relative fitness. This predicted outcome does not occur in the empirical experiments, suggesting that the accuracy of the K_S measurements was exceeded under the slow dilution rate chemostat competition experiments between Δ*rrnB* and the control strain. The K_S measurements are relatively accurate considering that reported K_S values for *E. coli* can differ by orders of magnitude depending on the strain, the history of the culture, and the laboratory in which the measurements were made (70). The simulation results of the slow dilution rate competition experiments between Δ*rrnB* and the control illustrate how the model can be used to identify inaccurate parameter values.

This model contributes to the study of microbial ecology in several ways. It offers tremendous power in predicting the outcome of direct competitions between populations for a limiting nutrient through the use of growth characteristics measured in pure culture, thus eliminating the need for mixed cultures. The comparison of empirical to simulation results can also be used as an indication of other parameters that may be affecting the competition (production of inhibitory compounds, cross feeding, etc.). The limitations of the model are also linked to its attributes. The accuracy of growth parameters determined in pure culture can have an impact on the predicted outcomes, especially in the case of maximal growth rate and K_S (70). These variables are determined during steady state growth in batch cultures and K_S for instance, may actually change during chemostat or non-equilibrium conditions (35, 49). Further study of the assumptions behind these measured growth parameters and their effect on modeled systems would increase the accuracy and dependability of

predictions made by the model, and could provide useful insight into the forces that drive population dynamics during resource competition.

CHAPTER 6

SUMMARY AND CONCLUSIONS

The research in this dissertation investigated the role of rRNA operon copy number as a life history trait and its connection with competitive ability in prokaryotes. Several central observations about rRNA operon copy number in prokaryotes suggest this trait should be considered in terms of the life history of a species. Multiple copies of the rRNA operons can be found on the chromosome of certain prokaryotes, whereas almost all other genes are present as single copies. The number of rRNA operons is highly conserved among isolates of the same species (as in 13) with a few known exceptions (4, 43). Although conserved among isolates of the same species, rRNA operon copy number is not strictly conserved between different species, regardless of phylogeny (69). The strict conservation of rRNA operon copy numbers within a species but not between different species is a common pattern for life history.

The hypotheses tested in this dissertation were based on the presumption that the number of rRNA operons in prokaryotes is largely an adaptation to environmental conditions; genome size, genetic drift, and phylogenetic constraints are not major deterministic factors (see Chapter 1). The first hypothesis states that multiple rRNA operons are an advantage in environments that are defined by fluctuations in nutrient availability. The advantage of multiple rRNA operons is thought to be due to higher rates of rRNA synthesis that permit quicker responses to favorable growth conditions and faster growth rates. The

second hypothesis states that fewer rRNA operons are an advantage in environments with stable, limiting nutrient availability, and is based on the metabolic expense of over-expressing multiple rRNA operons at slow growth rates.

To test these hypotheses, the effect of rRNA operon copy number on cell physiology and competitive ability was measured in otherwise isogenic strains of *E. coli*. The number of rRNA operons was manipulated in these strains by either the introduction of rRNA operon-containing plasmids (Chapter 2, (74)), or the deletion of one or two rRNA operons from the chromosome (Chapter 3). In previous studies, strains of *E. coli* containing manipulations of the rRNA operons were used to test the effect of rRNA operon copy number on various aspects of cell physiology. The strains constructed in these previous studies were unsuitable for the experiments in this dissertation because of the methods used to manipulate rRNA operon copy numbers, and therefore, some of the results of the previous studies are also called into question. Some limitations of using plasmid-borne rRNA operons, as in (41) and Chapter 2 (74), are that the plasmid copy number is either unknown or can vary, the plasmid can be lost without proper selection, and the present rRNA operon copy number can only be increased, not decreased. Other alterations of *E. coli* rRNA operons either contained additional antibiotic resistance genes that were expressed from the promoters of the inactivated rRNA operon (18), produced truncated rRNA transcripts from intact promoters of partially deleted rRNA operons (3, 5), or affected adjacent genes on the chromosome (23). The experiments in this

dissertation required that the effect of altering rRNA operon copy numbers be discernable from the secondary effects of manipulating the rRNA operons on the chromosome. It was therefore necessary to construct new strains with deletions of the chromosome that included the rRNA promoters and a large portion of the rRNA operon, but not other genes (discussed in Chapter 3). The effect of altering the rRNA operon copy number on cell physiology and competitive ability was directly measured in the resulting strains because the known promoters of effected rRNA operons were deleted and other genes on the chromosome were not disrupted.

It was postulated that the seven rRNA operons of *E. coli* are linked to the cell's ability to respond quickly to fluctuations in nutrient availability (1, 47). Direct evidence for this connection was the increased amount of time a strain of *E. coli* required to respond to more favorable growth conditions after the inactivation of rRNA operons (17). The inactivation of up to four of the seven rRNA operons did not have "a significant impact" upon maximal growth rates (17), which led to the conclusion that the benefit of *E. coli*'s multiple rRNA operons was not higher maximal growth rates, but quicker responses to fluctuations in nutrient availability. Unfortunately, the strains used in this study leave some doubt as to whether the increased amount of time it took for a strain to respond to favorable growth conditions was due to having fewer intact rRNA operons or expressing the additional antibiotic resistance genes used to inactivate the rRNA operons.

The results from Chapter 4 support the connection between rRNA operon copy number and *E. coli's* ability to respond quickly to fluctuating nutrient availability (Chapter 4, Table 4.1). There is also a correlation between rRNA operon copy number and relative fitness in batch culture competition experiments (Chapter 4, Figure 4.4), which further supports the hypothesis that multiple rRNA operons were an advantage when nutrient availability fluctuates. When compared to Δ*rrnAB*, the higher relative fitness of the control strain (7 rRNA operons) in batch culture conditions was largely due to its ability to more quickly respond to an influx of nutrients (i.e. shorter lag time). Relative fitness, as measured in batch culture competition experiments, can be largely affected by seemingly minor differences in lag time and maximal growth rate between two competing populations. The relative impact of each growth parameter is illustrated in the batch culture sensitivity analyses of the computer model (Chapter 5, Figure 5.2), and their effect on empirical relative fitness measurements (Chapter 4, Figure 4.8).

Increasing the rRNA operon copy number of *E. coli* by the addition of plasmid-borne rRNA operons had a negative effect on growth rate, accompanied by an over expression of RNA, in media that supported slow doubling times (Chapter 2, 74). These data suggested that multiple rRNA operons are a metabolic burden at slow growth rates. A decrease in this metabolic burden however, was not measured with strains containing fewer rRNA operons in chemostat competition experiments (Chapter 4, Figures 4.5-4.7). Under the chemostat conditions tested, strains of *E. coli* with fewer rRNA operons were not

at an advantage in environments with stable nutrient conditions. These results suggest that, under stable slow growth conditions, multiple rRNA operons in *E. coli* are not a metabolic expense that can be relieved by deleting two of its seven rRNA operons. These cells can either control the level of constitutive expression equally well from 5 and 7 rRNA operons, or the decrease in metabolic expense could not compensate for some detrimental effect of deleting the rRNA operons.

The number of rRNA operons on the chromosome of a prokaryotic species may be a component of its life history. An observed life history is the lifetime pattern of growth, differentiation, storage and, most importantly, reproduction. The availability of nutrients is arguably one of the major selective forces imposed upon populations of prokaryotes. The effect of rRNA copy number on *E. coli* in batch culture competition experiments suggests that multiple rRNA operons contribute to *E. coli's* fitness in environments characterized by fluctuating nutrient availability. The hypotheses tested in this dissertation would extend these findings to all prokaryotic species and suggest that the number of rRNA operons on the chromosome is an indication of the life history of a prokaryotic species. These hypotheses are also supported by the correlation between rRNA operon copy number and the rate of colony appearance of soil isolates (46). After spreading a soil sample onto dilute nutrient agar, isolates that form visible colonies in the first few days have about 5 rRNA operons, whereas isolates that form colonies up to two weeks later have 1 to 2 rRNA operons on their chromosomes.

Additional circumstantial evidence that support the hypotheses of this dissertation can be found in the abundant examples in which the number of rRNA operons on the chromosome of certain prokaryotes coincide with their presumed life history. Prokaryotic species such as the bioluminescent symbiont *Kryptophanaron alfredi* from the Caribbean flashlight fish (78), the parasitic mycoplasmas (2) and mycobacteria (31), and the marine oligotrophic ultramicrobacterium *Sphingomonas* sp. strain RB2256 (25) have one to two rRNA operons. These prokaryotes exist in stable and/or poor nutrient environments, tend to have relatively slow growth rates, and respond slowly, if at all, to fluctuations in nutrient availability. Prokaryotic species with a relatively high number of rRNA operons on their chromosome include *E. coli* with 7, *Vibrio* spp. with 8 to 10, and *Bacillus subtillus* with 10 rRNA operons. Compared to the prokaryotes with one or two rRNA operons listed above, these high rRNA operon copy number prokaryotes tend to respond more quickly to fluctuations in nutrient availability with relatively fast growth rates.

It is necessary to consider other possible explanations for the experimental results in this dissertation. One step of the procedure used to delete the rRNA operons in this study could have led to the incorporation of donor DNA other than the intended allele during generalized transduction with phage P1 (discussed in Chapter 3). The deletion of rRNA operons in this study needs to be complemented by replacing the deleted region of the chromosome with the full rRNA operon. The resulting strains would therefore be "reconstructed" controls that would allow any effect of co-transformed DNA

regions to be directly measured and accounted for. Also as discussed in Chapter 4, it is not possible to distinguish the effect of the deletion of rRNA genes from the deletion of tRNA genes on the *rrnA* and *rrnB* operons. Interestingly, there was a much larger effect when the *rrnA* operon was deleted from the chromosome of *E. coli* than when the *rrnB* operon was deleted, which was most obvious under slow dilution rate chemostat conditions (Chapter 4, Figure 4.5). Previously, the effect of deleting tRNA genes along with the rest of the rRNA operons was not apparent, but it is possible that the secondary effects of rRNA operon deletions could have obscured the impact of deleting the tRNA genes in these studies. Additionally, the effects of rRNA operon deletions have not been studied in chemostats at dilution rates as slow as in this dissertation (0.11 h^{-1}).

Deleting the *rrnA* operon in the Δ*rrnA* and Δ*rrnAB* strains resulted in a much larger decrease in relative fitness than measured for the Δ*rrnB* strain in chemostat competition experiments with slow dilution rates (Chapter 4, Figure 4.5). The large decrease in relative fitness was due to an increase in K_S for both *rrnA* deletion strains. Also at slow dilution rates, Δ*rrnA* and Δ*rrnAB* strains had lower yields and larger cell volumes than either the Δ*rrnB* or control strains (Chapter 4, Figure 4.3). A possible explanation for these results is presented in Chapter 4, which suggests that the tRNA genes present in the internally transcribed spacer (ITS) regions of the *rrnA* and *rrnB* operons may be causing the measured effects.

The *rrnA* ITS region contains the two tRNA genes $tRNA^{Ala}_{1B}$ and $tRNA^{Ile}_{1}$ whereas, the *rrnB* ITS region contains $tRNA^{Glu}_{2}$ gene. The tRNA genes in each

rRNA operon ITS region represent three of the most abundant and most frequently used tRNAs in the cell. There is a direct correlation between the number of copies of each tRNA gene and the concentration of their respective tRNAs. Additionally, the molar ratio of tRNA per ribosome increases as growth rate decreases (21). All of these factors may explain why a disruption in the tRNA gene pool could cause large effects under slow chemostat conditions, as with the *rrnA* operon. The differential effect of deleting *rrnA* or *rrnB* could be related to the two tRNA genes in the *rrnA* ITS region, which are present in only three copies on the chromosome, versus the single tRNA gene in the *rrnB* ITS region that is present in four copies.

It is also possible that either the expression or the products of the *rrnA* operon are somehow more essential under the slow growth, low nutrient conditions of the slow dilution rate chemostats. Specialization of rRNA operons might occur when multiple rRNA operons are maintained on the same chromosome. Any detrimental effect of mutations in one copy of an essential gene might be lessened by the expression of remaining unaffected copies on the same chromosome. The specialization of rRNA operons in *E. coli* could also explain the data in Chapter 4, which showed a substantial negative effect on relative fitness when *rrnA* was deleted, but not *rrnB*. Previous studies suggest there is some differential expression of *E. coli's* seven rRNA operons (up to 1.4-fold), but not specifically between the *rrnA* and *rrnB* operons (18). The expression of individual *E. coli* rRNA operons however, has not been

investigated under the slow chemostat conditions used in the research reported here.

The work in this dissertation highlights the differential effect between complete deletions of the *rrnA* and *rrnB* operons at slow growth rates. Previously, the deletion of tRNA genes along with the rest of the rRNA operon was considered to play only a minor role as long as intact copies of these genes either remained elsewhere on the chromosome (17) or were provided on a plasmid (5). The results of this dissertation illustrate the importance of discerning the effect of deleting tRNA genes from deleting the rRNA genes on an rRNA operon. Work continues in an effort to identify which portions of the *rrnA* operon (including the tRNA genes) can be linked to the phenotype observed in the Δ*rrnA* and Δ*rrnAB* strains.

APPENDIX A

P1*vir* LYSATE PREPARATION

The protocol for the preparation of P1*vir* lysates was adapted from L. Snyder (personal communication), and uses LB agar plates with a LB soft agar overlay. A culture of donor cells that was in late log or early stationary growth phase in LB was amended to 1 mM $CaCl_2$ from a 1 M stock. A 100 µl aliquot of the amended culture and 50 ml of phage P1*vir* at a titer of approximately 10^9-10^{10} PFU/ml was added to 5 ml of soft agar also amended to 1 mM $CaCl_2$. The soft agar was mixed and then poured onto moist LB_{Kan} agar. These overlayed plates were incubated overnight at 37°C. Three discernable, isolated plaques were picked with sterile toothpicks, which were then placed in 0.2 ml sterile saline (amended to 1 mM $CaCl_2$) in a sterile 14 ml disposable polypropylene culture tube. The phage were allowed to diffuse away from the toothpicks into the saline for 30 min to several hours. Next, 50 µl of donor bacteria (as above) was added and the phage were allowed to adsorb to the bacteria for 3 min. After the phage had adsorbed to the donor bacteria, 3 ml of soft agar (50°C, 1 mM $CaCl_2$) was added, mixed, poured onto an LB_{Kan} agar plate, and incubated overnight at 37°C. When confluent plaques are visible, 4 ml of sterile saline was layered on the agar surface and the phage are allowed to diffuse into the saline at 4°C overnight. The saline is then decanted into a sterile polypropylene centrifuge tube and centrifuged for 10 min at 5,000 x g and 4°C to pellet any bacterial cells and

debris. The supernatant is decanted into a fresh centrifuge tube and 100 µl of chlorophorm is added to lyse any remaining bacteria. The phage titer of the lysate was determined (usually 10^9 to 10^{10} PFU/ml) and transduction was performed as described in Chapter 3.

APPENDIX B

VISUALIZATION OF rRNA OPERONS USING SOUTHERN HYBRIDIZATION

Approximately 1 μg of genomic DNA was digested with 10-20 units of the restriction endonuclease *Pvu*II in a total volume of 50 μl at 37°C for >2 hours to allow for complete digestion. There is one *Pvu*II restriction site in the 23S gene of all seven rRNA operons, and one in the ITS region of *rrnA, D,* and *H.* A second restriction site lies upstream of the rRNA operons, giving each 16S-containing restriction fragment a different, distinctive size. Each of the 16S-containing fragments represents an rRNA operon and can be resolved by electrophoresis on an agarose gel (0.6% agarose in 0.5x TBE buffer). By using the *E. coli* genome sequence to find each unique upstream restriction site, the expected fragment size of each rRNA operon was determined and used for positive identification of each operon.

The separated DNA fragments were transferred to a Magnacharge nylon transfer membrane (Micron Separations Inc.; Westborough, MA) using the VacuGene XL Vacuum Blotting System (Amersham Pharmacia Biotech; Piscataway, NJ). The vacuum blotting was performed with a vacuum of 50 mbar, using the protocol provided with the vacuum blotting system. The DNA was then UV cross-linked to the membrane using the Stratlinker UV Crosslinker, model 1800 (Stratagene; La Jolla, CA) and the autocrosslink function (120 mjoules/cm^2 from a 254 nm light source).

Hybridization of the probe to the target DNA, post-hybridization washing of the membrane, and detection of the probe was all performed according to the protocols provided with the DIG High Prime labeling and detection kit (Boehringer Mannheim Corporation (BMB); Indianapolis, IN). The probe used to hybridize the 16S-containing fragments was synthesized by PCR-amplification of *E. coli* 16S DNA with the universal Eubacterial primers 8 Forward (5'-AGAGTTTGATCCTGGCTCAG-3') and 519 Reverse (5'-GTATTACCGCGGCTGCTGG-3'), resulting in a DNA fragment that is homologous with a conserved region (positions 8-356) of the *E. coli* 16S rDNA gene. This probe was labeled with digoxigenen-dUTP following the protocol provided with the DIG High Prime labeling and detection kit. After 12-16 hours of hybridization, post-hybridization washes, and the addition of the detection (CSPD) reagent, the membrane was wrapped in Saran Wrap and exposed to Lumi-Film Chemiluminescent Detection Film (BMB) for 30-60 min. The individual rRNA operons, if present, were visualized after the film was developed.

APPENDIX C

STATISTICAL ANALYSES OF RELATIVE FITNESS VALUES IN BATCH CULTURE COMPETITION EXPERIMENTS

The differences between mean relative fitness values of each strain were analyzed for significance using a single factor ANOVA and planned comparisons among means (73). The ANOVA showed a significant difference among the mean relative fitness values ($F_{3,28} = 11.18$, $P = 5.35 \times 10^{-5}$). The planned comparisons showed which differences were significant, and were based upon predetermined hypotheses about the effect of rRNA operon deletions on relative fitness in batch culture competition experiments. Table C.1 shows the comparisons, the *F* statistic, and whether the difference can be considered significant.

Table C.1

Comparison	$F_{1,24}$	Significance[a]
Control vs. Δ*rrnA* and Δ*rrnB*	6.06	***
Control vs. Δ*rrnAB*	32.46	***
Δ*rrnA* and Δ*rrnB* vs. Δ*rrnAB*	16.95	***
Δ*rrnA* vs. Δ*rrnB*	0.05	NS
Δ*rrnA* vs. Δ*rrnAB*	13.54	***
Δ*rrnB* vs. Δ*rrnAB*	11.92	***

[a] *** indicates $P < 0.025$, NS indicates not significant or $P > 0.1$

REFERENCES

1. **Alton, T. H., and A. L. Koch.** 1974. Unused protein synthetic capacity of *Escherichia coli* grown in phosphate-limited chemostats. J Mol Biol. **86**(1):1-9.

2. **Amikam, D., G. Glaser, and S. Razin.** 1984. Mycoplasmas (Mollicutes) have a low number of rRNA genes. J Bacteriol. **158**(1):376-8.

3. **Ammons, D., J. Rampersad, and G. E. Fox.** 1999. 5S rRNA gene deletions cause an unexpectedly high fitness loss in *Escherichia coli.* Nucleic Acids Res. **27**(2):637-42.

4. **Anderson, P., and J. Roth.** 1981. Spontaneous tandem genetic duplications in *Salmonella typhimurium* arise by unequal recombination between rRNA (*rrn*) cistrons. Proc Natl Acad Sci U S A. **78**(5):3113-7.

5. **Asai, T., C. Condon, J. Voulgaris, D. Zaporojets, B. Shen, M. Al-Omar, C. Squires, and C. L. Squires.** 1999. Construction and initial characterization of *Escherichia coli* strains with few or no intact chromosomal rRNA operons. J Bacteriol. **181**(12):3803-9.

6. **Asai, T., D. Zaporojets, C. Squires, and C. L. Squires.** 1999. An *Escherichia coli* strain with all chromosomal rRNA operons inactivated: complete exchange of rRNA genes between bacteria [see comments]. Proc Natl Acad Sci U S A. **96**(5):1971-6.

7. **Bachellier, S., E. Gilson, M. Hofnung, and C. W. Hill.** 1996. Repeated sequences, p. 2015-7. *In* F. C. Neidhardt, R. C. III, J. L. Ingraham, E. C. C. Lin, K. B. Low, B. Magasanik, W. S. Reznikoff, M. Riley, M. Schaechter, and H. E. Umbarger (ed.), *Escherichia coli* and *Salmonella typhimurium*: Cellular and Molecular Biology, vol. 2. ASM Press, Washington, DC.

8. **Baracchini, E., and H. Bremer.** 1991. Control of rRNA synthesis in *Escherichia coli* at increased *rrn* gene dosage. Role of guanosine tetraphosphate and ribosome feedback. J Biol Chem. **266**(18):11753-60.

9. **Begon, M., J. L. Harper, and C. R. Townsend.** 1996. Ecology, 3rd ed. Blackwell Sciences International, Oxford, UK.

10. **Blomfield, I. C., V. Vaughn, R. F. Rest, and B. I. Eisenstein.** 1991. Allelic exchange in *Escherichia coli* using the *Bacillus subtilis sacB* gene and a temperature-sensitive pSC101 replicon. Mol Microbiol. **5**(6):1447-57.

11. **Bremer, H., and P. P. Dennis.** 1996. Modulation of chemical composition, p. 1561-1562. *In* F. C. Neidhardt, R. C. III, J. L. Ingraham, E. C. C. Lin, K. B. Low, B. Magasanik, W. S. Reznikoff, M. Riley, M. Schaechter, and H. E. Umbarger (ed.), *Escherichia coli* and *Salmonella typhimurium*: Cellular and Molecular Biology, 2 ed, vol. 2. ASM Press, Wahsington, DC.

12. **Brosius, J., A. Ullrich, M. A. Raker, A. Gray, T. J. Dull, R. R. Gutell, and H. F. Noller.** 1981. Construction and fine mapping of recombinant plasmids containing the *rrnB* ribosomal RNA operon in *Escherichia coli.* Plasmid. **6:**112-118.

13. **Bruce, J. L., R. J. Hubner, E. M. Cole, C. I. McDowell, and J. A. Webster.** 1995. Sets of EcoRI fragments containing ribosomal RNA sequences are conserved among different strains of *Listeria monocytogenes* [published erratum appears in Proc Natl Acad Sci U S A 1995 Oct 24;92(22):10441]. Proc Natl Acad Sci U S A. **92**(11):5229-33.

14. **Button, D. K.** 1985. Kinetics of nutrient-limited transport and microbial growth. Microbiol Rev. **49**(3):270-97.

15. **Carlton, B. C., and B. J. Brown.** 1981. Gene Mutation, p. 222-242. *In* P. Gerhardt (ed.), Manual of methods for general bacteriology. American Society for Mirobiology, Washington, D.C.

16. **Condon, C., S. French, C. Squires, and C. L. Squires.** 1993. Depletion of functional ribosomal RNA operons in *Escherichia coli* causes increased expression of the remaining intact copies. Embo J. **12**(11):4305-15.

17. **Condon, C., D. Liveris, C. Squires, I. Schwartz, and C. L. Squires.** 1995. rRNA operon multiplicity in *Escherichia coli* and the physiological implications of *rrn* inactivation. J Bacteriol. **177**(14):4152-6.

18. **Condon, C., J. Philips, Z. Y. Fu, C. Squires, and C. L. Squires.** 1992. Comparison of the expression of the seven ribosomal RNA operons in *Escherichia coli.* Embo J. **11**(11):4175-85.

19. **Condon, C., C. Squires, and C. L. Squires.** 1995. Control of rRNA transcription in *Escherichia coli.* Microbiol Rev. **59**(4):623-45.

20. **Daniels, L., R. S. Hanson, and J. A. Phillips.** 1994. Chemical Analysis, p. 512-554. *In* P. Gerhardt (ed.), Methods for General and Molecular Bacteriology. American Society for Microbiology, Wahsington, D. C.

21. **Dong, H., L. Nilsson, and C. G. Kurland.** 1996. Co-variation of tRNA abundance and codon usage in *Escherichia coli* at different growth rates. J Mol Biol. **260**(5):649-63.

22. **Ellwood, M., and M. Nomura.** 1982. Chromosomal locations of the genes for rRNA in *Escherichia coli* K-12. J Bacteriol. **149**(2):458-68.

23. **Ellwood, M., and M. Nomura.** 1980. Deletion of a ribosomal ribonucleic acid operon in *Escherichia coli.* J Bacteriol. **143**(2):1077-80.

24. **Essener, A. A., J. A. Roels, and N. W. F. Kossen.** 1983. Theory and application of unstructured growth models: Kinetic and energetic aspects. Biotechnol. Bioeng. **25**:2803-2841.

25. **Fegatella, F., J. Lim, S. Kjelleberg, and R. Cavicchioli.** 1998. Implications of rRNA operon copy number and ribosome content in the marine oligotrophic ultramicrobacterium Sphingomonas sp. strain RB2256. Appl Environ Microbiol. **64**(11):4433-8.

26. **Fleischmann, R. D., M. D. Adams, O. White, R. A. Clayton, E. F. Kirkness, A. R. Kerlavage, C. J. Bult, J. F. Tomb, B. A. Dougherty, J. M. Merrick, and et al.** 1995. Whole-genome random sequencing and assembly of *Haemophilus influenzae* Rd [see comments]. Science. **269**(5223):496-512.

27. **Fogel, G. B., C. R. Collins, J. Li, and C. F. Brunk.** 1999. Prokaryotic genome size and SSU rDNA copy number: Estimation of microbial relative abundance from a mixed population. Microb Ecol. **38**(2):93-113.

28. **Garrett, R. A., J. Dalgaard, N. Larsen, J. Kjems, and A. S. Mankin.** 1991. Archaeal rRNA operons. Trends Biochem Sci. **16**(1):22-6.

29. **Gay, P., D. Le Coq, M. Steinmetz, T. Berkelman, and C. I. Kado.** 1985. Positive selection procedure for entrapment of insertion sequence elements in gram-negative bacteria. J Bacteriol. **164**(2):918-21.

30. **Gay, P., D. Le Coq, M. Steinmetz, E. Ferrari, and J. A. Hoch.** 1983. Cloning structural gene *sacB*, which codes for exoenzyme levansucrase of *Bacillus subtilis*: expression of the gene in *Escherichia coli*. J Bacteriol. **153**(3):1424-31.

31. **Gonzalez-y-Merchand, J. A., M. J. Garcia, S. Gonzalez-Rico, M. J. Colston, and R. A. Cox.** 1997. Strategies used by pathogenic and nonpathogenic mycobacteria to synthesize rRNA. J Bacteriol. **179**(22):6949-58.

32. **Gourse, R. L., T. Gaal, M. S. Bartlett, J. A. Appleman, and W. Ross.** 1996. rRNA transcription and growth rate-dependent regulation of ribosome synthesis in *Escherichia coli*. Annu Rev Microbiol. **50**:645-77.

33. **Gourse, R. L., and M. Nomura.** 1984. Level of rRNA, not tRNA, synthesis controls transcription of rRNA and tRNA operons in *Escherichia coli*. J Bacteriol. **160**(3):1022-6.

34. **Gourse, R. L., Y. Takebe, R. A. Sharrock, and M. Nomura.** 1985. Feedback regulation of rRNA and tRNA synthesis and accumulation of free ribosomes after conditional expression of rRNA genes. Proc Natl Acad Sci U S A. **82**(4):1069-73.

35. **Grover, J. P.** 1991. Resource competition in a variable environment: Phytoplankton growing according to the variable-internal-stores model. Am. Nat. **138**(4):811-835.

36. **Hamilton, C. M., M. Aldea, B. K. Washburn, P. Babitzke, and S. R. Kushner.** 1989. New method for generating deletions and gene replacements in *Escherichia coli*. J Bacteriol. **171**(9):4617-22.

37. **Hansen, S. R., and S. P. Hubbell.** 1980. Single-nutrient microbial competition: qualitative agreement between experimental and theoretically forecast outcomes. Science. **207**(4438):1491-3.

38. **Herzer, P. J., S. Inouye, M. Inouye, and T. S. Whittam.** 1990. Phylogenetic distribution of branched RNA-linked multicopy single-stranded DNA among natural isolates of Escherichia coli. J Bacteriol. **172**(11):6175-81.

39. **High Performance Systems, I.** 1997. Stella Technical Documentation. High Performance Systems, Inc., Hanover, NH.

40. **Hill, C. W., S. Harvey, and J. A. Gray.** 1990. Recombination between rRNA genes in *Escherichia coli* and *Salmonella typhimurium*, p. 335-340. *In* K. Drlica and M. Riley (ed.), The Bacterial Chromosome. American Society for Microbiology, Washington, D.C.

41. **Jinks-Robertson, S., R. L. Gourse, and M. Nomura.** 1983. Expression of rRNA and tRNA genes in *Escherichia coli*: evidence for feedback regulation by products of rRNA operons. Cell. **33**(3):865-76.

42. **Jinks-Robertson, S., and M. Nomura.** 1987. Ribosomes and tRNA, p. 1358-1385. *In* F. C. Neidhardt, J. L. Ingraham, K. B. Low, B. Magasanik, M. Schaechter, and H. E. Umbarger (ed.), *Escherichia coli* and *Salmonella typhimurium*: Cellular and Molecular Biology, 2 ed, vol. 2. American Society for Microbiology Press, Washington D.C.

43. **Khetawat, G., R. K. Bhadra, S. Nandi, and J. Das.** 1999. Resurgent *Vibrio cholerae* O139: rearrangement of cholera toxin genetic elements and amplification of *rrn* operon. Infect Immun. **67**(1):148-54.

44. **Kingston, R. E., R. R. Gutell, A. R. Taylor, and M. J. Chamberlin.** 1981. Transcriptional mapping of plasmid pKK3535: quantitation of the effect of guanosine tetraphsophate on binding to the *rrnB* promoters and a λ promoter with sequence homologies to the CII binding region. J Mol Biol. **146**:433-449.

45. **Kiss, A., B. Sain, and P. Venetianer.** 1977. The number of rRNA genes in *Escherichia coli*. FEBS Lett. **79**(1):77-9.

46. **Klappenbach, J. A., J. M. Dunbar, and T. M. Schmidt.** 2000. Ribosomal RNA operon copy number reflects ecological strategies of bacteria. Appl Environ Microbiol. **66**(4).

47. **Koch, A. L.** 1971. The adaptive responses of *Escherichia coli* to a feast and famine existence. Adv Microb Physiol. **6**:147-217.

48. **Koch, A. L.** 1982. Multistep kinetics: choice of models for the growth of bacteria. J Theor Biol. **98**(3):401-17.

49. **Kovarova-Kovar, K., and T. Egli.** 1998. Growth kinetics of suspended microbial cells: from single-substrate- controlled growth to mixed-substrate kinetics. Microbiol Mol Biol Rev. **62**(3):646-66.

50. **Kundig, C., H. Hennecke, and M. Gottfert.** 1993. Correlated physical and genetic map of the *Bradyrhizobium japonicum* 110 genome. J Bacteriol. **175**(3):613-22.

51. **Lederberg, S.** 1966. Genetics of host-controlled restriction and modification of dioxyribonulceic acid in *Escherichia coli.* J Bacteriol. **91**(3):1029-1036.

52. **Lenski, R. E.** 1988. Experimental studies of pleiotropy and epistasis in *Escherichia coli.* I. Variation in competitive fitness among mutants resistant to virus T4. Evolution. **42**:433-440.

53. **Lenski, R. E., J. A. Mongold, P. D. Sniegowski, M. Travisano, F. Vasi, P. J. Gerrish, and T. M. Schmidt.** 1998. Evolution of competitive fitness in experimental populations of E. coli: what makes one genotype a better competitor than another? Antonie Van Leeuwenhoek. **73**(1):35-47.

54. **Lenski, R. E., M. R. Rose, S. C. Simpson, and S. C. Tadler.** 1991. Long-term experimental evolution in *Escherichia coli.* I. Adaptation and divergence during 2,000 generations. Am Nat. **138**(6):1315-1341.

55. **Lenski, R. E., V. Souza, L. P. Duong, Q. G. Phan, T. N. M. Nguyen, and K. P. Bertrand.** 1994. Epistatic effects of promoter and repressor functions of the Tn10 tetracycline-resistance operon on the fitness of *Escherichia coli.* Mol Ecol. **3**:127-135.

56. **Lenski, R. E., and M. Travisano.** 1994. Dynamics of adaptation and diversification: a 10,000-generation experiment with bacterial populations. Proc Natl Acad Sci U S A. **91**(15):6808-14.

57. **Levin, B. R., F. M. Stewart, and L. Chao.** 1977. Resource-limited growth, competition, and predation: a model and experimental studies with bacteria and bacteriophage. Am Nat. **111**:3-24.

58. **Milkman, R.** 1996. Recombinational exchange among clonal populations, p. 2663-2684. *In* F. C. Neidhardt, R. C. III, J. L. Ingraham, E. C. C. Lin, K. B. Low, B. Magasanik, W. S. Reznikoff, M. Riley, M. Schaechter, and H. E. Umbarger (ed.), *Escherichia coli* and *Salmonella typhimurium*: Cellular and Molecular Biology, 2 ed, vol. 2. ASM Press, Wahsington, DC.

59. **Miller, J. H.** 1972. Experiments in Molecular Genetics, p. 201-205. Cold Spring Harbor Laboratory, Cold Spring Harbor, NY.

60. **Monod, J.** 1949. The growth of bacterial cultures. Ann Rev Microbiol. **3**:371-394.

61. **Morgan, E. A., T. Ikemura, L. Lindahl, A. M. Fallon, and M. Nomura.** 1978. Some rRNA operons in *E. coli* have tRNA genes at their distal ends. Cell. **13**(2):335-44.

62. **Morgan, E. A., T. Ikemura, and M. Nomura.** 1977. Identification of spacer tRNA genes in individual ribosomal RNA transcription units of *Escherichia coli*. Proc Natl Acad Sci U S A. **74**(7):2710-4.

63. **Poulsen, L. K., T. R. Licht, C. Rang, K. A. Krogfelt, and S. Molin.** 1995. Physiological state of *Escherichia coli* BJ4 growing in the large intestines of streptomycin-treated mice. J Bacteriol. **177**(20):5840-5.

64. **Provence, D. L., and R. C. III.** 1994. Gene transfer in Gram-negative bacteria, p. 332-334. *In* P. Gerhardt, R. G. E. Murray, W. A. Wood, and N. R. Kreig (ed.), Methods for General and Molecular Bacteriology. ASM Press, Washington, DC.

65. **Roels, J. A., and N. W. F. Kossen.** 1978. On the modeling of microbial metabolism. Prog Indust Microbiol. **14**:95-203.

66. **Russell, C. B., D. S. Thaler, and F. W. Dahlquist.** 1989. Chromosomal transformation of *Escherichia coli recD* strains with linearized plasmids. J Bacteriol. **171**(5):2609-13.

67. **Sambrook, J.** 1989. Appendix A: Bacterial media, antibiotics, and bacterial strains, p. A.1-A.6. *In* E. F. Fritsch and T. Maniatis (ed.), Molecular Cloning: A Laboratory Manual, 2 ed, vol. 3. Cold Spring Harbor Laboratory Press, Cold Spring Harbor, NY.

68. **Sarmientos, P., J. E. Sylvester, S. Contente, and M. Cashel.** 1983. Differential stringent control of the tandem *E. coli* ribosomal RNA promoters from the *rrnA* operon expressed in vivo in multicopy plasmids. Cell. **32**(4):1337-46.

69. **Schmidt, T. M.** 1997. Multiplicity of Ribosomal RNA Operons in Prokaryotic Genomes, p. 221-229. *In* F. J. deBruijn, J. R. Lupski, and G. M. Weinstock (ed.), Bacterial Genomes: Physical Structure and Analysis. International Thomson Publishing, New York.

70. **Senn, H., U. Lendenmann, M. Snozzi, G. Hamer, and T. Egli.** 1994. The growth of *Escherichia coli* in glucose-limited chemostat cultures: a re-examination of the kinetics. Biochim Biophys Acta. **1201**(3):424-36.

71. **Sharp, P. M., J. E. Kelleher, A. S. Daniel, G. M. Cowan, and N. E. Murray.** 1992. Roles of selection and recombination in the evolution of type I restriction-modification systems in enterobacteria. Proc Natl Acad Sci U S A. **89**(20):9836-40.

72. **Snyder, L.** 1998. Phage P1 strain and transduction protocol.

73. **Sokal, R. R., and F. J. Rohlf.** 1995. Biometry: the principles and practice of statistics in biological research, 3 ed. W. H. Freeman and Company, New York.

74. **Stevenson, B. S., and T. M. Schmidt.** 1998. Growth rate-dependent accumulation of RNA from plasmid-borne rRNA operons in *Escherichia coli*. J Bacteriol. **180**(7):1970-2.

75. **Tilman, D.** 1977. Resource competition between planktonic algae: an experimental and theoretical approach. Ecology. **58**:338-348.

76. **Vasi, F., M. Travisano, and R. E. Lenski.** 1994. Long-term experimental evolution in *Escherichia coli*. II. Changes in life-history traits during adaptation to a seasonal environment. Am Nat. **144**(3):432-456.

77. **Wilkinson, S. R., D. I. Young, J. G. Morris, and M. Young.** 1995. Molecular genetics and the initiation of solventogenesis in *Clostridium beijerinckii* (formerly *Clostridium acetobutylicum*) NCIMB 8052. FEMS Microbiol Rev. **17**(3):275-85.

78. **Wolfe, C. J., and M. G. Haygood.** 1993. Bioluminescent symbionts of the Caribbean flashlight fish (*Kryptophanaron alfredi*) have a single rRNA operon. Mol Mar Biol Biotechnol. **2**(4):189-97.